The Pennsylvania State University
The Graduate School

TOWARDS AN EFFECTIVE THEORY OF OPEN QUANTUM SYSTEMS THROUGH OPEN QUBIT SYSTEMS

A Dissertation in
Physics
by
Sean T. Prudhoe

Submitted in Partial Fulfillment
of the Requirements
for the Degree of

Doctor of Philosophy

August 2024

The dissertation of Sean T. Prudhoe was reviewed and approved by the following:

Sarah Shandera
Associate Professor of Physics
Chair of Committee

Eugenio Bianchi
Associate Professor of Physics
Committee Member

Irina Moiciou
Associate Professor of Physics
Committee Member

Sahin Ozdemir
Professor of Engineering Science and Mechanics
Committee Member

Mauricio Terrones
Verne M. Willaman Professor of Physics
Professor of Chemistry, Materials Science & Engineering
Department Head

Abstract

We explore procedures to approximate the reduced dynamics of open qubit systems, to understand the construction of effective open theories in more general systems. We provide constructions both for infinitesimal time-evolution i.e. master equations, and for discrete time-evolution through random ensembles of quantum channels. An argument is made that the ensemble approach is a much better suited method to tackle the open dynamics experienced in more novel open systems, such as those with time-dependent boundaries that are found in quantum cosmology. We also explore the idea that quantum subsystems may appear through a process of spontaneous symmetry breaking, which serves as the prequel to the appearance of an open quantum system.

Table of Contents

List of Figures

List of Tables

Acknowledgments

The author is grateful to Sarah Shandera and fellow research group members Unnati Akhouri, Sarka Blahnik, and Tommy Chin for much discussion on the topics presented in this dissertation. Particularly on the topic of emergent quantum subsystems, the author thanks Rishabh Kumar for his work on the project and Sarang Gopolakrishnan for introducing and discussing the paper that the project was based on. Further, the author acknowledges ample discussions provided by colleagues from the university of Massachusetts, Lowell, including Nishant Argawal, Archana Kamal, Red O'Keefe, and Brendan Bowen. And finally the author thanks the remaining members of the committee for time spent reviewing the dissertation thus far; they include Eugenio Bianchi, Irina Moiciou, and Sahin Ozdemir.

The work in this dissertation was supported by the National Science Foundation under the grants PHY-1719991 and PHY-2310662 and partially supported by the Department of Energy under DE-SC0020360. The work herein does not necessarily reflect the views of the National Science Foundation or the Department of Energy.

Chapter 1
Introduction

1.1 The theory of open quantum systems

Quantum mechanics is arguably the most successful set of physical laws yet uncovered by the scientific community. It describes physical phenomena from the microscopic (e.g. molecular, atomic, and sub-atomic processes) to the macroscopic (e.g. formation of neutron stars). And despite the wide applicability, the framework used to build quantum mechanics is remarkably simple. It includes the quantum state $|\psi\rangle$ which contains all information about the probabilistic outcome of measuring observable quantities, as well as the (possibly time-dependent) Hamiltonian which governs time-evolution as

$$\begin{aligned} |\psi_t\rangle &= U(t,t_0)|\psi_{t_0}\rangle \\ U(t,t_0) &= \mathrm{T}\exp\Big(-i\int H(t')dt'\Big) \end{aligned} \tag{1.1}$$

where T is the time-ordering operator and $U(t,t_0)$ is the unitary time-evolution operator. Unitarity is sufficient to ensure that probability is conserved under time-evolution i.e. $\langle\psi_t|\psi_t\rangle = \langle\psi_{t_0}|\psi_{t_0}\rangle = 1$. Or stated differently, given a complete set of outcomes for an experiment when a measurement is performed one of these outcomes must occur.

However, unitarity alone cannot explain all phenomena that emerge from quantum mechanics. Notable non-unitary processes are projective measurements, for example the measurements that appear in Stern-Gerlach setups. Further, since unitary processes are completely reversible (i.e. invertible), any irreversible process requires some degree of non-unitary. Such processes include decoherence and thermalization, which are fundamentally important for a classical universe to exist. Therefore, non-unitary dynamics is necessary for classicality to emerge from quantum mechanics.

To produce non-unitary operations, the unitarity of quantum mechanics need not be

fully broken, only the construct of quantum subsystems needs to be introduced [1–3]. That is the Hilbert space, the space of quantum states, decomposes as $\mathcal{H}_{\mathrm{S}} \otimes \mathcal{H}_{\mathrm{E}}$. The subspace $\mathcal{H}_{\mathrm{S}}$ contains the degrees of freedom of interest, and $\mathcal{H}_{\mathrm{E}}$ contains the residual degrees of freedom. The label S denotes system, and for historical reasons the label E denotes environment, but note that these degrees of freedom are not always a thermal reservoir. By coupling system and environment through an interaction Hamiltonian and tracing out the environment degrees of freedom, the system degrees of freedom will undergo non-unitary time-evolution. These types of quantum mechanical systems are referred to as **open quantum systems**, and they play a central role in this dissertation.

To appreciate the full set of non-unitary dynamics possible, the quantum state must be promoted to an object known as the density matrix (ρ). The density matrix is a statistical mixture of quantum states. If the mixture contains only a single state, then the density matrix is called pure, otherwise it is referred to as a mixed state. Any mixed state can be constructed as a convex combination of pure states, although such a construction is not unique. However, the minimum number of pure states required in such a construction equals the matrix rank of the density matrix. For a given open quantum system, the set of density matrices are the Hermitian operators such that

$$\begin{aligned} &\mathrm{tr}_{\mathrm{S}}\left(\rho_{\mathrm{S}}\right) = 1 \\ &\mathrm{tr}_{\mathrm{S}}\left(\rho_{\mathrm{S}}^{2}\right) \leq 1\,. \end{aligned} \tag{1.2}$$

These inequalities imply that a density matrix must be a positive operator with eigenvalues between 0 and 1. The second inequality is only saturated in the case that the density matrix is a pure state. In a given matrix representation of a density matrix, the diagonal elements are called populations and the off-diagonal elements are called coherences. And finally, the expectation of an observable ($\mathcal{O}_{\mathrm{S}}$) with respect to the state ρ_{S} is

$$\langle \mathcal{O}_{\mathrm{S}} \rangle = \mathrm{tr}_{\mathrm{S}}\left(\mathcal{O}_{\mathrm{S}}\rho_{\mathrm{S}}\right)\,. \tag{1.3}$$

The action of a non-unitary map will transform the density matrix associated to an open system. The notable example is that of a projective measurement, but the notion can be extended to so called generalized measurements. A generalized measurement is equivalent to acting on the reduced density with a non-unitary operation known as a quantum channel ($\mathcal{E}$)

$$\rho_{\mathrm{S}} \to \mathcal{E}\left[\rho_{\mathrm{S}}\right]\,. \tag{1.4}$$

At a technical level a quantum channel is a completely-positive trace-preserving map (CPTP). The trace preservation is equivalent to probability preservation. Complete-positivity guarantees that the post measurement state remains a density matrix, no matter the input state. Further, if a quantum channel only mixes the populations of a density matrix it is referred to as a classical channel or stochastic matrix. Perhaps the most important property of quantum channels is that they never increase the trace-distance of any pair of input states

$$\mathcal{D}\Big(\mathcal{E}\left[\rho_{\mathrm{S}}\right], \mathcal{E}\left[\sigma_{\mathrm{S}}\right]\Big) \leq \mathcal{D}\Big(\rho_{\mathrm{S}}, \sigma_{\mathrm{S}}\Big). \tag{1.5}$$

Physically speaking, a quantum channel never makes pairs of states more distinguishable. This is precisely why non-unitary processes are said to destroy information.

Complete-positivity of a quantum channel is equivalent to a few properties that we detail here. Most famously, complete-positivity of an quantum operation is equivalent to the existence of a Kraus decomposition [4]

$$\begin{aligned} \sum_i K_i \rho_{\mathrm{S}} K_i^\dagger &= \mathcal{E}\left[\rho_{\mathrm{S}}\right] \\ \sum_i K_i^\dagger K_i &= \mathbb{1}_{\mathrm{S}} \end{aligned} \tag{1.6}$$

where the K_i are known as Kraus operators. Note that the Kraus decomposition is not unique, but there is a minimal number of Kraus operators required to decompose a given quantum channel, referred to as the Kraus rank. The Kraus rank is equal to the matrix rank of the Choi matrix, which we define shortly.

The Kraus decomposition is useful for constructing and distinguishing quantum channels. For example, the unitality of a quantum channel may be deduced from the Kraus decomposition. A channel is said to be unital if $\mathcal{E}\left[\mathbb{1}_{\mathrm{S}}\right] = \mathbb{1}_{\mathrm{S}}$, that is it fixes the maximally mixed state. Distinguishing channels based on their unitality is helpful for the following reasons. First, any non-unital channel increases the purity of certain initial states, most obviously the maximally mixed state. Further, non-unital channels are strictly contracting over the space of states, therefore their fixed points are unique [2]. We provide examples of non-unital qubit channels in Chapter 2 and Chapter 3.

From the conditions for complete-positivity and the unital condition, it follows that a channel is unital iff a Kraus decomposition exists consisting entirely of normal operators. Recall that an operator is called normal if it commutes with its Hermitian conjugate. A natural construction of unital channels in any open system is to average over unitary channels. It is clear that such a construction satisfies the conditions of a

Kraus decomposition. However in the case of open systems larger than a qubit, unitary averages are not the only form of unital channels.

Another method to determine the complete-positive of a non-unitary map, is by determining if the Choi matrix is positive [5]. To define the Choi matrix associated to a non-unitary map, consider a composite quantum system $\mathcal{H} = \mathcal{H}_{\rm S} \otimes \mathcal{H}_{\rm S}$ and construct the maximally entangled state

$$|\Psi\rangle = \frac{1}{\sqrt{N}} \sum_{i=1}^{N} |i, i\rangle \,, \tag{1.7}$$

where N=dim$\mathcal{H}_{\rm S}$. Then the Choi matrix is defined as

$$C_{\mathcal{E}} = (\mathcal{E} \otimes \mathbb{1})|\Psi\rangle\langle\Psi| \tag{1.8}$$

and the non-unitary operation is completely-positive iff $C_{\mathcal{E}}$ is positive. The utility of the Choi matrix is that positivity of a matrix is a simple property to verify. Further, the Choi matrix may be used to determine the space of quantum channels for simple systems as was done for qubit channels in [6]. Connecting to the Kraus decomposition, the matrix rank of $C_{\mathcal{E}}$ is equal to the Kraus rank of the channel $\mathcal{E}$.

And perhaps the most physically relevant property of completely-positive maps is that of the Stinespring dilation [7]. That is $\mathcal{E}$ is completely-positive iff a composite unitary (V) and ancillary pure state ($\psi_{\rm E}$) exist such that

$$\mathcal{E}\left[\rho_{\rm S}\right] = {\rm tr}_{\rm E}\left[V\rho_{\rm S} \otimes \Big(|\psi_{\rm E}\rangle\langle\psi_{\rm E}|\Big)V^{\dagger}\right] \,. \tag{1.9}$$

The pure state $\psi_{\rm E}$ must reside in a Hilbert space with at least as many dimensions as the Kraus rank of the channel. From the physics point of view one often starts with the R.H.S of Eq.(1.9), where the unitary transformation is replaced with the time-evolution operator. Further, the auxiliary system is allowed to be in mixed state, however the resulting map will be completely-positive. To see this notice that Eq.(1.9) is invariant change of basis over the auxiliary Hilbert space, therefore the channel may be computed in an eigenbasis of the mixed state. The resulting expression is then a convex linear combination of quantum channels. From the Kraus decomposition it may be deduced that convex combinations of quantum channels remain completely-positive.

Performing the replacement $V \to U(t, t_0)$ in Eq.(1.9) we have

$$\Lambda(t, 0)\left[\rho_{\rm S}(0)\right] = {\rm tr}_{\rm E}\left[U(t, 0)\Big(\rho_{\rm S}(0) \otimes \rho_{\rm E}(0)\Big)U^{\dagger}(t, 0)\right] \tag{1.10}$$

which is a 1-parameter family of quantum channels known as a dynamical map. We have changed symbols here to emphasis the difference between a quantum channel and a dynamical map. The dynamical map is a non-unitary generalization of the unitary time-evolution operator from closed quantum systems. Besides of course the non-unitary features previously mentioned, it differs from a time-evolution operator in the possible lack of divisibility. Recall that the unitary operator defined in Eq.(1.1) may be split into products of unitary operators

$$U(t_2, t_0) = U(t_2, t_1)U(t_1, t_0) \tag{1.11}$$

for any values of time such that $t_0 \leq t_1 \leq t_2$. The process of dividing unitary time-evolution may be repeated indefinitely, used for example in the derivation of the path integral formulation in quantum mechanics. But for dynamical maps, the process of dividing the time-evolution into smaller pieces must be done with more care. The time-evolution over intermediate times is governed by the propagator, or interweaving map

$$\Lambda(t_2, t_0) = \Phi(t_2, t_1)\Lambda(t_1, t_0) \tag{1.12}$$

which is not guaranteed to be positive let alone completely-positive. Dynamical maps where Φ is positive for all intermediate times are known as P-divisible, and are CP-divisible if Φ is a quantum channel for all intermediate times [8]. For example, unitary channels are always CP-divisible which follows from Eq.(1.11).

CP-divisible dynamical maps are a widely used generalization of classical Markovian stochastic processes. There is however not a consensus on the correct definition of the quantum Markov property, as there is no true quantum analogue of the classical propagator [9–11]. Dynamical maps that are P-divisible are called weakly non-Markovian, and processes that are not even P-divisible are called strongly non-Markovian [12]. The physical relevance of the divisibility of a dynamical map is that it constrains the equations of motion that can generate a given process. The dynamical map may be thought of as a non-perturbative description of an open systems dynamics, where as the equations of motion or master equation is often a tool to obtain approximate solutions for the open system dynamics.

The most commonly employed master equation is that of the time-dependent Lindblad equation

$$\partial_t \rho_{\mathrm{S}}(t) = -i\left[H(t), \rho_{\mathrm{S}}(t)\right] + \sum_i \left(\gamma_i(t) L_i \rho_{\mathrm{S}} L_i^\dagger - \frac{1}{2}\{L_i^\dagger L_i, \rho_{\mathrm{S}}(t)\}\right) \tag{1.13}$$

with $H(t)$ the effective Hamiltonian, L_i the Lindblad or jump operators, and $\gamma_i(t)$ the time-dependent rates. In the case that the rates are constant and positive this equation is known as the Gorini–Kossakowski–Sudarshan–Lindblad (GKSL) equation [13,14]. The rates are crucial in determining the divisibility of the dynamics. For rates that are non-negative at any time, the obtained dynamical map is CP-divisible, but note this is only a sufficient condition. In Chapter 2 we provide examples of CP-divisible dynamics with negative rates in the case of an open qubit system.

However, a time-local description must include divergent rates in the case that the reduced dynamics is irreversible at some finite time. Such a divergence is unphysical and thus a suitable master equation in these settings must be non-time-local. A non-time-local master equation takes the general form

$$\partial_t \rho_{\mathrm{S}}(t) = K_{\mathrm{TL}}(t)\left[\rho_{\mathrm{S}}(t)\right] + \int_{t_0}^{t} K_{\mathrm{NTL}}(t,\tau)\left[\rho_{\mathrm{S}}(\tau)\right] d\tau \,. \tag{1.14}$$

A well known example of such a master equation is the Nakajima-Zwanzig equation [15,16]. The issues with non-time-local equations is that being integro-differential equations they are difficult to solve. Further while the Nakajima-Zwanzig equations is an exact master equation, it is only formally so as it uses the formal solution to the total system Schrödinger equation. Actual solutions still must be obtained perturbatively, for example using the cumulant expansion.

1.2 Effective descriptions of open quantum systems

The main approach to study open systems thus far is to derive, either from first principles or propose through other means, a master equation of the form given in Eq.(1.13). There are certainly cases where equations that are non-time-local have been used, for example the post-Markovian equation proposed in [17]. More typical though is a non-time-local equation derived perturbatively from the Nakajima-Zwanzig equation, from which a time-local equation is derived in certain limits. And while there are certainly similarities between how an effective time-local equation can be derived in a variety of open systems, there is still no general procedure for obtaining such a result.

There are several obstacles to construct such an effective master equation in open quantum systems. One obstacle is the initial state of the environment, which for a given open system can be generic. One may already see that the state of the environment plays a crucial role at the level of unitary effective theories. For example, in quantum

field theory when the ultra-violet degrees of freedom form a vacuum state, they may be integrated out by re-normalizing Hamiltonian parameters. However, when the ultra-violet degrees of freedom are in a higher temperature thermal state the description can dramatically change as excitations not present in the low energy effective theory become relevant. So it is reasonable to suspect that the initial state of the environment plays an important role in determining the form of an effective master equations, which is seen from results derived in Chapter 2.

The other major obstacle is the potential for time-locality breaking. That is to say building an effective master equation requires more than determining the allowed set of jump operators, and an approximate form for the time-dependent rates. One must also determine if a non-time-local generator is necessary, and the shape of the memory kernel. However, it is difficult to address this question non-perturbatively, although the presence of non-invertibilities may be deduced from trace-distance measures over a sufficient number of initial states, if such measurements are possible.

So far the difficulty in using non-time-local master equations has lead much of the investigation of open quantum cosmology to remain in the time-local domain (a non-exhaustive list [18–23]). In most of these works an argument is made that the late-time dynamics will be governed by a time-local master equation, which may be true in the scenarios considered. But we find in Chapter 2 that an open system coupled to a changing landscape of environmental degrees of freedom requires a non-time-local description. And depending on the details of the changing landscape, the locality breaking can persist to late-times.

Because of the sheer difficultly met when trying to derive the reduced dynamics in quantum cosmology (see for example [24]), we choose to pursue effective theories in open systems through analytic studies of open qubit networks. Ostensibly, one may argue that such models may be too simple to say anything useful about quantum gravity or open quantum cosmology, but it is known in the literature that non-perturbative quantum gravity will be described using a Type I Von-Neumann algebra (take for example quantum spin-foams).

We construct our effective theory in the following manner. In Chapter 2 we construct exact dynamical maps for a three qubit network, where two of the qubits serve the role of a growing environment. We study two aspects that are relevant for the construction of effective master equations. First, when only two of the qubits are interacting we determine in detail how the Hamiltonian parameters and initial environment state conspire to form non-time-local reduced dynamics. We find that there is both a strong-coupling condition

and special class of initial states required for non-time-local reduced dynamics.

We further consider making the active degrees of freedom in the environment time-dependent. We consider the case where the third qubit breaks a symmetry of the interaction between the previous pair at a point during their evolution. We find that in the presence of phase-covariance breaking, the reduced dynamics of the system qubit becomes non-time-local for all times afterwards. We take this as evidence that in an open quantum system with a changing environmental landscape, a non-time-local master equation is necessary to approximate the reduced dynamics.

In Chapter 3 we pivot towards a different construction of effective open theories that moves away from the master equation. To make the construction simple, but still widely applicable, we consider only phase-covariant reduced dynamics, which is generated over a qubit network. That is each 1-qubit dynamical map is phase-covariant, no matter which qubit is chosen to be the system or focal qubit. In this way we are able to obtain an exact ensemble of phase-covariant dynamical maps. From these ensembles we extract out how the network and long time averaged channel approaches its steady value. From the form of the steady channel, and its approach to equilibrium, we construct random distributions of phase-covariant channels that approximate the network dynamics at late-times.

And finally in Chapter 4, we explore a model of spontaneous generation of qubit subsystems, which serve as a potential prequel to the models considered in the previous chapters. The motivation is to understand how quantum subsystems emerge in a dynamical process, and what drives the form of typical interaction, say the propensity towards many-body and local interactions. In principle, the model allows for the eventual tuning of subsystems that appear, through both the subsystem decompositions and the form of typical interactions.

Chapter 2
Pursuit of Effective Master Equations

2.1 Preamble

This chapter is a reprint of [25]. In this work we studied the types of master equations that describe the exact reduced dynamics of a triplet of qubits. We show how the non-time-local vs. time-local nature of the master equation depends both on the Hamiltonian parameters and the class of the initial environment state. Further, we show that when breaking the phase-covariance of the reduced dynamics by activating a dormant environmental qubit, the reduced dynamics becomes eternally non-time-local. We take this as a justification for the need of non-time-local master equations in open quantum systems with time-dependent boundaries, such as those encountered in quantum cosmology.

2.2 Introduction

The evolution of quantum systems coupled to unobserved or unobservable degrees of freedom can be much more complex than the evolution of closed systems [1]. Information may flow back and forth between the observed and unobserved parts of the system, leading to equations of motion that may not be local in time, and that give rise to non-unitary, non-Markovian evolution [26]. While formal expressions for the evolution of open systems exist, and exact expressions can be derived in particular cases where the unobserved physics is known, there is not yet a procedure for systematically constructing effective theories of open systems that can encapsulate the full range of possible phenomena.

A particular class of complex open systems appears in cosmology, where the volume

of the universe accessible to a single observer is generically bounded. An open-systems approach in cosmology has been advocated by some researchers for decades [27, 28], and recent theoretical developments have led to a resurgence of interest in these ideas. For example, the possibility of detecting primordial non-Gaussianity in the statistics of the cosmic microwave background fluctuations [29] motivated to a comprehensive study of the effects of interacting fields during or after inflation. Those interactions can couple Fourier modes of different wavelengths in different ways. The finite extent of the observable universe means that very long wavelength modes are irretrievably in the 'environment'. Modes with very short wavelength are practically unobservable as well. Tracing out either, or both, sets of unobservable modes generates an effective description for the observable modes, which form an open system [30]. The appropriate framework for understanding the space of models that generate the data is that of an open effective theory. Moreover, the field or fields relevant for inflation are expected to be accompanied by many other degrees of freedom which may move from passive to active as inflation proceeds. Indeed, it is postulated that if the inflationary field explores too large of a range, a large number of fields will become relevant, limiting the validity of the original model as an effective description [31–33]. Using an open system effective theory for the inflaton, rather than a traditional low-energy effective theory, one can treat these light degrees of freedom as a time-dependent environment. These open systems are complex, since many results that are known require non-perturbative techniques [34] and the associated open systems are frequently non-Markovian [35]. However, one has symmetry constraints to guide the effective theory [36]. A similar story of complexity restricted by symmetry applies to another well-studied system where open effective theories are applicable, black holes [19, 20, 37–41]. Cosmologists, then, would like to understand how to construct effective theories of open systems that are non-perturbative and non-Markovian, with time-dependent environments, but constrained by symmetries.

To address these questions requires a non-perturbative understanding of the evolution of the reduced system. For finite-dimensional quantum systems this can be addressed using the dynamical map, the operator that governs the dynamics of the reduced degrees of freedom. Of course, determining the dynamical map is as difficult as solving the Schrödinger equation governing the system/environment dynamics. Thus for this work we consider simple open systems, constructing dynamical maps for a single system qubit. In this setting the dynamical map can be determined as an analytic function of the Hamiltonian parameters, for a generic initial environment state.

Due to their relative simplicity, much is understood about the general structure of

qubit dynamical maps [6,42–44]. Such maps appear frequently in quantum computational settings, where they model noisy interactions of qubits with the environment. Optimal dynamical maps have been found for performing communication tasks that leverage qubit entanglement to transmit quantum information securely [45–49]. So, while interacting qubits are far simpler systems than those found in cosmology, it is an appropriate starting point to connect the questions of interest to cosmologists to the recent advances in the understanding of open systems that have been driven by laboratory and quantum computational considerations.

We begin by investigating a solvable example of coupled qubits to explore how non-Markovianity and the non-time-local aspects of the master equation for one qubit depend on the initial state of the unobserved qubit and on the symmetries and coupling constants of the full Hamiltonian. The first Hamiltonian we consider has (1) a conserved quantity, and (2) a block-diagonal structure of two equal-size pieces, allowing additional symmetry structures at special points in parameter space. Since non-time-local master equations can be particularly difficult to work with, we examine how much of the parameter space requires a time non-local equation, and the perturbations or approximations in both the Hamiltonian or the state of the unobserved qubit that will generate time-local equations of motion.

We then extend the study of the two qubit model, using a subset of the Hamiltonian family and initial environment states that allow for the appearance of additional degree of symmetry. We introduce a third qubit that remains a spectator for a time and is later switched on using an interaction that explicitly breaks the extra symmetry appearing in the two qubit interaction. The study focuses on the radical change in the invertibility of the dynamical map obtained by tracing out the two qubits that act as the environment, indicating that a time-local master equation cannot be used after symmetry breaking.

In the rest of the introduction we briefly review the formalism for open system dynamics and master equations in the context of our goals and model. Then, in Section 2.3, we introduce the example systems. In Section 2.4 we derive the reduced dynamics for a single-qubit systems, tracing out the environment qubit(s). Section 2.5 derives the conditions for non-time-local dynamics via the non-invertibility of the dynamical map and discusses several features we use to classify the dynamical map including the non-Markovianity, divisibility, and symmetries of the Hamiltonian. We determine how these depend on Hamiltonian parameters, in particular whether it is strongly coupled or not, and what role the initial environment state plays in non-time-locality. In Section 2.6 we use perturbed initial environment states to construct approximate time-local master

equations. And we conclude in Section 3.7.

2.2.1 Open system evolution

For some open systems, the master equation governing the evolution of the density matrix for the observed system, $\rho_{\rm S}(t)$, is [13, 50–52]

$$\partial_t \rho_{\rm S}(t) = -i[H_{\rm free}(t) + H_{\rm open}(t), \rho_{\rm S}(t)] + \sum_k \gamma_k(t) \left(L_k \rho_{\rm S}(t) L_k^\dagger - \frac{1}{2}\{L_k^\dagger L_k, \rho_{\rm S}(t)\} \right) . \quad (2.1)$$

Here $H_{\rm free}(t) + H_{\rm open}(t) = H_{\rm eff}(t)$ is the effective Hamiltonian of the system, containing both the original system Hamiltonian $H_{\rm free}(t)$ and a piece, $H_{\rm open}(t)$, generated by the coupling to an environment. The L_k are operators acting on the system, and the $\gamma_k(t)$ are functions describing the flow of information between the system and environment. The $\gamma_k(t)$, which control the subset of all possible operators L_k that appear with non-zero coefficients, depend on the system-environment coupling and the state of the environment. $H_{\rm eff}(t)$ and $\gamma_k(t)$ are given by environment correlation functions calculated using the initial environment state $\rho_{\rm E}(0)$.

If the environment and full Hamiltonian are unknown, one might begin constructing an effective theory for the system by writing all possible L_k and a generic $H_{\rm eff}$ from the complete set of operators that act on the system. Then, the work in the effective theory comes in specifying some structure for the dissipation functions $\gamma_k(t)$, determining any approximations that may allow some possible terms in $H_{\rm eff}$ to be discarded, and in determining consistency between effects captured in $H_{\rm open}(t)$ and in the non-unitary part of Eq.(2.1). Some broad guidelines for this process are known: the simplest choice would be all $\gamma_k \geq 0$ and constant, restricting the system to non-unitary however time-independent, Markovian evolution. Time-dependent Markovian dynamics would be described by $\gamma_k(t) \geq 0$ at all times. Finally a restricted set of non-Markovian dynamics would be captured by considering generic functions $\gamma(t)$.

However, the most general case allows the master equation to be non-local in time. Then, in addition to the time-local part one adds an integral term. This is the Nakajima-Zwanzig equation [15, 16],

$$\partial_t \rho_{\rm S}(t) = K_{\rm TL}(t)\rho_{\rm S}(t) + \int K_{\rm NZ}(t,\tau)\rho_{\rm S}(\tau) d\tau \, , \quad (2.2)$$

where the time-local piece, $K_{\rm TL}(t)$, generates the same action on $\rho_{\rm S}(t)$ as given in Eq.(2.1). The integral is over the history of the evolution $[t_0, t]$ where t_0 is a time where the system

and environment are uncorrelated and t is the time where one is interested in calculating ensemble averages. In constructing a parameterized effective theory for the open system dynamics, one would like to know how to systematically address whether a non-local equation is necessary. In addition, which qualitative aspects of information flow can be captured in either the $\gamma(t)$ or the time non-local kernel $K_{\rm NZ}(t,\tau)$, and how they should be implemented?

To address these questions in a simple case, we explore the relationship between the full Hamiltonian for system and environment, together with the initial state of the environment, to several features of the reduced dynamics. We consider measures of non-Markovianity and the conditions under which time non-local evolution is required. We do this by first computing the exact reduced dynamics via the dynamical map. This is a non-unitary generalization of the time evolution operator, a completely positive and trace preserving (CPTP) map from the initial density matrix to the density matrix at a later time t,

$$\rho_S(t) = \Lambda(t,0) \circ \rho_S(0)\,. \tag{2.3}$$

For qubit dynamical maps the complications arising from non-Markovianity are less severe. Non-Markovian qubit dynamical maps can be tractably studied, more so than their master equation counterparts. For example the divisibility (how the time evolution can be broken into steps) and how it relates to non-Markovianity has been exhaustively studied in the case of qubit dynamical maps [9–11, 53]. For the model we consider it is therefore possible to make detailed statements about the relation between properties of the dynamical map and its non-Markovianity.

Dynamical maps do not have to be invertible; maps with $\mathrm{Det}\Lambda(\tau_i) = 0$ for some times τ_i require either a time-local description that diverges at each τ_i or a non-time-local integral kernel, as written in Eq.(2.2) [54]. For a simple system, we will use the non-invertibility of the dynamical map to derive the conditions on the full Hamiltonian and the environment that make a non-time-local master equation necessary. We find that, independent of the Hamiltonian, there are always a set of initial environment states which support time-local reduced dynamics. This allows a time-local, approximate, master equation to be constructed by shifting the initial state of the environment. For an initial environment state, $\rho_{\rm E}(t_0)$, and dynamics that requires a non-time-local piece, there exist environment states nearby in trace distance norm, $\{\rho^{'}_{\rm E}(t_0)\}$, which can be used to define

a master equation of the form

$$\begin{aligned}\partial_t \rho_S(t;\rho_{\rm E}(t_0)) = & K_{\rm TL}(t;\rho_{\rm E}^{'}(t_0))\rho_S(t;\rho_{\rm E}(t_0)) \\ & + \int K_{\rm NTL}(t,\tau;\delta\rho_{\rm E})\rho_{\rm S}(\tau;\rho_{\rm E}(t_0))d\tau\,.\end{aligned} \tag{2.4}$$

Here the non-time-local component is linear in $\delta\rho_{\rm E} = \rho_{\rm E}(t_0) - \rho_{\rm E}^{'}(t_0)$, and the integral is over the evolution history $[t_0, t]$.

2.3 The system-environment Hamiltonians and the unitary dynamics

This section introduces both the family of two-qubit Hamiltonians considered, as well as a more restrictive family of three-qubit interactions. The two-qubit model has an associated parity symmetry, which splits the Hamiltonian into two equal-sized blocks. Such models are interesting as they have an intermediate level of symmetry: more than the class with no non-trivial symmetries, however not as much as Hamiltonians that preserve the total angular momentum of the two qubits. Physically, dynamics of the type we use here describe a pair of non-interacting qubits, most clearly seen through a change of meronomic frame [55]. We also characterize features of the non-Markovianity of the single-qubit evolution, according to parameter choices in the full Hamiltonian.

2.3.1 Two-qubit family

The two-qubit Hamiltonian that we study is

$$\begin{aligned}H =& H_{\rm free} + H_{\rm int} \\ =& \omega_{\rm S}(Z_{\rm S}\otimes\mathbb{1}_{\rm E}) + \omega_{\rm E}(\mathbb{1}_{\rm S}\otimes Z_{\rm E}) + \kappa_{\rm SE}(Y_{\rm S}\otimes X_{\rm E}) + \kappa_{\rm ES}(X_{\rm S}\otimes Y_{\rm E})\,.\end{aligned} \tag{2.5}$$

The free parameters $\omega_{\rm S}$ and $\omega_{\rm E}$ provide the time scales associated to the free dynamics of each individual qubit (with $\hbar = 1$), and the parameters κ_{SE} and κ_{ES} are coupling strengths. H has a symmetry, $[H, Z_{\rm S}\otimes Z_{\rm E}] = 0$, so the eigenstates have definite parity associated to $P_{zz} = Z_{\rm S}\otimes Z_{\rm E}$. This $\mathbb{Z}_2$ symmetry allows H to be split into even and odd blocks, where the even block is spanned by states with correlated spins (e.g. $|\uparrow\uparrow\rangle$) and the odd block is spanned by states with anti-correlated spins (e.g. $|\uparrow\downarrow\rangle$).

The block diagonalization is achieved by splitting H into symmetric and anti-

symmetric parts under exchange of system and environment operators. Defining new parameters,

$$\begin{aligned} 2\Delta_\pm &= \omega_\mathrm{S} \pm \omega_\mathrm{E} \\ 2\kappa_\pm &= \kappa_\mathrm{SE} \pm \kappa_\mathrm{ES}\,, \end{aligned} \tag{2.6}$$

the Hamiltonian can be written as

$$\begin{aligned} H =& \Delta_+(Z_\mathrm{S}\otimes \mathbb{1}_\mathrm{E} + \mathbb{1}_\mathrm{S}\otimes Z_\mathrm{E}) + \kappa_+\left[Y_\mathrm{S}\otimes X_\mathrm{E} + X_S\otimes Y_\mathrm{E}\right] \\ &+\Delta_-(Z_\mathrm{S}\otimes \mathbb{1}_\mathrm{E} - \mathbb{1}_\mathrm{S}\otimes Z_\mathrm{E}) + \kappa_-\left[Y_\mathrm{S}\otimes X_\mathrm{E} - X_\mathrm{S}\otimes Y_\mathrm{E}\right] \\ \equiv& H_+ + H_-\,, \end{aligned} \tag{2.7}$$

where the $\pm$ labels correspond to the $\mathbb{Z}_2$ (parity) eigenvalues of each block. The block diagonalization of H introduces a subspace decomposition $\mathcal{H} = \mathcal{Q}_+ \oplus \mathcal{Q}_-$, where the spaces $\mathcal{Q}_\pm$ are spanned by the eigenstates of $H_\pm$. As we show below, there is also a tensor product decomposition for which the two subsystems decouple.

Using $|0\rangle$ and $|1\rangle$ to label the eigenstates of Z_S and Z_E, the stationary states of H are

$$\begin{aligned} |0_+\rangle &= \cos\frac{\phi_+}{2}|0_\mathrm{S},0_\mathrm{E}\rangle + i\sin\frac{\phi_+}{2}|1_\mathrm{S},1_\mathrm{E}\rangle \\ |1_+\rangle &= \sin\frac{\phi_+}{2}|0_\mathrm{S},0_\mathrm{E}\rangle - i\cos\frac{\phi_+}{2}|1_\mathrm{S},1_\mathrm{E}\rangle \\ |0_-\rangle &= \cos\frac{\phi_-}{2}|0_\mathrm{S},1_\mathrm{E}\rangle + i\sin\frac{\phi_-}{2}|1_\mathrm{S},0_\mathrm{E}\rangle \\ |1_-\rangle &= \sin\frac{\phi_-}{2}|0_\mathrm{S},1_\mathrm{E}\rangle - i\cos\frac{\phi_-}{2}|1_\mathrm{S},0_\mathrm{E}\rangle\,, \end{aligned} \tag{2.8}$$

with eigenvalues

$$\pm\omega_\pm = \pm 2\sqrt{\Delta_\pm^2 + \kappa_\pm^2}\,. \tag{2.9}$$

In Equation (2.8), the angles

$$\phi_\pm = \arctan\frac{\kappa_\pm}{\Delta_\pm} \tag{2.10}$$

indicate the relative size of the interaction and free Hamiltonian parameters, and if either provide a dominate contribution to the energy eigenvalues $\omega_\pm$. As long as at least one of the blocks is interacting i.e. $\kappa_\pm \neq 0$, the stationary states in the subsystem decomposition $\mathcal{H} = \mathcal{Q}_\mathrm{S}\otimes\mathcal{Q}_\mathrm{E}$ are entangled, and maximally entangled as $\frac{\kappa_\pm}{\Delta_\pm} \to \pm\infty$.

We will see below that the reduced dynamics may acquire a non-time-local component if $\phi_+ + \phi_- \geq \frac{\pi}{2}$. Since this condition requires that one or both of $\kappa_\pm \geq \Delta_\pm$, the part of

parameter space where non-time-local master equations can be required coincides with strong coupling, although not all strongly coupled Hamiltonians will have non-time-local dynamics.

So far, we have defined subsystems assuming a laboratory-based notion of locality for operations on qubits, established by the system/environment labels. However, the block-diagonal structure of the Hamiltonian suggests that we also consider a re-organization of the Hilbert space into degrees of freedom that decouple. That is, we can define qubits A and B, with orthonormal basis states $\{1_{\rm A}, 0_{\rm A}\}$ and $\{1_{\rm B}, 0_{\rm B}\}$, so that $\mathcal{H} = \mathcal{Q}_{\rm A} \otimes \mathcal{Q}_{\rm B}$. This is a change of meronomic frame [55]. Explicitly, a (non-unique) mapping between these bases is given by

$$\begin{aligned} |0_+\rangle &= |0_{\rm A}, 0_{\rm B}\rangle \\ |1_+\rangle &= |1_{\rm A}, 1_{\rm B}\rangle \\ |0_-\rangle &= |0_{\rm A}, 1_{\rm B}\rangle \\ |1_-\rangle &= |1_{\rm A}, 0_{\rm B}\rangle \,. \end{aligned} \tag{2.11}$$

One finds $H = \omega_+ \left(|0_+\rangle\langle 0_+| - |1_+\rangle\langle 1_+|\right) + \omega_- \left(|0_-\rangle\langle 0_-| - |1_-\rangle\langle 1_-|\right)$, it is straightforward to change to the frame given in Eq.(2.11), where

$$H_{AB} = \omega_{\rm A} Z_{\rm A} \otimes \mathbb{1}_{\rm B} + \omega_{\rm B} \mathbb{1}_{\rm A} \otimes Z_{\rm B} \,. \tag{2.12}$$

Here $\omega_{\rm A} = \frac{1}{2}(\omega_+ + \omega_-)$, $\omega_{\rm B} = \frac{1}{2}(\omega_+ - \omega_-)$, and $Z_{\rm A} = |0_{\rm A}\rangle\langle 0_{\rm A}| - |1_{\rm A}\rangle\langle 1_{\rm A}|$, etc. Comparing to Eq.(2.7), the two terms in Eq.(2.12) are just the A/B frame expressions for H_+ and H_-. An advantage of this frame is that it is easy to characterize the regions of parameter space with extra symmetry. A particularly useful region of parameter space is

$$\omega_+ = \omega_- \Leftrightarrow \omega_{\rm B} = 0 \;\; (\textbf{the degenerate family}) \tag{2.13}$$

which is symmetric under local rotations on the B qubit subsystem. Since symmetries are clearest in the A/B frame, we will continue to use it for that purpose in Table 2.1 below, where we classify the reduced system dynamics possible with this Hamiltonian, Eq.(2.5).

Returning to the system/environment frame, we characterize the entangling properties of the time evolution. Using the computational basis for system and environment qubits,

the time evolution operator, $U(t)$, is

$$U(t) = e^{-iHt} = \begin{bmatrix} \alpha_+(t) & 0 & 0 & -\beta_+(t) \\ 0 & \alpha_-(t) & -\beta_-(t) & 0 \\ 0 & \beta_-(t) & \bar{\alpha}_-(t) & 0 \\ \beta_+(t) & 0 & 0 & \bar{\alpha}_+(t) \end{bmatrix} , \tag{2.14}$$

where

$$\begin{aligned} \alpha_\pm(t) &= \cos\omega_\pm t - i\cos\phi_\pm \sin\omega_\pm t\,, \\ \beta_\pm(t) &= \sin\phi_\pm \sin\omega_\pm t\,, \end{aligned} \tag{2.15}$$

and $\bar{\alpha}_\pm(t)$ is the complex conjugate of $\alpha_\pm(t)$. The pair of functions from each doublet satisfy $|\alpha_\pm(t)|^2 + |\beta_\pm(t)|^2 = 1$.

The functions $\beta_\pm(t)$ are generated by the interaction between system and environment, so they determine both the entanglement and, as we see below, the invertibility of the reduced dynamics for the system.

2.3.2 Three-qubit model of dynamical symmetry breaking

We further study a model where the reduced dynamics is phase covariant. Reduced dynamics is phase covariant or time translation symmetric if the following constraints hold [56]

I $[H_{\text{free}}, H_{\text{int}}] = 0$

II $[H_{\text{free}}, \rho_{\text{E}}(0)] = 0$.

These constraints have thermodynamic implications. The first constraint is a strict energy conservation condition i.e. energy is not built up between the system and environment boundary. The second assumption is that the initial environment state is a Gibbs' state defined with respect to the free environment Hamiltonian. If these assumptions hold, then the set of time evolution operator generated by the free system Hamiltonian commutes with the action of the dynamical map. Hence the designation as a time translation symmetry. To incorporate phase-covariance breaking into our model we consider the

Hamiltonian

$$\begin{aligned}\tilde{H}(t) =& H_{\text{free}} + H_{\text{int}}(t) \\ & \omega(Z_{\text{S}} \otimes \mathbb{1}_{\text{E}} \otimes \mathbb{1}_{\text{E}'} + \mathbb{1}_{\text{S}} \otimes Z_{\text{E}} \otimes \mathbb{1}_{\text{E}'}) + \omega \left[X_S \otimes Y_{\text{E}} \otimes \mathbb{1}_{\text{E}'} - Y_{\text{S}} \otimes X_{\text{E}} \otimes \mathbb{1}_{\text{E}'}\right] \\ & + \gamma\Theta(t-\tau) \left[X_{\text{S}} \otimes \mathbb{1}_{\text{E}} \otimes X_{\text{E}'}\right] ,\end{aligned} \tag{2.16}$$

where $\Theta(t)$ is the Heaviside theta function. The choice of the time-independent portion of the Hamiltonian satisfies strict energy conservation. The second assumption is satisfied if the initial state of the E qubit is restricted to the form $\rho_{\text{E}}(0) = \frac{1}{2}(\mathbb{1}_{\text{E}} + z_{\text{E}}(0)Z_{\text{E}})$. For what follows $\tilde{H}_{t<\tau}$ is the Hamiltonian for $t < \tau$ and $\tilde{H}_{t\geq\tau}$ is the Hamiltonian for $t \geq \tau$, as we can note the Hamiltonian is a piece-wise defined function.

$\tilde{H}_{t\geq\tau}$ is chosen to break the phase covariance of the reduced dynamics, but in the process also breaks the parity symmetry. But other global symmetries appear for $t \geq \tau$, which we can exploit to determine the stationary states when the interaction changes. Using the Pauli anti-commutation relations, it is not difficult to see $[\tilde{H}_{t\geq\tau}, Z_{\text{S}} \otimes Z_{\text{E}} \otimes Z_{\text{E}'}] = 0$. But from the block structure in the eigendecomposition of the Hamiltonian, one can note the presence of another symmetry. We find that the observable,

$$\mathcal{O}_2 = Y_{\text{S}} \otimes \mathbb{1}_{\text{E}} \otimes Y_{\text{E}'} - Z_{\text{S}} \otimes X_{\text{E}} \otimes Y_{\text{E}'} \tag{2.17}$$

commutes with $\tilde{H}_{t\geq\tau}$. Therefore $\tilde{H}_{t\geq\tau}$ splits into four 2×2 blocks with definite values of $\mathcal{O}_1$ and $\mathcal{O}_2$

Thus a familiar path may be taken to determine the time evolution generated by $\tilde{H}_{t\geq\tau}$, which we denote by $\tilde{U}_{t\geq\tau}(t)$. We begin with the eigenvalues which are found to be

$$\pm\Omega_{\pm} = \pm\sqrt{\gamma^2 \pm 2\sqrt{2}\gamma\omega + 4\omega^2} \tag{2.18}$$

and are doubly degenerate. We shall start the computation in the eigenbasis of $\mathcal{O}_2$ (called the polarized basis), and then go back to the computational basis. To this end define the angles,

$$\tan\psi_{\pm} = 1 \pm 2\sqrt{2}\frac{\omega}{\gamma} \tag{2.19}$$

from which we obtain the time dependent functions (note the similarity to the previous

section),

$$\begin{aligned}\tilde{\alpha}_{\pm}(t) &= \cos\Omega_{\pm}t - i\cos\psi_{\pm}\sin\Omega_{\pm}t \\ \tilde{\beta}_{\pm}(t) &= \sin\psi_{\pm}\sin\Omega_{\pm}t\end{aligned} \tag{2.20}$$

With these functions one can construct the unitary operator $\tilde{U}_{t\geq\tau}(t)$ in the polarized basis. In the computational basis, the following combinations of functions will be most useful

$$\begin{aligned}a_{\pm}(t) &= \frac{1}{2}\Re(\tilde{\alpha}_{+} \pm \tilde{\alpha}_{-}) \\ b_{\pm}(t) &= \frac{1}{2}\Im(\tilde{\alpha}_{+} \pm \tilde{\alpha}_{-}) \\ g_{\pm}(t) &= \frac{1}{2}(\tilde{\beta}_{+} \pm \tilde{\beta}_{-}) \\ h_{\pm}(t) &= \frac{1}{2}(\tilde{\alpha}_{+} \pm \bar{\tilde{\alpha}}_{-})\end{aligned} \quad . \tag{2.21}$$

We have all we need to compute the total time evolution operator, which is given by the following time ordered exponential

$$\tilde{U}(t,0) = \mathcal{T}\exp\left[-i\int_0^t \tilde{H}(\tau)d\tau\right]. \tag{2.22}$$

Breaking the time interval into N pieces, and using the Baker-Campbell-Hausdorff relation, one can show that in the limit N goes to infinity the time ordered exponential approaches

$$\tilde{U}(t,0) = [\Theta(t) - \Theta(t-\tau)]\,\tilde{U}_{t<\tau}(t) + \Theta(t-\tau)\tilde{U}_{t\geq\tau}(t-\tau)\tilde{U}_{t<\tau}(\tau) \tag{2.23}$$

where we have just seen how to compute $\tilde{U}_{t\geq\tau}(t)$, and we can use the results of the previous section to determine $\tilde{U}_{t<\tau}(t)$.

2.4 The reduced dynamics

The reduced dynamics of the system is obtained from the full dynamics by tracing out the environment. Restricting to factorized initial states ensures that the reduced dynamics is completely positive [13]. In that case, the density matrix of the system qubit alone, at time t, is

$$\rho_{\mathrm{S}}(t) = tr_{\mathrm{E}}[U(t)\rho_{\mathrm{S}}(0)\otimes\rho_{\mathrm{E}}(0)U^{\dagger}(t)]\,. \tag{2.24}$$

The state of the system qubit at any time can be found using the dynamical map, represented by a matrix acting on the vectorization of the reduced density matrix [26]. For a qubit density matrix this is the Bloch representation

$$\rho_{\mathrm{S}}(0) = \frac{1}{2}(\mathbb{1}_{\mathrm{S}} + \vec{r}_{\mathrm{S}}(0) \cdot \vec{\sigma}_{\mathrm{S}}), \tag{2.25}$$

where $\vec{r}_{\mathrm{S}}(0)$ is a real, 3-dimensional vector with Euclidean norm $||\vec{r}_{\mathrm{S}}(0)|| \leq 1$. The evolved density matrix can then be written as

$$\rho_{\mathrm{S}}(t) = \Lambda(t, 0) \circ \rho_{\mathrm{S}}(0). \tag{2.26}$$

where $\Lambda(t, 0)$ is a 4×4 matrix. Note that as the Hamiltonian is time independent, the dynamical map depends on the initial and final times only through the difference $t - t_0$, so for what follows we can simply write $\Lambda(t)$ and suppress the initial time dependence. It is helpful to further define a 3×3 matrix with components $T^{ij} = \Lambda^{ij}$ and a 3-vector $d^i = \Lambda^{0i}$ [6], so that the action of the dynamical map can be written

$$\begin{aligned} \rho_{\mathrm{S}}(t) =& \frac{1}{2}(\mathbb{1}_{\mathrm{S}} + \vec{r}_{\mathrm{S}}(t) \cdot \vec{\sigma}_{\mathrm{S}}) \\ =& \frac{1}{2}\left(\mathbb{1}_{\mathrm{S}} + \left(\vec{\vec{T}}(t) \circ \vec{r}_{\mathrm{S}}(0) + \vec{d}(t)\right) \cdot \vec{\sigma}_{\mathrm{S}}\right) . \end{aligned} \tag{2.27}$$

This presentation has the advantage that the trace fixing requirement is immediate. For Λ to be physical, $\vec{\vec{T}}$ and $\vec{d}$ must be real so that $\rho_{\mathrm{S}}(t)$ is Hermitian. Unlike unitary maps, dynamical maps need not be divisible. For example, one is generally unable to split the time evolution as $\Lambda(t+\tau) = \Lambda(\tau)\Lambda(t)$. The reduced dynamics further differs from unitary dynamics by exhibiting hallmark features of open systems, including purity change and decoherence.

As with ordinary operators, we can define components of the dynamical map with respect to an operator basis on $\mathcal{Q}_{\mathrm{S}}$,

$$\Lambda^{ab}(t) = \frac{1}{2} tr_{\mathrm{S}}[\sigma^a_{\mathrm{S}} \Lambda(t) \circ \sigma^b_{\mathrm{S}}] = \frac{1}{2} tr[(\sigma^a_{\mathrm{S}} \otimes \mathbb{1}_{\mathrm{E}}) U(t) (\sigma^b_{\mathrm{S}} \otimes \rho_{\mathrm{E}}(0)) U^\dagger(t)] \tag{2.28}$$

where a and b can take the values $0, x, y, z$ where $\sigma^0_S = \mathbb{1}_{\mathrm{S}}$.

2.4.1 Two-qubit family

Carrying out this calculation, we find the non-zero dynamical map components, in terms of the environment qubit's initial state, $\vec{r}_E(0)$, and the functions $\alpha_\pm(t)$ and $\beta_\pm(t)$ appearing in the time evolution operator, Eq.(2.15), to be

$$\begin{aligned}
\Lambda^{z0}(t) =& \frac{1}{2}\left[|\alpha_+(t)|^2 - |\beta_+(t)|^2 - |\alpha_-(t)|^2 + |\beta_-(t)|^2\right] z_E(0) \\
\Lambda^{xx}(t) =& \Re[\alpha_+(t)\alpha_-(t) - \beta_+(t)\beta_-(t)] \\
\Lambda^{xy}(t) =& \Im[\alpha_+(t)\alpha_-(t) + \beta_+(t)\beta_-(t)] \\
\Lambda^{xz}(t) =& \Re[\alpha_+(t)\beta_-(t) + \alpha_-(t)\beta_+(t)]x_E(0) - \Im[\alpha_+(t)\beta_-(t) - \alpha_-(t)\beta_+(t)]y_E(0) \\
\Lambda^{yx}(t) =& -\Im[\alpha_+(t)\alpha_-(t) - \beta_+(t)\beta_-(t)] \\
\Lambda^{yy}(t) =& \Re[\alpha_+(t)\alpha_-(t) + \beta_+(t)\beta_-(t)] \\
\Lambda^{yz}(t) =& -\Im[\alpha_+(t)\beta_-(t) + \alpha_-(t)\beta_+(t)]x_E(0) - \Re[\alpha_+(t)\beta_-(t) - \alpha_-(t)\beta_+(t)]y_E(0) \\
\Lambda^{zx}(t) =& -\Re[\alpha_+(t)\beta_+(t) + \alpha_-(t)\beta_-(t)]x_E(0) + \Im[\alpha_+(t)\beta_+(t) - \alpha_-(t)\beta_-(t)]y_E(0) \\
\Lambda^{zy}(t) =& -\Im[\alpha_+(t)\beta_+(t) + \alpha_-(t)\beta_-(t)]x_E(0) - \Re[\alpha_+(t)\beta_+(t) - \alpha_-(t)\beta_-(t)]y_E(0) \\
\Lambda^{zz}(t) =& \frac{1}{2}\left[|\alpha_+(t)|^2 - |\beta_+(t)|^2 + |\alpha_-(t)|^2 - |\beta_-(t)|^2\right] .
\end{aligned} \tag{2.29}$$

Note the difference in how the components of the initial environment state enter, with $z_{\rm E}(0)$ appearing separately from $x_{\rm E}(0)$ and $y_{\rm E}(0)$. It is instructive to see how the symmetry of the full Hamiltonian simplifies the dynamical map dependence on the initial state of the environment qubit, $\vec{r}_{\rm E}(0)$. To that end, define the partial components of the dynamical map by

$$\begin{aligned}
\Lambda^{ab} &= \frac{1}{2}\Lambda^{abc} r^c_{\rm E}(0) \\
\Lambda^{abc} &= tr[(\sigma^a_{\rm S} \otimes \mathbb{1}_{\rm E}) U(t) (\sigma^b_{\rm S} \otimes \sigma^c_{\rm E}) U^\dagger(t)] .
\end{aligned} \tag{2.30}$$

The parity symmetry $P_{zz} = Z_{\rm S} \otimes Z_{\rm E}$ essentially halves the number of non-zero Λ^{abc}, and separates the xy and z components of initial environment state in the dynamical map.

Then, since P_{zz} commutes with $U(t)$ and satisfies $P_{zz}^2 = \mathbb{1}$, we see that

$$\begin{aligned}\Lambda^{abc} &= tr[P_{zz}^2(\sigma_{\rm S}^a \otimes \mathbb{1}_{\rm E})U(t)(\sigma_{\rm S}^b \otimes \sigma_{\rm E}^c)U^\dagger(t)] \\ &= (-1)^{\pi_a+\pi_b+\pi_c} tr[P_{zz}(\sigma_{\rm S}^a \otimes \mathbb{1}_{\rm E})U(t)(\sigma_{\rm S}^b \otimes \sigma_{\rm E}^c)U^\dagger(t)P_{zz}]\,, \\ &= (-1)^{\pi_a+\pi_b+\pi_c}\Lambda^{abc}\end{aligned} \tag{2.31}$$

where the π_d are defined such that,

$$P_{zz}(\sigma_{\rm S}^e \otimes \sigma_{\rm E}^f) = (-1)^{\pi_e+\pi_f}(\sigma_{\rm S}^e \otimes \sigma_{\rm E}^f)P_{zz}\,. \tag{2.32}$$

Considering the cases where either e=0 or f=0, allows one to speak of the parity of local system and environment operators. For example the parity of the operator $\mathbb{1}_{\rm S} \otimes \sigma_{\rm E}^f$ is determined by π_f. The condition $\pi_a + \pi_b + \pi_c = 1 \pmod 2$ if satisfied implies that Λ^{abc} vanishes. This is equivalent to the following: given Λ^{ab} if the parity of $(\pi_a + \pi_b)$ is even (odd) then the only contributing partial components have π_c even (odd). Λ^{zzz} also vanishes as a consequence of the parity symmetry. However this is obviously not a consequence of the previous argument. Instead it follows using the P_{zz} symmetry and that $tr_{\rm S}(Z_{\rm S}) = 0$.

Several additional partial components vanish, although not enforced by Eq.(2.31). For example,

$$\begin{aligned}\Lambda^{xtx} &= \Lambda^{xty} = 0 \\ \Lambda^{ytx} &= \Lambda^{yty} = 0\end{aligned} \tag{2.33}$$

which imposes that the shift $\vec{d}$ must be parallel to the z axis. Finally,

$$\Lambda^{xxz} = \Lambda^{xyz} = \Lambda^{yxz} = \Lambda^{yyz} = 0\,. \tag{2.34}$$

Important to mention is that the shift of the dynamical map is restricted to having only a non-zero z-component. Thus the dynamical map is unital if $z_{\rm E}(0) = 0$. A dynamical map is unital if

$$\Lambda(t)\mathbb{1}_{\rm S} = \mathbb{1}_{\rm S}\,, \tag{2.35}$$

which requires $\vec{d} = \vec{0}$. These maps have the distinct property that they never increase the initial purity $(tr\rho_{\rm S}^2)$ of any state. When restricting to qubit dynamical maps, they can always be Kraus decomposed using unitary Kraus operators. That is the reduced dynamics generated by unital channels may be constructed by averaging over unitary

channels.

It is worth noting that for the 2-qubit model there is a connection between the free Hamiltonian and the magnitude of the shift. The magnitude of the shift is zero iff the state $\Omega_{\rm E} = \frac{1}{2}(\mathbb{1}_{\rm S} \otimes \rho_{\rm E}(0))$ and $H_{\rm free}$ are orthogonal operators i.e. $\mathrm{Tr}(\Omega_{\rm E} H_{\rm free})$=0. But as we see in the next section, there are special choices of Hamiltonian parameters that make the dynamical map unital independent of the choice of initial environment state.

2.4.2 Three-qubit model of dynamical symmetry breaking

The reduced dynamics for the three qubit model is computed from

$$\tilde{\Lambda}^{ab}(t,0) = \frac{1}{4} tr\left[\sigma_{\rm S}^{a} \otimes \mathbb{1}_{\rm E} \otimes \mathbb{1}_{\rm E'} \tilde{U}(t,0) \sigma_{\rm S}^{b} \otimes (\mathbb{1}_{\rm E} + z_{\rm E}(0) Z_{\rm E}) \otimes \rho_{\rm E'}(0) \tilde{U}^{\dagger}(t,0)\right] \tag{2.36}$$

where we assume that the second qubit is in an initial state compatible with phase covariance. For this reason we do not include initial correlations between subsystems E and E', although this is not necessary for the reduced dynamics to be CP.

For $t < \tau$, we claim that the dynamical map is phase covariant. Using the results of the previous section we find

$$\tilde{\Lambda}_{t<\tau}(t) = \begin{bmatrix} 1 & 0 & 0 & 0 \\ 0 & \cos^2 2\omega t & -\cos 2\omega t \sin 2\omega t & 0 \\ 0 & \cos 2\omega t \sin 2\omega t & \cos^2 2\omega t & 0 \\ z_{\rm E} \sin^2 2\omega t & 0 & 0 & \cos^2 2\omega t \end{bmatrix} \tag{2.37}$$

If we now focus on the unital action of $\tilde{\Lambda}_{t<\tau}$

$$\tilde{T}_{t<\tau}(t) = \begin{bmatrix} \cos 2\omega t & -\sin 2\omega t & 0 \\ \sin 2\omega t & \cos 2\omega t & 0 \\ 0 & 0 & 1 \end{bmatrix} \begin{bmatrix} \cos 2\omega t & 0 & 0 \\ 0 & \cos 2\omega t & 0 \\ 0 & 0 & \cos^2 2\omega t \end{bmatrix}, \tag{2.38}$$

it is evident that any rotation about the z-axis will commute with $\tilde{T}_{t<\tau}(t)$. Since the shift is left fixed by rotations about the z-axis, it follows that

$$\tilde{\Lambda}_{t<\tau}(t)[e^{-i\omega t Z_{\rm S}} \rho_{\rm S} e^{i\omega t Z_{\rm S}}] = e^{-i\omega t Z_{\rm S}} [\tilde{\Lambda}_{t<\tau}(t) \rho_{\rm S}] e^{i\omega t Z_{\rm S}}, \tag{2.39}$$

i.e. the reduced dynamics is phase covariant as it has a time-translation symmetry generated by $\omega Z_{\rm S}$. The phase-covariant map presented here is known as the generalized

amplitude damping channel, which appears in quantum information to describe dissipative processes [42].

For $t \geq \tau$, where we introduce the phase covariance breaking into the interaction, the dynamical map is found to be

$$\tilde{\Lambda}_{t\geq\tau}(t) = \begin{bmatrix} 1 & 0 & 0 & 0 \\ \tilde{d}_x(t) & 0 & 0 & 0 \\ \tilde{d}_y(t) & 0 & 0 & 0 \\ \tilde{d}_z(t) & 0 & 0 & 0 \end{bmatrix}, \tag{2.40}$$

where

$$\begin{aligned}
\tilde{d}_x(t) &= \frac{z_{\mathrm{E}} x_{\mathrm{E}'}}{\sqrt{2}} \Bigg[\Big(g_+ g_- - \Re[b_- g_+] - \Im[g_- h_-] + \Re[a_+]\Re[h_-] - \Re[b_-]\Im[h_-] \Big) \\
&\quad + \Big(g_+ g_- - \Im[g_+ h_+ + g_- h_-] + \Re[h_+ h_-] \Big) \cos 4\omega\tau \\
&\quad + \Big(\Im[h_+ h_-] - \Re[g_+ h_+ + g_- h_-] \Big) \sin 4\omega\tau \Bigg] \\
\tilde{d}_y(t) &= \frac{z_{\mathrm{E}} x_{\mathrm{E}'}}{\sqrt{2}} \Bigg[\Big(\Re[g_- h_-] - \Re[a_+ g_+] + \Re[b_-]\Re[h_-] + \Re[a_+]\Im[h_-] \Big) \\
&\quad + \Big(\Re[g_+ h_+] + \Re[g_- h_-] + \Im[h_+ \bar{h}_-] \Big) \cos 4\omega\tau \\
&\quad + \Big(- g_+ g_- + \Im[g_+ \bar{h}_+] + \Im[g_- h_-] + \Re[h_+ h_-] \Big) \sin 4\omega\tau \Bigg] \\
\tilde{d}_z(t) &= \frac{z_{\mathrm{E}}}{2} \Bigg[\Big(|a_+|^2 - |b_-|^2 + g_-^2 + 2\Im[g_+ h_-] \Big) + \Big(g_-^2 - |h_+|^2 - 2\Im[g_+ h_-] \Big) \cos 4\omega\tau \\
&\quad + 2 \Big(\Re[g_- h_+] - \Re[h_-]\Im[h_-] \Big) \sin 4\omega\tau \Bigg]
\end{aligned} \tag{2.41}$$

and $a_\pm$, $b_\pm$, $g_\pm$, and $h_\pm$ are defined in Eq.(2.21), and are all evaluated at $t - \tau$. The dynamical map after phase covariance breaking is a time-dependent SWAP operation, mapping all initial states to $\vec{\tilde{d}}(t)$. The transition of the reduced dynamics is continuous iff $\tau = \frac{\pi}{2\omega}(n + \frac{1}{2})$ for some positive integer n; i.e. only if τ coincides with a time when $\Lambda_{t<\tau}$ is non-invertible. If τ is not finely tuned, the image of $\Lambda_{t<\tau}(\tau)$ will suddenly collapse to the point $\vec{\tilde{d}}(\tau) = z_{\mathrm{E}}(0)\hat{z}$.

2.5 Features of the reduced dynamics

This section reviews important non-unitary features of the dynamical map families that we have found in the previous section. We begin with a look at the invertibility of the dynamical maps, as this determines the structure of possible master equations used to generate the reduced dynamics. We also look at the classes of dynamical maps for the 2-qubit model, which we characterize by their degree of symmetry.

2.5.1 Invertibility

Of paramount interest is the invertibility structure, which determines when time-local master equations are viable for use as generators. In the case of the 3-qubit example it is clear that the map is always non-invertible as $\tilde{T}_{t\geq\tau}(t) = 0$.

But the invertibility of the dynamical map for the two-qubit is non-trivial, and we show in this section how it depends on the Hamiltonian and the state of the environment. We find that there are in fact three independent ingredients that play a role in defining the invertibility: the strength of the system/environment coupling, the ratio between eigenenergies, and the initial environment state. The fact that these are distinct criteria is seen from the special row structure of Λ

$$\mathrm{Det}\,\Lambda(\tau) = \mathrm{Det}\,\vec{\vec{T}}(\tau) = |\vec{T}_z(\tau)|^2 \tag{2.42}$$

where $\vec{T}_z$ is the third row of $\vec{\vec{T}}$. This now leads to three conditions that determine when the dynamical map is non-invertible as we have

$$\mathrm{Det}\,\Lambda(\tau) = 0 \Leftrightarrow \vec{T}_z(\tau) = \vec{0}\,. \tag{2.43}$$

Starting with the z-component, $\Lambda^{zz}(\tau) = 0$ implies

$$\sin^2\phi_+ \sin^2(\omega_+\tau) + \sin^2\phi_- \sin^2(\omega_-\tau) = 1\,. \tag{2.44}$$

Eq.(2.44) may only be satisfied at a discrete set of times, and only if $\sin^2\phi_+ + \sin^2\phi_- \geq 1$. The set of $\phi_\pm$ that satisfy this condition constitute the strong coupling regime of parameter space. Figure 2.1 shows that this region of parameter space partially overlaps with the space where $U(t)$ is a perfect entangler.

However, strong coupling between system and environment is not a sufficient for the map to be non-invertible. Eq.(2.44) also depends on the energy eigenvalues. For example

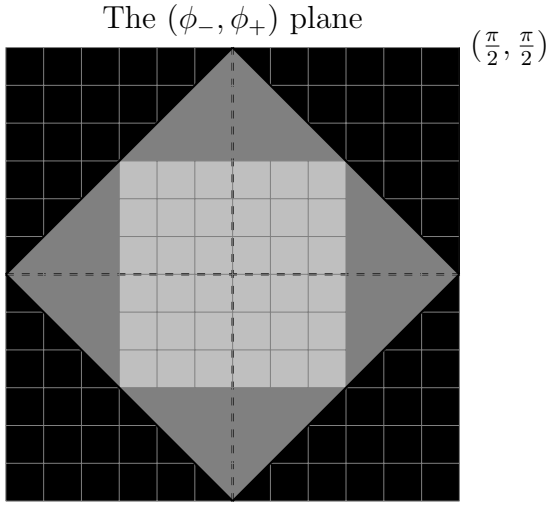

Figure 2.1: The (ϕ_+, ϕ_-) plane split into regions based on the non-local properties of the dynamics. The light gray region contains Hamiltonians that are not perfect entanglers, whereas the other regions (black+dark grey) are perfect entanglers. The entire gray region supports time local dynamics. The black region is the strong coupling region and contains the only Hamiltonians that may have $\mathrm{Det}\Lambda = 0$.

consider the boundary between the dark gray and black regions of Figure 2.1 where $\sin^2\phi_+ + \sin^2\phi_- = 1$ (excluding the corners where either $\phi_+ = 0$ or $\phi_- = 0$). In this region Eq.(2.44) is satisfied iff,

$$\sin^2\omega_+\tau = \sin^2\omega_-\tau = 1\,. \tag{2.45}$$

In order for this to be possible integers k and l must exist such that,

$$\frac{\omega_+}{\omega_-} = \frac{2k+1}{2l+1}\,. \tag{2.46}$$

Defining ν such that $\omega_+ = (2k+1)\nu$ and $\omega_- = (2l+1)\nu$; for any positive integer n a non-invertiblity can appear in the reduced dynamics at times given by,

$$\tau_n = \frac{(2n+1)\pi}{2\nu}\,. \tag{2.47}$$

So on this boundary only Hamiltonians with commensurate eigenenergies require time-non-local dynamics (although incommensurate Hamiltonians on the boundary can generate dynamical maps with small determinant). On the other hand, away from the boundary, farther into the blue region, most frequency pairs will generate dynamics with non-time-locality for some initial environment states.

So far, we have considered only one of the conditions for non-invertibility, $\Lambda^{zz}(\tau) = 0$, which imposes conditions on the Hamiltonian that must be satisfied for the map to be non-invertible. However, constraining the Hamiltonian to be in the strong-coupling regime is not sufficient: the initial environment state also plays a role. The class of initial states of the environment that lead to non-time-local dynamics is found by setting the remaining components of $\vec{T}_z(\tau)$ to zero,

$$\begin{aligned} \Lambda^{zx}(\tau) &= \Lambda^{zxx}(\tau)x_E + \Lambda^{zxy}(\tau)y_E = 0\,, \\ \Lambda^{zy}(\tau) &= \Lambda^{zyx}(\tau)x_E + \Lambda^{zyy}(\tau)y_E = 0\,. \end{aligned} \tag{2.48}$$

We can characterize the set of initial states for which non-invertibility will occur by finding the vector $\vec{\eta}(\tau)$ in the xy plane associated to the environment qubit state for which both

$$V(\tau_i)\vec{\eta}(\tau) = \begin{bmatrix} \Lambda^{zxx}(\tau) & \Lambda^{zxy}(\tau) \\ \Lambda^{zyx}(\tau) & \Lambda^{zyy}(\tau) \end{bmatrix} \vec{\eta}(\tau) = 0 \tag{2.49}$$

and $\mathrm{Det}\, V(\tau) = 0$ at some fixed τ. The solution is

$$\vec{\eta}(\tau) = \Lambda^{zyy}(\tau)\hat{x} - \Lambda^{zyx}(\tau)\hat{y}\,, \tag{2.50}$$

and the orthogonal direction is

$$\vec{\eta}^{\perp}(\tau) = \Lambda^{zxx}(\tau)\hat{x} + \Lambda^{zxy}(\tau)\hat{y}\,. \tag{2.51}$$

A non-invertibility at time τ can be removed by shifting the initial state to contain a component in the direction $\vec{\eta}^{\perp}(\tau)$. Furthermore, there can only be a discrete set of times, $\tau_i < T$, where the condition $\Lambda^{zz}(\tau_i) = 0$ can be satisfied. Assume there are N non-invertible times,

$$0 < \tau_1 < ... < \tau_{\mathrm{N}} < T, \tag{2.52}$$

with the associated initial environment states that preserve the non-invertibility $\{\hat{\eta}_1, ..., \hat{\eta}_N\}$. Single out $\hat{\eta}_1$ and note that so long as $\hat{\eta}_1^{\perp} \cdot \hat{\eta}_k^{\perp} \neq 0$, then the non-invertibility at τ_k is eliminated by the presence of $\hat{\eta}_1^{\perp}$ in $\vec{r}_{\mathrm{E}}(0)$. The remaining directions all must satisfy $\hat{\eta}_1^{\perp} \cdot \hat{\eta}_k^{\perp} = 0$. Since these initial environment states lie in a two dimensional space, all the remaining $\hat{\eta}_i^{\perp}$ must equal $\hat{\eta}_1$. The question of removing all non-invertibilities up to T is then equivalent to finding a θ such that,

$$\eta_i^{\perp} \cdot (\cos\theta\hat{\eta}_1^{\perp} + \sin\theta\hat{\eta}_1) \neq 0, \tag{2.53}$$

for all $i \in \{1, N\}$.

We have demonstrated that certain off diagonal components (coherences) of the initial environment state in the eigenbasis of the free environment Hamiltonian ($H_{\mathrm{E;free}}$) control the appearance of time-non-locality in the reduced dynamics. In Section 2.6 we use this knowledge of the time-local environment states in order to construct exact non-local master equations as well as approximate time-local master equations.

2.5.2 Dynamical map families

We saw above how the invertibility of the dynamical map can be dramatically changed by symmetry breaking during the dynamics. On the other hand, for the time-independent Hamiltonian, non-invertibility only occured in a subset of the parameter space. In this section we classify all the dynamics possible with the Hamiltonian in Eq.(2.5). This classification illustrates the relationship between symmetry, non-invertibility, and two other key properties of open system dynamics: non-Markovianity and unitality.

Table 2.1 lists the various dynamical map families contained in this model, together with each family's characteristics that we derive below. The largest family is the non-commensurate family ($\mathcal{N}$), with two independent frequencies. If we consider the time evolution in the Bloch ball, the trajectories generated are dense for any initial state $\vec{r}_{\mathrm{S}}(0)$. As mentioned previously, we use the (AB) frame to discuss the symmetries as they are simplest in this frame. For example the symmetries present in the entire family of Hamiltonians are $Z_{\mathrm{A}} \otimes \mathbb{1}_{\mathrm{B}}$ and $\mathbb{1}_{\mathrm{A}} \otimes Z_{\mathrm{B}}$. Of course these are equivalent to H and P_{zz}, however we find that this frame compresses the discussion of Hamiltonian families that have additional symmetries beyond these two.

The Hamiltonians which generate the family $\mathcal{D}$ have more symmetries than those corresponding to $\mathcal{N}$; these Hamiltonians commute with all rotations performed in the B subsystem. The apparent symmetry between A and B in Eq.(2.12) is broken by the relationship to the S/E frame. The presence of more symmetries simplifies the time-dependence of the dynamical map, thus less complicated trajectories are generated and the non-Markovian measures are periodic. The witnesses of non-Markovianity become periodic even in the case that the eigenfrequencies of the Hamiltonian are commensurate ($\mathcal{C}$). $\Lambda \in \mathcal{D}$ are not structurally different than those in $\mathcal{N}$ i.e. no additional components or partial components vanish. $\mathcal{D}$ does not have conserved quantities at the level of reduced dynamics.

There are special subfamilies of $\mathcal{D}$ that support conserved quantities at the level of reduced dynamics. These families $\mathcal{D}_{\pm}$ contain dynamical maps that are phase damping

channels, which are unital channel with the additional condition that $\lambda_x = 1$ and $\lambda_y = \lambda_z = \lambda$. They are generated from the Hamiltonians with parameters such that $\phi_+ = \pm\phi_-$. These families are simple to study and allow us to easily determine the set of initial environment states that yield invertible dynamics. For example in the family $\mathcal{D}_+$, there is only 1 distinct direction $\vec{\eta}(\tau)$ that allows non-invertibility namely $\vec{\eta} = \hat{y}$.

Restricting further the allowed set of initial environment states uncovers a set of Markovian families $\mathcal{M}_\pm$. These families contain the maps in $\mathcal{D}_\pm$ generated using $\vec{r}_{\mathrm{E}}(0) = \hat{x}$ $(\mathcal{M}_+)$ and $\vec{r}_{\mathrm{E}}(0) = \hat{y}$ $(\mathcal{M}_-)$. This is simply explained by looking at the Kraus decomposition of these channels. To illustrate this take an element of $\mathcal{D}_+$. The minimal Kraus decomposition has the form

$$\Lambda_+\rho_{\mathrm{S}} = \frac{1+x_{\mathrm{E}}}{2}U_+\rho_{\mathrm{S}}U_+^\dagger + \frac{1-x_{\mathrm{E}}}{2}(Z_{\mathrm{S}}U_+Z_{\mathrm{S}})\rho_{\mathrm{S}}(Z_{\mathrm{S}}U_+^\dagger Z_{\mathrm{S}}) \tag{2.54}$$

thus when the initial environment state is pure and in the x-direction the channel becomes unitary. We say the dynamics is Markovian as the dynamical map is unitary and thus generated by a time-dependent Lindblad equation with non-negative rates. Note that unitary reduced dynamics is the only kind of Markovian dynamics possible, since the environment Hilbert space is of finite dimension, so necessarily has a free Hamiltonian that is bounded from below [8]. As in all Markovian open systems, the initial environment state remains fixed under the time evolution in $\mathcal{M}_\pm$.

So far we have not mentioned the family of maps that are phase covariant i.e. the generalized amplitude damping channels $\mathcal{A}_\pm$, often referred to by the acronym GADC. These families do not neatly fit within the previous families, but instead have non-zero overlap with $\mathcal{N}$, $\mathcal{C}$, and $\mathcal{D}$. These maps have singular values satisfying $\lambda_z = \lambda_x^2 = \lambda_y^2$, and are non-unital with the only non-zero component given by $d_z = z_{\mathrm{E}}(1-\lambda_z)$. For $z_{\mathrm{E}} = 1$ the maps are simply known as amplitude damping channels. These maps are generated when either $\Delta_- = \kappa_+ = 0$ $(\mathcal{A}_+)$ or $\Delta_+ = \kappa_- = 0$ $(\mathcal{A}_-)$ and $\vec{r}_{\mathrm{E}}(0) = z_{\mathrm{E}}(0)\hat{z}$.

It is worth noting that the families $\mathcal{D}_\pm, \mathcal{A}_\pm$,and $\mathcal{M}_\pm$ consist entirely of extreme channels; i.e. channels that live in the boundary of the set of qubit channels [6]. The extreme channels form a tetrahedron, and consist of minimal rank Kraus operators, where maps on the interior have non-minimal Kraus rank. The families $\mathcal{M}_\pm$ are contained in the corner representing the trivial channel. The families $\mathcal{D}_\pm$ live on an edge connected to the trivial channel. And the families $\mathcal{A}_\pm$ live on a face of the tetrahedron.

The method we devise later for constructing effective master equations relies on there being a set of fundamental time scales that can be used to determine all non-invertible

Dynamical Map Families			
Family	Time Evolution	Extra Symmetries	Unital
Non-Commensurate ($\mathcal{N}$) $\omega_+ \neq q\omega_-$	Aperiodic Non-Markovian	None	If $z_{\mathrm{E}}(0) = 0$
Commensurate ($\mathcal{C}$) $\omega_+ = q\omega_-$	Periodic Non-Markovian	None	If $z_{\mathrm{E}}(0) = 0$
Degenerate ($\mathcal{D}$) $\omega_+ = \omega_-$	Periodic Non-Markovian	$\{\mathbb{1}_{\mathrm{A}} \otimes X_{\mathrm{B}}, \mathbb{1}_{\mathrm{A}} \otimes Y_{\mathrm{B}}\}$	If $z_{\mathrm{E}}(0) = 0$
Phase Damping($\mathcal{D}_\pm$) $\phi_+ = \pm\phi_-$	Periodic Non-Markovian	$\{\mathbb{1}_{\mathrm{A}} \otimes X_{\mathrm{B}}, \mathbb{1}_{\mathrm{A}} \otimes Y_{\mathrm{B}}\}$	Any $\vec{r}_{\mathrm{E}}(0)$
Markovian ($\mathcal{M}_\pm$) $\vec{r}_{\mathrm{E}}(0) = \hat{x}(+)$ or $\hat{y}(-)$	Markovian	$\{\mathbb{1}_{\mathrm{A}} \otimes X_{\mathrm{B}}, \mathbb{1}_{\mathrm{A}} \otimes Y_{\mathrm{B}}\}$	Always
Amplitude Damping ($\mathcal{A}_\pm$)	Aperiodic NM ($\mathcal{A}_\pm \cap \mathcal{N}$) Periodic NM ($\mathcal{A}_\pm \cap \mathcal{D}$)	None $\{\mathbb{1}_{\mathrm{A}} \otimes X_{\mathrm{B}}, \mathbb{1}_{\mathrm{A}} \otimes Y_{\mathrm{B}}\}$	If $z_{\mathrm{E}}(0) = 0$

Table 2.1: Here various dynamical map families are defined for the 2-qubit model. They are distinguished by the Hamiltonian parameters and initial environment state used in their generation.

times of the reduced dynamics. Such a task is especially simple for the families $\mathcal{D}_\pm$ and $\mathcal{A}_\pm \cap \mathcal{D}$, where only one such time scale exists. But for the set of Hamiltonians where the parameters are not carefully chosen ($\mathcal{N}$), such a construction is unfavorable as the non-invertible times behave as essentially random.

2.5.3 Entanglement generation and non-Markovianity

For the range of parameters possible in the two-qubit Hamiltonian, we can characterize the flow of information between system and environment by examining the non-Markovianty and the degree to which the system and environment can become entangled.

The parameters required for the time-evolution to be (periodically) perfectly entangling can be found using the criteria of Makhlin [57, 58], that the convex hull of the eigenvalues of the matrix $m(U) = (Q^\dagger U Q)^{\mathrm{T}} Q^\dagger U Q$ contains zero, where Q is the operator that changes to the Bell basis. Evaluating the eigenvalues of $m(U)$, the convex hull condition becomes (see details in Appendix A.1)

$$\cos^2\varphi\beta_+^2(t) + \sin^2\varphi\beta_-^2(t) = \frac{1}{2}\,, \tag{2.55}$$

where $\varphi \in [0, 2\pi)$ parameterizes the remaining convex combinations. This can be satisfied

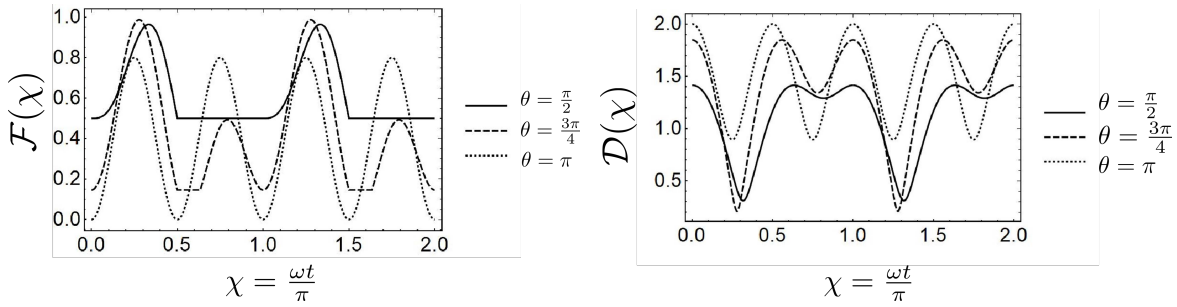

Figure 2.2: The fidelity and trace distance between time evolved reduced states using the initial conditions $\vec{r}_1(0) = \hat{x}$ and $\vec{r}_2(0) = \cos\theta\hat{x} + \sin\theta\hat{y}$ are plotted. The parameters used are $\omega = \omega_+ = \omega_- = \frac{\sqrt{5}}{2}$, $\tan\phi_+ = \tan\phi_- = 2$, and $\vec{r}_{\rm E}(0) = \vec{0}$. The non-Markovian nature of the reduced dynamics is evident from the oscillations of $\mathcal{D}$ and $\mathcal{F}$.

iff the largest of $\beta_+^2(t)$ and $\beta_-^2(t)$ is greater than or equal to $\frac{1}{2}$, which will hold at some times as long as $\text{Max}(\phi_+, \phi_-) \geq \frac{\pi}{4}$. This condition on the parameter space of the Hamiltonian is shown in Figure 2.1, compared with other conditions we derive below related to properties of the reduced dynamics.

For nearly all parameter values in the Hamiltonian, Eq.(2.7), and initial states, the dynamical map is non-Markovian. This is expected since the system and environment are the same (small) size. The non-Markovianity is diagnosed by information back-flow into the system from the environment [59], with standard indicators being non-monotonicity in the evolution of trace distance and fidelity. For any two states on the reduced system, $\vec{r}_1(t)$ and $\vec{r}_2(t)$, the trace distance ($\mathcal{D}$) and fidelity ($\mathcal{F}$) are [60],

$$\begin{aligned} 2\mathcal{D}(\vec{r}_1(t), \vec{r}_2(t)) &= ||\vec{r}_1(t) - \vec{r}_2(t)|| \\ 2\mathcal{F}(\vec{r}_1(t), \vec{r}_2(t)) &= 1 + \vec{r}_1(t)\cdot\vec{r}_2(t) + \sqrt{(1 - r_1^2(t))(1 - r_2^2(t))}\,. \end{aligned} \tag{2.56}$$

Generically these measures are oscillatory, and aperiodic unless $\omega_+ = q\omega_-$ for some $q \in \mathbb{Q}$.

The degenerate family, Eq.(2.13), always has periodic measures of non-Markovianity and is a useful case to look at in more detail. Figure 2.2 shows the trace distance and fidelity in the degenerate family, demonstrating the non-Markovian character of the reduced dynamics. The dimensionless parameter $\chi = \frac{\omega t}{\pi}$ ($\omega = \omega_+ = \omega_-$) is used to construct these plots, and the environment memory time-scale can be read off as $\tau_{\rm NM} \sim \mathcal{O}(\frac{\pi}{2\omega})$.

Figure 2.2 is generated with $\phi_+ = \phi_-$ allowing for interesting features to appear in $\mathcal{F}$. If $\phi_\pm$ are perturbed so that $\phi_+ \neq \phi_-$, these interesting features also vanish. First note the plateaus, which indicate there is a unitary phase (i.e. $\mathcal{F}$=constant) if we further require

that $\vec{r}_{\rm E}(0) = \hat{x}$. Additionally, preceding the plateaus are discontinuities in $\dot{\mathcal{F}}$. In some other finite open systems, such discontinuities indicate dynamical phase transitions [61].

Non-Markovianity of the dynamics has been equated to the indivisibility of the dynamical map into channels (CPTP maps) [59], however the actual relationship is more complicated as non-Markovian dynamical maps can be CP divisible [9–11]. To study the divisibility of the dynamical map one looks at the interweaving maps (Φ), defined using two times $\tau_2 > \tau_1 \geq 0$,

$$\Lambda(\tau_2) = \Phi(\tau_2, \tau_1)\Lambda(\tau_1)\,. \tag{2.57}$$

For invertible reduced dynamics the interweaving map is computed as $\Phi(\tau_2, \tau_1) = \Lambda(\tau_2)\Lambda^{-1}(\tau_1)$, although Φ may still be defined even when Λ^{-1} does not exist [10].

The degree of positivity of $\Phi(\tau_2, \tau_1)$ determines the divisibility class of the map $\Lambda(\tau_2)$, as $\Lambda(\tau_1)$ is completely positive by construction. It is important to note that divisibility is meant in a holistic sense i.e. the reduced dynamics is considered CP divisible up to time τ_2 only if $\Phi(\tau_2, \tau_1)$ is completely positive for all $\tau_1 < \tau_2$. A qubit channel is (infinitesimally) P-divisible if $\mathrm{Det}\Lambda(t) \geq 0$ for all $t \geq 0$ [8]. We have shown this to be true for the 2-qubit family studied. So the dynamical maps presented here may be arbitrarily split into positive maps, each made close to the identity channel.

The question of CP divisibility is in general more subtle. For qubit dynamical maps of full rank, these maps are CP divisible if $s_1 s_2 s_3 > 0$, where s_i are the singular values of the Lorentz normal form of the channel [11]. For unital channels, this is equivalent to requiring $\mathrm{Det}\Lambda(t) > 0$. We are able to find many examples of such maps. Take $\Lambda(t) \in \mathcal{N}$ and $z_{\rm E}(0) = 0$. As long as the initial environment state is not pure, $\Lambda(t)$ will be a full Kraus rank unital channel. Therefore it will be CP divisible iff it is invertible. Of course these maps generate oscillation in non-Markovian measures, so do not constitute Markovian reduced dynamics. In Appendix A.2, we study the CP divisibility of deficient Kraus rank maps in $\mathcal{D}_+$. We find that even when these maps are invertible, there typically exist time intervals s.t. for $\tau \in [\tau_a, \tau_b]$ the map $\Phi(\tau_2, \tau)$ fails to be CP.

2.6 Master equations

We present the standard master equations that can be associated to any $\Lambda(t, 0)$, both local and non-local in time. We find that by changing $\vec{r}_{\rm E}(0)$, different partitions of the singularity between non-local and local terms can be achieved. We show that we can capture some non-unitarity features of the reduced dynamics just using the local term.

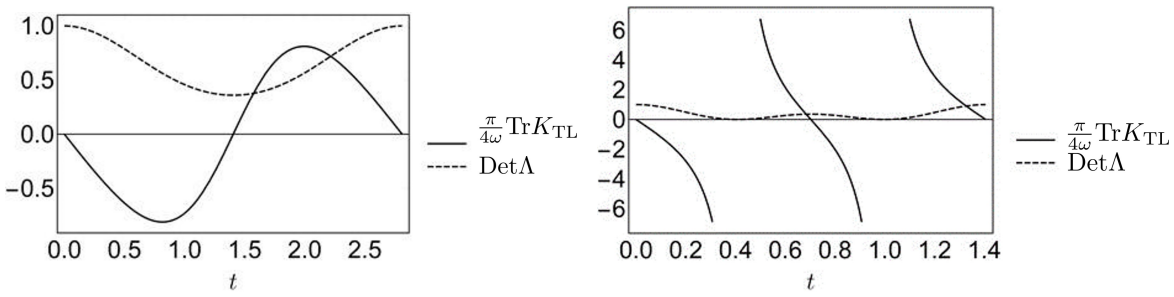

Figure 2.3: $\mathrm{Tr}K_{\mathrm{TL}}$ (scaled by $\frac{\pi}{4\omega}$) and $\mathrm{Det}\Lambda$ are plotted with $\vec{r}_{\mathrm{E}}(0) = \vec{0}$. a) Uses parameters $\omega = \omega_+ = \omega_- = \frac{\sqrt{17}}{4}$ and $\tan\phi_+ = \tan\phi_- = \frac{1}{2}$; the dynamics is invertible with $\mathrm{Det}\Lambda$ separated from zero. b) Uses parameters $\omega = \omega_+ = \omega_- = \sqrt{5}$ and $\tan\phi_+ = \tan\phi_- = 4$; $\mathrm{Det}\Lambda$=0 has solutions, where the dynamical map becomes a projection onto the $\hat{Q}_1(\tau)$ direction in the Bloch ball.

2.6.1 Standard master equations

The dynamical map can be used to construct the time-local, although possibly singular, generator for the master equation

$$\partial_t \rho_S(t) = K_{\mathrm{TL}}(t)\rho_S(t) = \dot{\Lambda}(t)\Lambda^{-1}(t)\rho_S(t)\,. \tag{2.58}$$

Since the inverse dynamical map is

$$\Lambda^{-1}(t) = \frac{1}{T_z^2}\begin{bmatrix} T_z^2 & 0 & 0 & 0 \\ -d_z\vec{T}_z & \vec{T}_y\times\vec{T}_z & \vec{T}_z\times\vec{T}_x & \vec{T}_z \end{bmatrix}, \tag{2.59}$$

the time-local generator is expressed in terms of the dynamical map components as

$$K_{\mathrm{TL}}(t) = \frac{1}{T_z^2}\begin{bmatrix} 0 & 0 & 0 & 0 \\ -d_z(\dot{\vec{T}}_x\cdot\vec{T}_z) & \dot{\vec{T}}_x\cdot(\vec{T}_y\times\vec{T}_z) & \dot{\vec{T}}_x\cdot(\vec{T}_z\times\vec{T}_x) & \dot{\vec{T}}_x\cdot(\vec{T}_z) \\ -d_z(\dot{\vec{T}}_y\cdot\vec{T}_z) & \dot{\vec{T}}_y\cdot(\vec{T}_y\times\vec{T}_z) & \dot{\vec{T}}_y\cdot(\vec{T}_z\times\vec{T}_x) & \dot{\vec{T}}_y\cdot(\vec{T}_z) \\ -d_z(\dot{\vec{T}}_z\cdot\vec{T}_z) & \dot{\vec{T}}_z\cdot(\vec{T}_y\times\vec{T}_z) & \dot{\vec{T}}_z\cdot(\vec{T}_z\times\vec{T}_x) & \dot{\vec{T}}_z\cdot(\vec{T}_z) \end{bmatrix}. \tag{2.60}$$

Fig (2.3) contains plots of $\mathrm{Det}\Lambda$ and $\mathrm{Tr}K_{\mathrm{TL}}$ using $\Lambda(t) \in \mathcal{D}_+$, which demonstrate that singularities in K_{TL} occur where $\mathrm{Det}\Lambda = 0$.

The generator K_{TL} can be put into Lindblad form,

$$\partial_t\rho_S(t) = -i[(\vec{H}_{\mathrm{eff}}(t)\cdot\vec{\sigma}_{\mathrm{S}}),\rho_{\mathrm{S}}(t)] + \sum_{i=1}^{3}\sum_{j=1}^{3}\gamma_{ij}(t)(\sigma_{\mathrm{S}}^j\rho_{\mathrm{S}}(t)\sigma_{\mathrm{S}}^i - \frac{1}{2}\{\sigma_{\mathrm{S}}^i\sigma_{\mathrm{S}}^j,\rho_{\mathrm{S}}(t)\})\,, \tag{2.61}$$

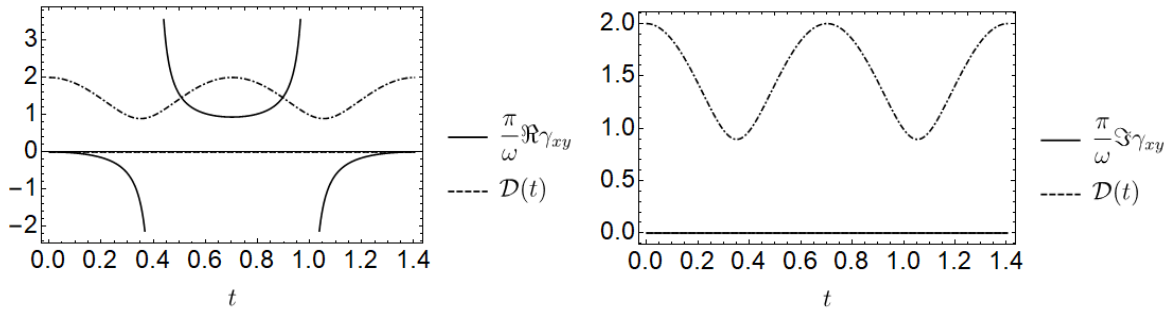

Figure 2.4: Plotted are the real and imaginary parts of the off diagonal Lindblad coefficients. Plots are generated using the parameters $\omega_+ = \omega_- = \frac{\sqrt{5}}{2}$ and $\tan\phi_+ = \tan\phi_- = 2$. Included in the plots is the trace distance evaluated using the same parameters and initial states $\vec{r}_1(0) = -\vec{r}_2(0) = \hat{x}$. We include the trace distance to demonstrate that experimentally accessible quantum information measures can constrain the parameters that appear in effective master equations; in this case oscillation frequencies of the Lindblad coefficients.

where $\vec{H}_{\text{eff}}(t) = \omega_{\text{S}}\hat{z} + \vec{H}_{\text{open}}(t)$ generates unitary evolution on $\mathcal{Q}_{\text{S}}$ with a contribution from internal parameters and a portion that knows about the environment and interaction, $\vec{H}_{\text{open}}(t)$. The coefficients $\gamma_{ij}(t)$ are the Lindblad coefficients which generate the non-unitarity that appears in the reduced dynamics.

Obtaining the Lindblad form of the master equation amounts to a change of basis, for example the effective Hamiltonian has components

$$H^i_{\text{eff}}(t) = \frac{1}{2}\epsilon^{ijk}K_{jk}(t)\,, \tag{2.62}$$

and similar expression exist for the $\gamma_{ij}(t)$, though we do not include them here. Figure 2.4 shows how we can use the quantities such as the $\mathcal{D}(t)$ to determine the oscillation timescales that appear in the Lindblad coefficients, which is useful to set a scale for environment memory timescales that will inevitably appear in effective master equations.

In the strong coupling region where the time-local description has singular behavior, we instead use an integral master equation known as the Nakajima-Zwanzig equation. The Hamiltonian being time independent allows the NZ generator to take the form $K_{NZ}(t,\tau) = K_{NZ}(t-\tau)$. Thus the NZ equation is a convolution,

$$\partial_t\rho_{\text{S}}(t) = \int_0^t K_{\text{NZ}}(t-\tau)\rho_{\text{S}}(\tau)d\tau\,. \tag{2.63}$$

The convolution kernel may be obtained from the dynamical map using the Laplace

transform of the dynamical map $\Phi(s)$ (as in [62]),

$$\tilde{K}_{\rm NZ}(s) = s\mathbb{1}_4 - \Phi^{-1}(s) \tag{2.64}$$

The form of the functions $\alpha_\pm(t)$ and $\beta_\pm(t)$ restrict the dynamical map components to having few Fourier components. That is each Λ^{ab} has a Fourier decomposition of the form,

$$\begin{aligned}\Lambda^{ab}(t) = C^{ab} &+ F_1^{ab}e^{-i2\omega_+ t} + F_2^{ab}e^{-i2\omega_- t} + F_3^{ab}e^{-i(\omega_+ + \omega_-)t} + F_4^{ab}e^{-i(\omega_+ - \omega_-)t} \\ &+ G_1^{ab}e^{i2\omega_+ t} + G_2^{ab}e^{i2\omega_- t} + G_3^{ab}e^{i(\omega_+ + \omega_-)t} + G_4^{ab}e^{i(\omega_+ - \omega_-)t}\end{aligned} . \tag{2.65}$$

If ab is even (odd) then the component Λ^{ab} involves only even (odd) time dependent functions. It is now simple to go to the frequency domain, where we can write the generic Laplace transformed components,

$$\begin{aligned}\Phi^{ab}(s) = \frac{C^{ab}}{s} &+ \frac{F_1^{ab}}{s + i2\omega_+} + \frac{F_2^{ab}}{s + i2\omega_-} + \frac{F_3^{ab}}{s + i(\omega_+ + \omega_-)} + \frac{F_4^{ab}}{s + i(\omega_+ - \omega_-)} \\ &+ \frac{G_1^{ab}}{s - i2\omega_+} + \frac{G_2^{ab}}{s - i2\omega_-} + \frac{G_3^{ab}}{s - i(\omega_+ + \omega_-)} + \frac{G_4^{ab}}{s - i(\omega_+ - \omega_-)}\end{aligned} . \tag{2.66}$$

In principle one can use these formulae to construct the exact non-time-local master equation associated to the reduced dynamics, although the expressions involved are cumbersome. Instead for what follows we devise a method to expand the NZ kernel,

$$K_{\rm NZ}(t-\tau) = \delta(t-\tau)K_{\rm TL}(t) + K_{\rm NTL}(t,\tau)\,. \tag{2.67}$$

Such an expansion is available for each time-local initial environment state ($\vec{r}_{\rm TL}$), where the relative importance of the time-local vs non-time-local component is controlled by the magnitude of $\vec{r}_{\rm TL} - \vec{r}_{\rm E}(0)$.

2.6.2 Effective master equation

An exact time local master equation without singularities exists as long as either of the following conditions are met

I The Hamiltonian parameters are in the weak coupling region, i.e. $\sin^2\phi_+ + \sin^2\phi_- < 1$.

II $\vec{r}_{\rm E}(0)$ has off diagonal elements in the eigenbasis of $H_{\rm E;free}$ along certain directions

described in Section IIIB.

However, when neither of the above holds only a non-local equation can capture the exact time evolution of the reduced state. Such a master equation can be found using reduced dynamics from the time-local region.

Consider the case where the Hamiltonian parameters are in the strong coupling region and $\vec{r}_{\rm E}(0) = \vec{r}_{\rm NTL}$, yielding non-invertibilities in the reduced dynamics. By choosing a shifted initial environment state ($\vec{r}_{\rm E}^{'}$), we can engineer the time local component of a non-time local master equation. By using the exact non-time local dynamical map we can also determine the corresponding non-time-local component for the master equation. As the non-time-local piece is linear in $\delta\vec{r} = \vec{r}_{\rm NTL} - \vec{r}_{\rm E}^{'}$, the choice of shifted initial state controls its relevance.

We can choose $\vec{r}_{\rm E}^{'}$ by considering states near to $\vec{r}_{\rm E}(0)$ that are shifted along the direction(s) $\eta^{\perp}$ as defined in Eq.(2.51). The time derivative of $\rho_{\rm S}(t;\vec{r}_{\rm NTL})$ may be expanded as,

$$\begin{aligned}\dot{\rho}_{\rm S}(t;\vec{r}_{\rm NTL}) &= \partial_t \rho_{\rm S}(t;\vec{r}_{\rm E}^{'} + \delta\vec{r}) = \partial_t \left[\Lambda(t;\vec{r}_{\rm E}^{'}) + (\Lambda(t;\delta\vec{r}) - \Lambda(t;\vec{0}))\right]\rho_{\rm S}(0) \\ &= K_{\rm TL}(t;\vec{r}_{\rm E}^{'})\rho_{\rm S}(t;\vec{r}_{\rm E}^{'}) + \delta\vec{r}\cdot\left[\frac{\partial\dot{\Lambda}(t;\delta\vec{r})}{\partial\delta\vec{r}}\right]\rho_{\rm S}(0) \\ &= K_{\rm TL}(t;\vec{r}_{\rm E}^{'})\rho_{\rm S}(t;\vec{r}_{\rm NTL}) + \delta\vec{r}\cdot\left[\frac{\partial\dot{\Lambda}(t;\delta\vec{r})}{\partial\delta\vec{r}} - K_{\rm TL}(t;\vec{r}_{\rm E}^{'})\frac{\partial\Lambda(t;\delta\vec{r})}{\partial\delta\vec{r}}\right]\rho_{\rm S}(0)\,.\end{aligned} \tag{2.68}$$

Note that since the dynamical map is linear in the initial environment state, we can replace $\frac{\partial\Lambda(t;\delta\vec{r})}{\partial\delta\vec{r}}$ in the above equation with $\frac{\partial\Lambda(t;\vec{r}_{\rm E}^{'})}{\partial\vec{r}_{\rm E}^{'}}$

$$\dot{\rho}_{\rm S}(t;\vec{r}_{\rm NTL}) = K_{\rm TL}(t;\vec{r}_{\rm E}^{'})\rho_{\rm S}(t;\vec{r}_{\rm NTL}) + \delta\vec{r}\cdot\left[\frac{\partial\dot{\Lambda}(t;\vec{r}_{\rm E}^{'})}{\partial\vec{r}_{\rm E}^{'}} - K_{\rm TL}(t;\vec{r}_{\rm E}^{'})\frac{\partial\Lambda(t;\vec{r}_{\rm E}^{'})}{\partial\vec{r}_{\rm E}^{'}}\right]\rho_{\rm S}(0)\,. \tag{2.69}$$

This can be further simplified noting that $\dot{\Lambda}(t;\vec{r}_{\rm E}^{'}) - K_{\rm TL}(t;\vec{r}_{\rm E}^{'})\Lambda(t;\vec{r}_{\rm E}^{'}) = 0$, yielding the final expression

$$\dot{\rho}_{\rm S}(t;\vec{r}_{\rm NTL}) = K_{\rm TL}(t;\vec{r}_{\rm E}^{'})\rho_{\rm S}(t;\vec{r}_{\rm NTL}) + \delta\vec{r}\cdot\left[\frac{\partial K_{\rm TL}(t;\vec{r}_{\rm E}^{'})}{\partial\vec{r}_{\rm E}^{'}}\Lambda(t;\vec{r}_{\rm E}^{'})\right]\rho_{\rm S}(0)\,. \tag{2.70}$$

We have now explicitly isolated a time-local component which is evaluated at the same Hamiltonian parameters as $\Lambda(t;\vec{r}_{\rm TNL})$, but uses the initial environment state $\vec{r}_{\rm E}^{'}$

instead of $\vec{r}_{\rm NTL}$. How large $\delta\vec{r}$ is compared with $\vec{r}_{\rm TNL}$ determines the maximum value of ${\rm Tr}K_{\rm TL}(t;\vec{r}_{\rm E}^{'})$, which in turn determines how relevant the integral term is in capturing the non-invertibility.

An effective time local description is obtained keeping only the zeroth order term,

$$\partial_t\rho_S(t;\vec{r}_{\rm NTL}) \approx K_{\rm TL}(t;\vec{r}_{\rm E}^{'})\rho_S(t;\vec{r}_{\rm NTL}) \tag{2.71}$$

Using this equation to generate the reduced dynamics is equivalent to exchanging the dynamical map $\Lambda(t,\vec{r}_{\rm NTL})$ for the dynamical map $\Lambda(t;\vec{r}_{\rm E}^{'})$, so obviously defines a completely positivity master equation.

2.7 Conclusions

For a two-qubit system with symmetry, we have classified how the non-Markovianity, unitality, and time non-locality depend on the system/environment Hamiltonian and the initial state of the environment. We also considered a three-qubit example with a time-dependent interaction that broke a dynamical symmetry.

The oscillatory character of the reduced dynamics demonstrates that there is a continuous flow of information flow back and forth between system and environment. For sufficiently symmetric Hamiltonians, special initial environment states exist that support Markovian reduced dynamics, where the information flow becomes one-way. While this is not surprising, it is a reminder that the assumption of a Markovian master equations is not consistent with typical interacting Hamiltonians. This is true in the cosmological context as well [24, 63].

In typical effective theories of open systems, then, we need some guidance for how to parameterize the possible non-Makovian behavior. In the qubit model, whether the flow of information between system and environment was periodic or aperiodic depended on the degree of symmetry present in the Hamiltonian. There was no reason to assume that any of the parameters in the Hamiltonian take related values (for example, commensurate frequencies in the system/environment free Hamiltonians). In some cosmological contexts, however, there are effects that connect parameter values. For example, in inflation all modes undergo a common squeezing driven by the background expansion. This squeezing can determine a significant part of the time-dependence in the dissipative coefficients $\gamma(t)$ [24], including the periodicity. The background expansion may suggest the appropriate scale to use in an effective open model.

A further wrinkle in open effective theories is that the master equations need not be local in time. Most constructions in cosmology restrict to time-local equations for simplicity [22,35,64] although work in the context of black holes has shown that non-time-local evolution can be required [41]. Our work here explores the conditions necessary for time-local dynamics in small qubit models. We find that even in the regions of parameter space with the largest degrees of symmetry, it can be necessary to use a time-non-local master equation. We make this determination based on the non-invertibility of the dynamical map, which depends both on the Hamiltonian and the initial environment state. Strong coupling is a necessary condition for non-invertibility, however so is a rather restricted set of initial environment states. Those states are defined largely by the dynamics of the free Hamiltonian for the environment. Diagonal initial environment states in the eigenbasis of $H_{\mathrm{E;free}}$ are the most non-local, as their dynamical maps are non-invertible in the presence of strong coupling.

In cosmology, the Hamiltonian is generically time-dependent, so it is not uncommon for the relevant (active) degrees of freedom and couplings to evolve over time. We used a 3-qubit model to investigate how such a time-dependence effects the nature of the dynamical map. We found that introducing a degree of freedom that does not respect the symmetry of the initial interaction drastically altered the reduced dynamics. The dynamical map became non-invertible at all times after the activation of the spectator qubit. This strongly suggests that the framework of open effective theories in cosmology should include a time-non-local component.

Chapter 3
Effective Dynamics via Quantum Channel Ensembles

3.1 Preamble

This chapter is a reprint of [65]. From the previous chapter we determined that in open quantum system, such as those encountered in quantum cosmology, any effective master equation should include a non-time-local component. This does not rule out the master equation approach, but it certainly makes it much more challenging. Therefore instead of focusing on effective master equations, in this chapter we develop a method to approximate the long-time dynamics of open systems using ensembles of quantum channels. In order to narrow our focus, we consider open systems that may be described by phase-covariant dynamical maps, although we expect that this is not too restrictive.

3.2 Introduction

Most of the quantum systems used for measurement and computation are open, rather than isolated, systems. We are frequently interested in understanding the dynamics of an ensemble of such systems, such as the set of evolutions of some quantum state under many trials of a noisy circuit [66, 67]. An ensemble of noisy circuits is an approximate description of some more complex, closed system, and more generally ensembles of open systems provide an alternative description of closed systems. In that case, the ensemble is generated by a partition of the closed system into a set of subsystems, with the evolution of each subsystem described by an open-systems equation. The set of sub-system evolutions is constrained by conservation laws and symmetries of the closed,

unitary evolution. One might in practice be primarily interested only in the evolution of some special subsystems, for example the computational qubits or the probe systems for a measurement task. For other questions, such as studying thermalization, it may be useful to define a typical or average open evolution together with the deviations from the average.

In this work, we derive and characterize ensembles of open-system qubit evolutions. We consider cases where either all members of the ensemble are phase-covariant dynamical maps [68, 69], or ensembles whose average map is phase covariant. Prior work on random ensembles of open-system dynamics has largely been restricted to evolution that is time-homogeneous, Markovian and unital [70–79]. Phase-covariant maps provide a well-characterized way to consider more complex open-system evolution with none those restrictions [56, 80, 81], making them appealing for phenomenological studies of thermalization, quantum homogenization, dephasing process, quantum metrology and quantum optics [80, 82–84]. For computational questions, they carry the advantages of non-unitality [67, 85, 86].

The most general phase-covariant qubit channel can be parameterized as

$$\Lambda_{\mathrm{PC}} = \begin{bmatrix} 1 & 0 & 0 & 0 \\ 0 & \lambda_1 \cos\theta & -\lambda_1 \sin\theta & 0 \\ 0 & \lambda_1 \sin\theta & \lambda_1 \cos\theta & 0 \\ \tau_3 & 0 & 0 & \lambda_3 \end{bmatrix}, \tag{3.1}$$

where λ_1, λ_3, θ, and τ_3 are all real numbers and complete positivity imposes some restrictions on the parameters, discussed below. The action of this class of channels includes translations and xy-symmetric deformations of the Bloch sphere that commute with rotations about the z-axis. Phase covariant maps provide agnostic noise models, since they describe a combination of pure dephasing with energy absorption and emission. An additional useful property of phase-covariant channels is that they need not have the maximally mixed state as a fixed point. That is, they need not be unital. The state that is invariant under the action of the phase-covariant map, Eq.(3.1), is $\rho_* = \frac{1}{2}\left(\mathbb{1} + \left(\frac{\tau_3}{1-\lambda_3}\right) Z\right)$, where Z is the Pauli matrix. This state is different from the maximally mixed state (the Gibbs state at infinite temperature) whenever $\tau_3 \neq 0$, but it is still diagonal and can be understood as a classical ensemble or Gibb's state with $\beta_* = \log\left[\frac{2}{1-a_*}\right] > 0$, where $a_* = \frac{\tau_3}{1-\lambda_3}$. This simple steady state is useful for studying thermalization beyond the Markovian regime [69].

Evolution under a phase-covariant dynamical map (a smooth, time-parameterized

sequence of phase-covariant channels) can be generated for a system with free Hamiltonian $H_{\rm S}$ by coupling it via an interaction term $H_{\rm SE}$ to an environment with free Hamiltonian $H_{\rm E}$ in initial state $\rho_{\rm S} \otimes \rho_{\rm E}$, with the restrictions

$$[H_{\rm S} + H_{\rm E}, H_{\rm SE}] = [H_{\rm E}, \rho_{\rm E}] = 0\,. \tag{3.2}$$

These relations imply that (i) no energy builds up within interactions and (ii) the initial environment state is a Gibbs state with respect to H_0, and plays the role of a classical reservoir in the case that the reduced dynamics is Markovian. But, these maps are generically non-Markovian, allowing much richer dynamics [87].

By choosing Hamiltonians for N coupled spins with initial states that obey the conditions above, we can construct ensembles of open-system evolution where each member of the ensemble is a phase-covariant map for a single spin degree of freedom. Except in special cases, the full set of maps is time-consuming to derive for large N. However, we can take a useful limit that effectively averages over the oscillatory behavior associated with the finite system size. We will find that in useful cases this average map provides a stationary channel that depends only on the initial state and the symmetries of the interaction terms in the Hamiltonian.

To construct these channels from example systems, we first average over the set of individual dynamical maps at fixed time t associated with the evolution of the ith subsystem, $\Lambda_i(t')$, and then take the limit of a long time-average:

$$\overline{\Lambda}_N^{\infty} \equiv \lim_{t\to\infty} \frac{1}{t} \int_0^t \left[\frac{1}{N} \sum_{i=1}^{N} \Lambda_i(t') \right] dt'\,. \tag{3.3}$$

In useful cases, the limit of the long-time and ensemble averaged map will be a time-independent channel. Furthermore, for disordered Hamiltonians, $\overline{\Lambda}_N(t)$ (and the map averaged over the N sub-systems at any time) may be phase-covariant even when individual maps are not. This is most directly seen by working with the distribution of map parameters, inherited from the Hamiltonian disorder, over the N sub-systems. Then $\overline{\Lambda}_N^{\infty}$ may again be a time-independent, phase-covariant channel. We will demonstrate these points with specific examples below.

In the rest of the paper, we establish a procedure for generating ensembles of phase-covariant maps with a long-time average that is time-independent and with fluctuations about the average that mimic those found in finite-size spin networks. We begin in Section 3.3 by constructing ensembles of maps for spin networks where every division into

sub-system and environment satisfies Eq.(3.2). That is, every map is phase-covariant and differences in the map come from the inhomogeneity of the initial state. We derive the $\overline{\Lambda}_N^\infty$ for those ensembles. In Section 3.4 we provide a perturbative calculation justifying the use of $\overline{\Lambda}_N^\infty$ as defined in Eq.(3.3) as a large-N limit for at least some kinds of systems. Next, in Section 3.5, we consider a case where different members of the ensemble may also have different dynamics, for example as generated by different values for couplings within the full, closed Hamiltonian. There we show how moving from a distribution over Hamiltonian parameters to a distribution over map parameters facilitates the construction of additional scenarios whose average dynamics are phase covariant. We put these pieces together in Section 3.6, and provide a prescription for generating ensembles of open-system evolution that we conjecture to be useful for studying the ensemble of subsystems of large-N, closed systems. We conclude in Section 3.7.

3.3 Phase-covariant ensembles from XXZ networks

In this section we consider several examples of XXZ spin-networks in external magnetic fields, which we use as benchmark examples of the phase-covariant ensembles. We are interested in extracting features that can be usefully generalized to a construction that can be carried out using only the parameters of the maps in Eq.(3.1), without reference to an explicit Hamiltonian, although we will see how properties of the Hamiltonian are recognizable in the maps. The phase-covariant restrictions on XXZ models have a simple late-time averaged behavior, described by single phase-covariant channel (since these channels are closed under convex linear combinations [88]). Besides characterizing this channel, we use these models to extract a typical scaling with N of how maps vary around the average, which can be used to inform more general probability distributions over map parameters.

To begin, the dynamical map associated to the i^{th} qubit in the network is defined as

$$\Lambda_i(t)[\rho_i(0)] = \text{tr}_{j\neq i}\left[e^{-iHt}\rho_i(0)\otimes\rho_{\text{E}_\text{i}}(0)e^{iHt}\right] \tag{3.4}$$

where H is the full Hamiltonian describing the network dynamics. Λ_i(t) depends on time, the Hamiltonian parameters, and the initial state of the remaining qubits. To obtain phase-covariant dynamical maps for a given qubit network, we must ensure the thermodynamic constraints from Eq.(3.2) are satisfied. Therefore, we choose initial global states that are totally uncorrelated and diagonal in the computational basis (as

appropriate for XXZ type Hamiltonians)

$$\rho(0) = \frac{1}{2^N} \bigotimes_{i=1}^{N} \left(\mathbb{1}_i + z_i Z_i \right). \tag{3.5}$$

The initial state must be totally uncorrelated so that for all possible choices of focal qubit the reduced dynamics is completely positive. Then, all maps are of the form Eq.(3.1) and satisfy the following inequalities [6]

$$\begin{aligned} |\lambda_{3,i}| + |\tau_{3,i}| &\leq 1 \\ 4\lambda_{1,i}^2 + \tau_{3,i}^2 &\leq (1 + \lambda_{3,i})^2 . \end{aligned} \tag{3.6}$$

3.3.1 XXZ-networks

In this section, we consider homogeneous XXZ-networks with two different topologies. The first has nearest-neighbor interactions and periodic boundary conditions (a ring), with Hamiltonian

$$H_{\mathrm{XXZ}}^{\mathrm{ring}} = h \sum_{i=1}^{N} Z_i + \frac{J_\perp}{2} \sum_{i=1}^{N} (X_i X_{i+1} + Y_i Y_{i+1}) + \frac{J_\parallel}{2} \sum_{i=1}^{N} Z_i Z_{i+1} . \tag{3.7}$$

Here X, Y, Z are the usual Pauli matrices and the qubit indices take integer values mod N. The coupling constants $J_\parallel$ and $J_\perp$ determine the class of the model. For $J_\perp = 0$, H_{XXZ} reduces to the (anti)-ferromagnetic Ising model with $J_\parallel < 0$ ($J_\parallel > 0$). When $J_\perp = J_\parallel$ the model reduces to the XXX model. These models belong to different universality classes as they flow to distinct fixed points under renormalization.

Second, we consider completely connected networks, with all possible pairwise interactions:

$$H_{\mathrm{XXZ}}^{\mathrm{cc}} = h \sum_{i=1}^{N} Z_i + \frac{J_\perp}{2} \sum_{i,j} (X_i X_j + Y_i Y_j) + \frac{J_\parallel}{2} \sum_{i,j} Z_i Z_j . \tag{3.8}$$

Technically, the computation of the dynamical maps via Eq.(3.4) involves exponentiating the Hamiltonian and tracing over most of the system. This is easiest to do if the Hamiltonian is first diagonalized. Both topologies have a number of symmetries that can be exploited to perform this diagonalization. A detailed description can be found in Appendix B.1, but we summarize the key points here as they provide a helpful organization to understand some of the structure in the maps.

First, H_{XXZ} for either connectivity has a U(1) symmetry generated by the charge

operator $Q_N = \sum_i Z_i$. Therefore $H_{\rm XXZ}$ is block-diagonal in an excitation basis,

$$\mathcal{P}_N H_{\rm XXZ} \mathcal{P}_N^\dagger = H^0_{\rm XXZ} \oplus H^1_{\rm XXZ} \oplus ... \oplus H^N_{\rm XXZ}\,, \tag{3.9}$$

with dim $H^q_{\rm XXZ} = \binom{N}{q}$ and $\mathcal{P}_N$ is a $2^N \times 2^N$ permutation matrix taking the computational basis to a chosen excitation basis. There are many choices of excitation basis, as one can always reorder computational basis states within a given q-block to obtain a new basis.

Next, one can leverage the translation symmetry of the models. For homogeneous couplings and the two topologies considered here, the Hamiltonian is invariant under relabelings like $i \to i-1$. That is, the translation operator over N spins, T_N, satisfies $[T_N, H_{\rm XXZ}] = 0$. Thus the next stage in block-diagonalization for both models is achieved by using a Fourier basis, with blocks labelled by a:

$$\Gamma_N \mathcal{P}_N \left(H_{\rm XXZ}\right) \mathcal{P}_N^\dagger \Gamma_N^\dagger = \bigoplus_{q=0}^{N} \bigoplus_{a=0}^{N-1} H^{q,a}_{\rm XXZ}\,. \tag{3.10}$$

See Appendix B.1 for additional details and examples.

However, for $N > 3$, even these symmetries are not enough to achieve exact diagonalization (see, for example, Eq.(B.11) in the Appendix). The additional degeneracy in the eigenstates of T_N increases with N, and so eigenstates of $H_{\rm XXZ}$ are superpositions of these Fourier modes. That is, if eigenstates of the Hamiltonian are labelled by a complete set of quantum numbers $\{q,a,l\}$, and the index k runs over the Fourier modes in each block a, then

$$|E^a_q; l\rangle = \sum_{k=k_{\rm min}}^{k_{\rm max}} C^{kl}_q |\mathcal{F}^a_q; k\rangle\,. \tag{3.11}$$

Whenever $k_{\rm max} = k_{\rm min}$, the stationary states are just Fourier modes i.e. $|E^a_q; k_{\rm min}\rangle = |\mathcal{F}^a_q; k_{\rm min}\rangle$. For small $(k_{\rm max} - k_{\rm min})$, the time evolution may be computed analytically. That is the procedure we will follow in the examples below, but the maximum degree of degeneracy amongst Fourier modes grows linearly with N, and it becomes more difficult to perform the diagonalization.

To make this a bit more explicit, consider the $q = 1$ block for an XXZ-network with N qubits. The block has dimension N and T_N is non-degenerate within it, so diagonalization of $H^{q=1}_{\rm XXZ}$ is achieved through an N-dimensional discrete Fourier transformation. Explicitly

the eigenstates are given as discrete plane waves

$$|\mathcal{F}_1^a;0\rangle \equiv \frac{1}{\sqrt{N}} \sum_{k=0}^{N-1} e^{ik\theta_a} \sigma_k^+ |1...1\rangle \,, \tag{3.12}$$

where $\theta_a = \frac{2\pi a}{N}$ and σ_k^+ flips the kth spin from 1 to 0 and acts as the identity every where else. The $q = N-1$ block has essentially identical eigenstates, expect with the replacement

$$\sigma_k^+ |1...1\rangle \to \sigma_k^- |0...0\rangle \,. \tag{3.13}$$

For other values of q, the translation operator becomes more degenerate. In these cases an appropriately sized discrete Fourier transformation must be performed to reach the next step of block-diagonalization.

In the remainder of this subsection, we go through the computation of the dynamical maps for three qubits in detail. Then, in the rest of the section, we report map parameters and average maps for $N > 3$, leaving details of the process to Appendix B.1.

3.3.1.1 3-qubit XXZ-network

We shall now demonstrate how we compute the ensemble of phase-covariant maps and the average map, and characterize the fluctuations, for the example of a 3-qubit network. In this case, the ring and completely connected topologies are equivalent. We begin by diagonalizing H_{XXZ}, going first to the canonically ordered excitation basis

$$\mathcal{P}_3 H_{\mathrm{XXZ}} \mathcal{P}_3^\dagger = H_{\mathrm{XXZ}}^0 \oplus H_{\mathrm{XXZ}}^1 \oplus H_{\mathrm{XXZ}}^2 \oplus H_{\mathrm{XXZ}}^3 \,. \tag{3.14}$$

This example is especially simple as the only interacting blocks, H_{XXZ}^1 and H_{XXZ}^2, are both diagonalized through discrete Fourier transformation. The other blocks are non-interacting, and consist of the computational basis states $|1...1\rangle$ (q=0) and $|0...0\rangle$ (q=N). Using the exact diagonalization of the Hamiltonian, we determine explicit expression for the parameters appearing in the phase-covariant dynamical maps when the initial state

is of the form Eq.(3.5). We find

$$\begin{aligned}
\lambda_{1,i}(t,3) &= \sqrt{\alpha_i^2(t,3)+\beta_i^2(t,3)} \\
\theta_i(t,3) &= 2ht + \phi_i(t,3) \\
\lambda_{3,i}(t,3) &= \frac{1}{9}\Big(5+4\cos 3J_\perp t\Big) \\
\tau_{3,i}(t,3) &= \frac{2}{9}(\sum_{k\neq i} z_k)\Big(1-\cos 3J_\perp t\Big)
\end{aligned} \tag{3.15}$$

where we have made the definitions

$$\begin{aligned}
\alpha_i(t,3) = \frac{1}{18}\Big(&\Big(1-\prod_{k\neq i} z_k\Big)\Big(7+2\cos 3J_\perp t\Big) \\
&+\Big(1+\prod_{k\neq i} z_k\Big)\Big(3\cos\left(2J_\parallel-2J_\perp\right)t+6\cos\left(J_\parallel+2J_\perp\right)t\Big)\Big) \\
\beta_i(t,3) = \frac{1}{18}&\Big(\sum_{k\neq i} z_k\Big)\Big(3\sin\left(2J_\parallel-2J_\perp\right)t+6\sin\left(J_\parallel+2J_\perp\right)t\Big) \\
\phi_i(t,3) = \tan^{-1}&\left(\frac{\beta_i(t,3)}{\alpha_i(t,3)}\right).
\end{aligned} \tag{3.16}$$

Notice that the strength of the external magnetic field, h only enters into the rotation angle θ.

There are two relevant time scales in these maps, determined by $J_\parallel$ and $J_\perp$. For simplicity, we will illustrate results in Figure 3.1 for $J_\parallel = J_\perp$, and define a single time-scale

$$t_J = \frac{2\pi}{J_\perp}. \tag{3.17}$$

While a simplifying assumption, we do not expect this reduction to drastically change the primary aspects of our results for the average phase-covariant maps computed below. For example, the late-time average values of both λ_3 and τ_3 are independent of the ratio $\frac{J_\perp}{J_\parallel}$. Further, if we avoid certain commensurate values of Hamiltonian parameters, the steady-state values of λ_1 are also independent of the coupling ratio.

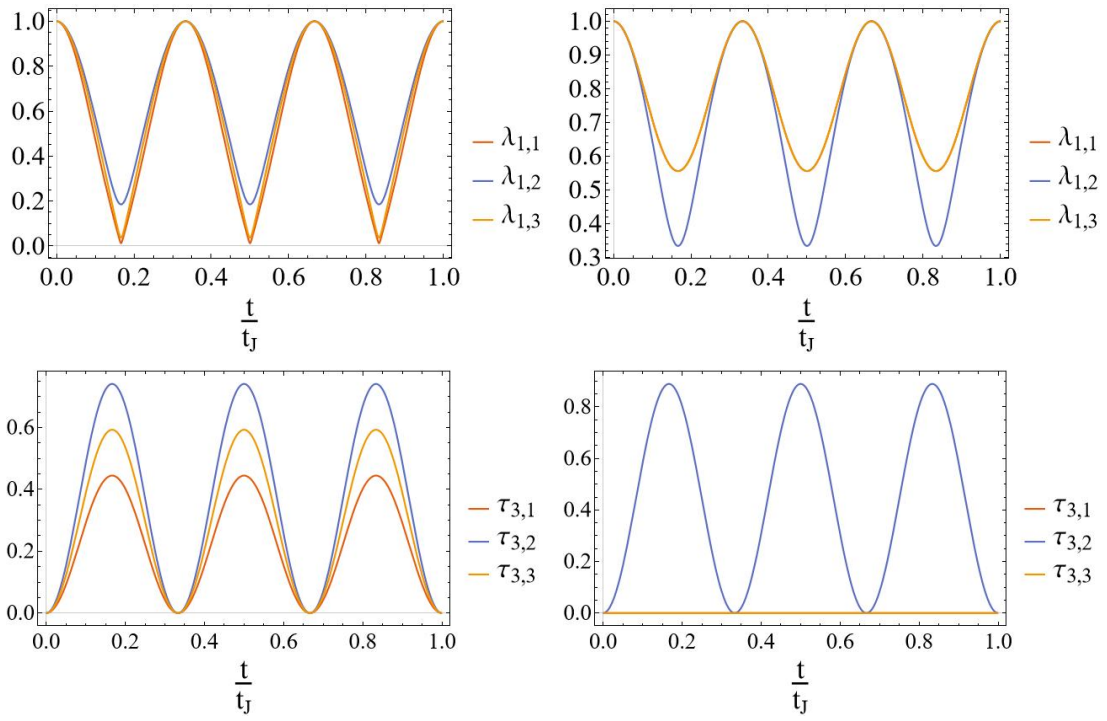

Figure 3.1: Examples of ensembles of two of the dynamical map functions, $\lambda_{1,i}(t)$ and $\tau_{3,i}(t)$. Each panel shows results for all spins ($i = 1, 2, 3$) in the network. Plots on the left are for initial state z_1=1, $z_2 = \frac{1}{3}$ and $z_3 = \frac{2}{3}$ (hierarchical), while those on the right had $z_1 = z_3 = -z_2 = 1$ (Néel). Both cases assume $J_\parallel = J_\perp$, which is used to define the time scale $t_J = \frac{2\pi}{J_\perp}$.

We now turn to the computation of the steady-channel, $\overline{\Lambda}_3^\infty$ and the normalized fluctuations. For generic values of h (i.e. not commensurate with $J_\perp$ or $J_\parallel$), $\Lambda_{xx}(t)$, $\Lambda_{xy}(t)$, $\Lambda_{yx}(t)$, and $\Lambda_{yy}(t)$, vanish under long-time averaging. Therefore we assume that h is generic, precluding this situation. Choosing to define the time average of $\lambda_1(t)$ as

$$\overline{\lambda}_1(t) = \sqrt{\overline{\Lambda}_{xx}^2(t) + \overline{\Lambda}_{xy}^2(t)} \tag{3.18}$$

we then find

$$\begin{aligned} \overline{\lambda}_1(t=\infty, N=3) &= 0\,, \\ \overline{\lambda}_3(t=\infty, N=3) &= \frac{5}{9}\,, \\ \overline{\tau}_3(t=\infty, N=3) &= \frac{4}{9}\frac{\mathfrak{e}_1(z_i)}{3}\,. \end{aligned} \tag{3.19}$$

Anticipating results for larger N, we express $\overline{\tau}_3^\infty$ in terms of elementary symmetric

polynomials in the initial state $\mathfrak{e}_k(z_i)$. These polynomials are defined for any N by the equation

$$\prod_{i=1}^{N}(z+z_i) = \mathfrak{e}_0(z_i)z^N + \mathfrak{e}_1(z_i)z^{N-1} + ... + \mathfrak{e}_N(z_i)\,. \tag{3.20}$$

Examples and related applications of the polynomials can be found in [89].

Before we move on to the next topic, it is useful to point out a few features of the dynamical map ensembles for the various N we consider.

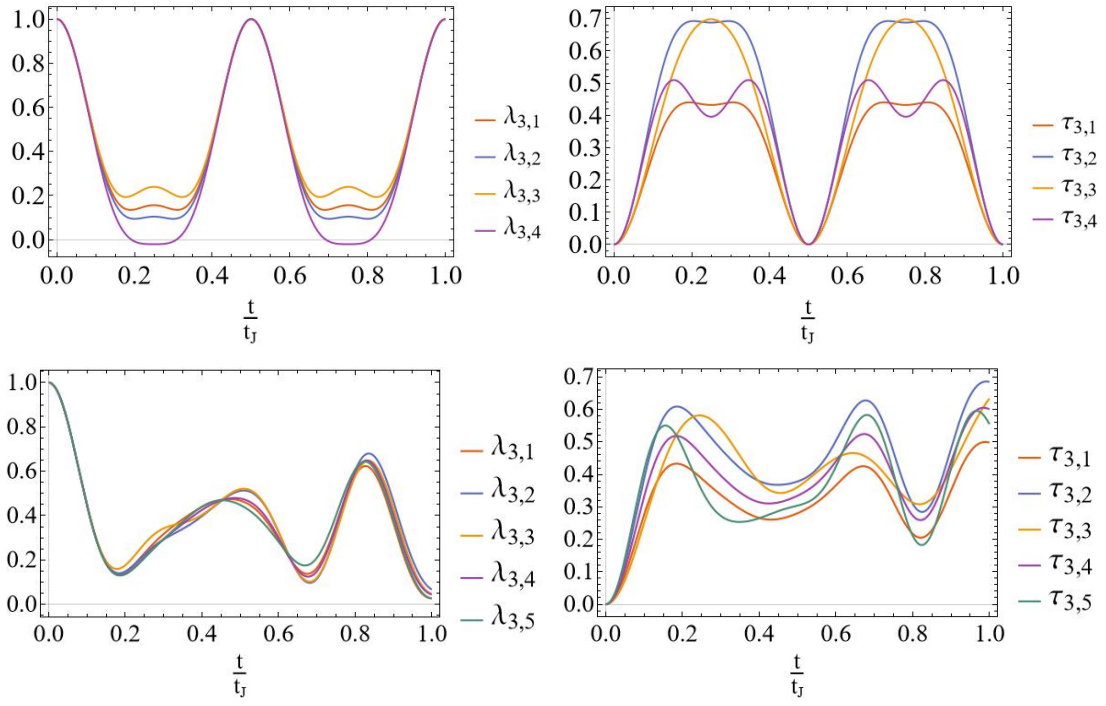

Figure 3.2: The ensembles of non-unitary parameters are plotted for the 4 and 5 qubit XXX-model for hierarchical initial states. The top set of plots are generated using the the initial state with $z_1 = 1$, $z_2 = \frac{1}{4}$, $z_3 = \frac{2}{4}$, and $z_4 = \frac{3}{4}$. The bottom set of plots are generated using the initial condition $z_1 = 1$, $z_2 = \frac{1}{5}$, $z_3 = \frac{2}{5}$, $z_4 = \frac{3}{5}$, and $z_5 = \frac{4}{5}$.

Figure 3.2 emphasizes the non-time-local nature or non-invertibility of our ensembles, following from the existence of zeros in the $\lambda_3(t)$ plots. The top left panel shows that while not every individual map is time-local for the $N = 4$ hierarchy state, the average dynamics will be. While not plotted here, the Néel serves as a maximal example of locality breaking, as even the average dynamical map is time-non-local.

We may also use these plots to draw a point of distinction between the two topologies of networks. In the completely connected case $\lambda_3(t)$ and $\tau_3(t)$ are always periodic over some multiple of t_J, while in the case of the XXX-ring the dynamics need not be periodic,

as can be seen from the lower panel of Figure 3.2. Of course if N is a perfect square then periodicity occurs, as can be seen for the case of $N = 4$. Equations (B.42) and (B.54) in Appendix B.2 makes this point clear, showing that for the XXX-ring $\sqrt{N}J_\perp$ appears in the various frequencies comprising the dynamical map components.

3.3.2 Long-time averaged channels

The individual maps and steady-channels for $N > 3$ require a similar, but longer computation. the two topologies of XXZ-clusters for. We also discuss features of the reduced dynamics found for the computed ensembles, i.e. whether they are time-local for certain initial states and other average properties. Details of the map components as a function of time, and some additional plots of that time-dependence, can be found in Appendix B.2.

3.3.2.1 Complete connectivity

Turing our attention to the completely-connected XXZ-network we compute the late-time network averaged quantum channels. For $N = 4$ we find

$$\begin{aligned}
\overline{\lambda}_1^\infty(N=4) &= 0 \\
\overline{\lambda}_3^\infty(N=4) &= \frac{7}{16}\frac{\mathfrak{e}_0(z_i)}{1} + \frac{3}{16}\frac{\mathfrak{e}_2(z_i)}{6} \\
\overline{\tau}_3^\infty(N=4) &= \frac{9}{16}\frac{\mathfrak{e}_1(z_i)}{4} - \frac{3}{16}\frac{\mathfrak{e}_3(z_i)}{4}\,.
\end{aligned} \tag{3.21}$$

For $N = 5$ we find

$$\begin{aligned}
\overline{\lambda}_1^\infty(N=5) &= 0 \\
\overline{\lambda}_3^\infty(N=5) &= \frac{7}{15}\frac{\mathfrak{e}_0(z_i)}{1} + \frac{16}{75}\frac{\mathfrak{e}_2(z_i)}{10} \\
\overline{\tau}_3^\infty(N=5) &= \frac{8}{15}\frac{\mathfrak{e}_1(z_i)}{5} - \frac{16}{75}\frac{\mathfrak{e}_3(z_i)}{10}\,.
\end{aligned} \tag{3.22}$$

and for $N = 6$ we find

$$\begin{aligned}
\overline{\lambda}_1^\infty(N=6) &= 0 \\
\overline{\lambda}_3^\infty(N=6) &= \frac{59}{144}\frac{\mathfrak{e}_0(z_i)}{1} + \frac{5}{12}\frac{\mathfrak{e}_2(z_i)}{15} - \frac{5}{48}\frac{\mathfrak{e}_4(z_i)}{15} \\
\overline{\tau}_3^\infty(N=6) &= \frac{85}{144}\frac{\mathfrak{e}_1(z_i)}{6} - \frac{5}{12}\frac{\mathfrak{e}_3(z_i)}{20} + \frac{5}{48}\frac{\mathfrak{e}_5(z_i)}{6}\,.
\end{aligned} \tag{3.23}$$

The relationship appearing between $\overline{\lambda}_3^\infty$ and $\overline{\tau}_3^\infty$ are in part due to constraints that must be satisfied. Namely if all $z_i = \pm 1$, the total global state is a fixed point of the unitary evolution therefore

$$\overline{\tau}_3^\infty\Big|_{z_i=\pm 1} \pm \overline{\lambda}_3^\infty\Big|_{z_i=\pm 1} = \pm 1\,. \tag{3.24}$$

Our results taken together with these constraint leads us to make the following conjectures for the values of any N where for odd values

$$\begin{aligned}
\overline{\lambda}_1^\infty(N=\text{odd}) &= 0 \\
\overline{\lambda}_3^\infty(N=\text{odd}) &= a_0\frac{\mathfrak{e}_0(z_i)}{1} + a_2\frac{\mathfrak{e}_2(z_i)}{\binom{N}{2}} + ... + a_{N-3}\frac{\mathfrak{e}_{N-3}(z_i)}{\binom{N}{N-3}} \\
\overline{\tau}_3^\infty(N=\text{odd}) &= (1-a_0)\frac{\mathfrak{e}_1(z_i)}{\binom{N}{1}} - a_2\frac{\mathfrak{e}_3(z_i)}{\binom{N}{3}} - ... - a_{N-3}\frac{\mathfrak{e}_{N-2}(z_i)}{\binom{N}{N-2}}
\end{aligned} \tag{3.25}$$

and for even values

$$\begin{aligned}
\overline{\lambda}_1^\infty(N=\text{even}) &= 0 \\
\overline{\lambda}_3^\infty(N=\text{even}) &= a_0\frac{\mathfrak{e}_0(z_i)}{1} + a_2\frac{\mathfrak{e}_2(z_i)}{\binom{N}{2}} + ... + a_{N-2}\frac{\mathfrak{e}_{N-2}(z_i)}{\binom{N}{N-2}} \\
\overline{\tau}_3^\infty(N=\text{even}) &= (1-a_0)\frac{\mathfrak{e}_1(z_i)}{\binom{N}{1}} - a_2\frac{\mathfrak{e}_3(z_i)}{\binom{N}{3}} - ... - a_{N-2}\frac{\mathfrak{e}_{N-1}(z_i)}{\binom{N}{N-1}}\,.
\end{aligned} \tag{3.26}$$

Another property of these long time averages, and in fact of the dynamical map components in general, is that λ_3 is an even function of $\{z_i\}$ while τ_3 is an odd function. This is a consequence of the symmetry generated by

$$\mathcal{P} = \prod_{i=1}^{N} Z_i. \tag{3.27}$$

which is a symmetry for both models considered, therefore $\lambda_3(t)$ and $\tau_3(t)$ have definite values of $\mathcal{P}$ in the ring topology as well.

To conclude the discussion, notice that the average map depends only on the initial state and symmetry of the Hamiltonian. We note that in this case the long time averages are invariant under any permutation of the initial z_i. Comparing the fully connected case to the ring, shown next, illustrates this dependence. In addition, notice that the invariant state of the average map is not the average of the initial states, but any explicit dependence on coupling strength is gone. As expected from the individual maps at any

time, there is also no dependence on magnetization. In the case of non-phase covariant maps, there will be terms depending on h, and, just as in the case of λ_1, special values of the coupling lead to different long time average values.

3.3.2.2 Ring connectivity

Computing the late-time and ring-averaged quantities we find for $N = 4$

$$\begin{aligned}
\overline{\lambda}_1^{\infty}(N=4) &= 0 \\
\overline{\lambda}_3^{\infty}(N=4) &= \frac{7}{16} + \frac{3}{16}\frac{\mathfrak{e}_2(z_i) - 4z_1z_3 - 4z_2z_4}{6} \\
\overline{\tau}_3^{\infty}(N=4) &= \frac{9}{16}\frac{\mathfrak{e}_1(z_i)}{4} + \frac{1}{16}\frac{\mathfrak{e}_3(z_i)}{4}\,,
\end{aligned} \tag{3.28}$$

and for $N = 5$

$$\begin{aligned}
\overline{\lambda}_1^{\infty}(N=5) &= 0 \\
\overline{\lambda}_3^{\infty}(N=5) &= \frac{71}{225} + \frac{2}{45}\frac{\mathfrak{e}_2(z_i)}{10} \\
\overline{\tau}_3^{\infty}(N=5) &= \frac{154}{225}\frac{\mathfrak{e}_1(z_i)}{5} - \frac{2}{45}\frac{\mathfrak{e}_3(z_i)}{10}\,.
\end{aligned} \tag{3.29}$$

Comparing to the complete connectivity, Eq.(3.26) and Eq.(3.25), demonstrates how the interaction structure appears in the maps. For example taking $N = 4$, the long-time average is only invariant under cyclic permutations of the initial state while in the fully connected case the invariance was with respect to the full permutation group. However, for $N = 5$ the full permutation symmetry is recovered in the infinity time limit. But we do not expect this to be a generic feature for larger N, and in principle only cyclic polynomials of the initial state should appear. As before, the invariant state of the average map does not correspond to the average initial state.

3.3.3 Fluctuations about the average channel

We now consider physical data to constrain the variance we expect in the distributions at late-times. We do this by considering the maximum distance from the finite-time average to the steady value. We define the fluctuations at finite-time about these average

quantities, estimated by the normalized fluctuations

$$\begin{aligned} \Delta\lambda_i &\equiv \frac{\overline{\lambda}_i(t) - \overline{\lambda}_i^{\infty}}{\overline{\lambda}_i^{\infty}} \\ \Delta\tau_3 &\equiv \frac{\overline{\tau}_3(t) - \overline{\tau}_3^{\infty}}{\overline{\tau}_3^{\infty}} \,. \end{aligned} \tag{3.30}$$

These quantities will be used to calibrate the second moments of the phase-covariant measures developed in Section 3.6. The normalized fluctuations are generally initial-state dependent. But to determine an approximate size of the fluctuations, we may simply consider a class of initial states that have essentially initial state independent fluctuations. To see that such a class of states exists, consider the completely connected network and assume that each qubit satisfies $0 \leq z_i \leq \mathcal{Z} < 1$. Then we may notice that

$$\frac{\mathfrak{e}_k(z_i)}{\binom{N}{k}} \leq \mathcal{Z}^k \tag{3.31}$$

therefore for small enough $\mathcal{Z}$, only the first terms in $\overline{\lambda}_3(t)$ and $\overline{\tau}_3(t)$ are relevant. In such a class the fluctuations about the long time average will be initial state independent.

In Figures 3.3 and 3.4, we have plotted the fluctuations about the long time averages for the completely and ring connected networks, using only the lowest order terms in the initial state from $\overline{\lambda}_3(t)$ and $\overline{\tau}_3(t)$. We confirm in Section 3.6 that these approximations do provide a good estimate of the fluctuation size, even when considering a generic initial state.

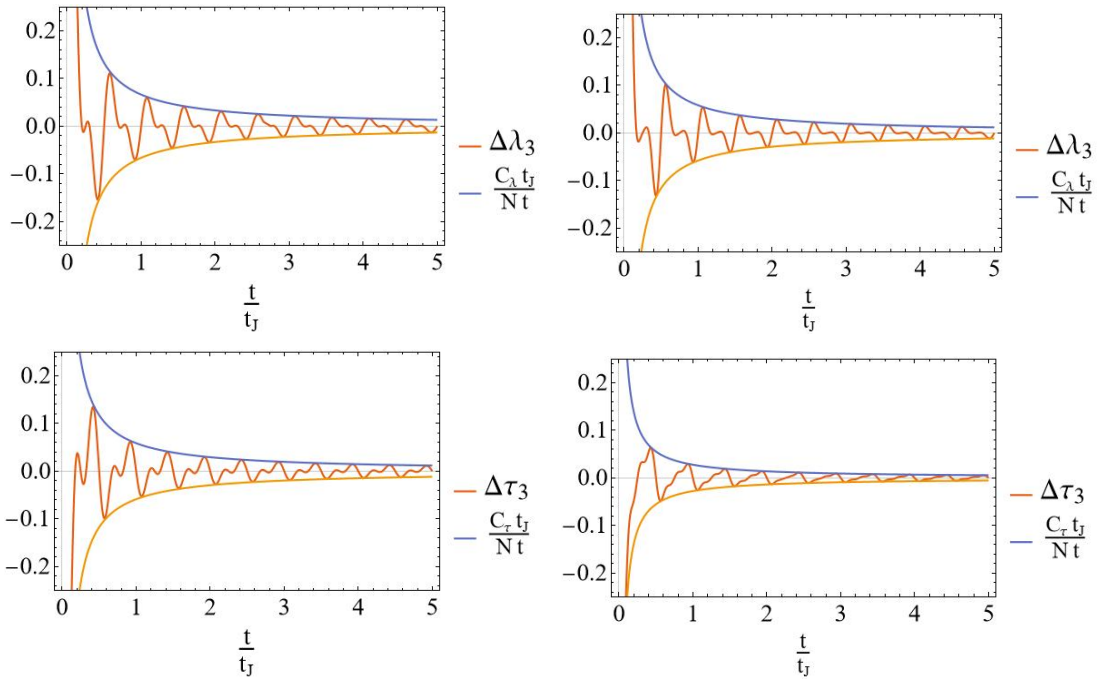

Figure 3.3: The normalized fluctuations of $\overline{\lambda}_3(t)$ and $\overline{\tau}_3(t)$ considering only lowest order terms are plotted for the completely-connected XXZ network. The bounding hyperbolas estimate the size of the late-time fluctuations, as in Eq.(3.32).

From these plots the late-time fluctuations are found to scale as

$$\Delta\zeta \approx \frac{C_\zeta t_J}{Nt}\,, \tag{3.32}$$

where $t_J = \frac{2\pi}{J_\perp}$ is the dynamical timescale defined in Eq.(3.17) and C_ζ is an order one constant. The completely connected network, for a fixed N, approaches the steady channel more quickly than in the case of the ring. Comparing the $N = 6$ completely connected network and the $N = 5$ ring network, we see that the fluctuations persist at least four times longer in the case of the ring. Note that the scale of the vertical axis of all plots are identical.

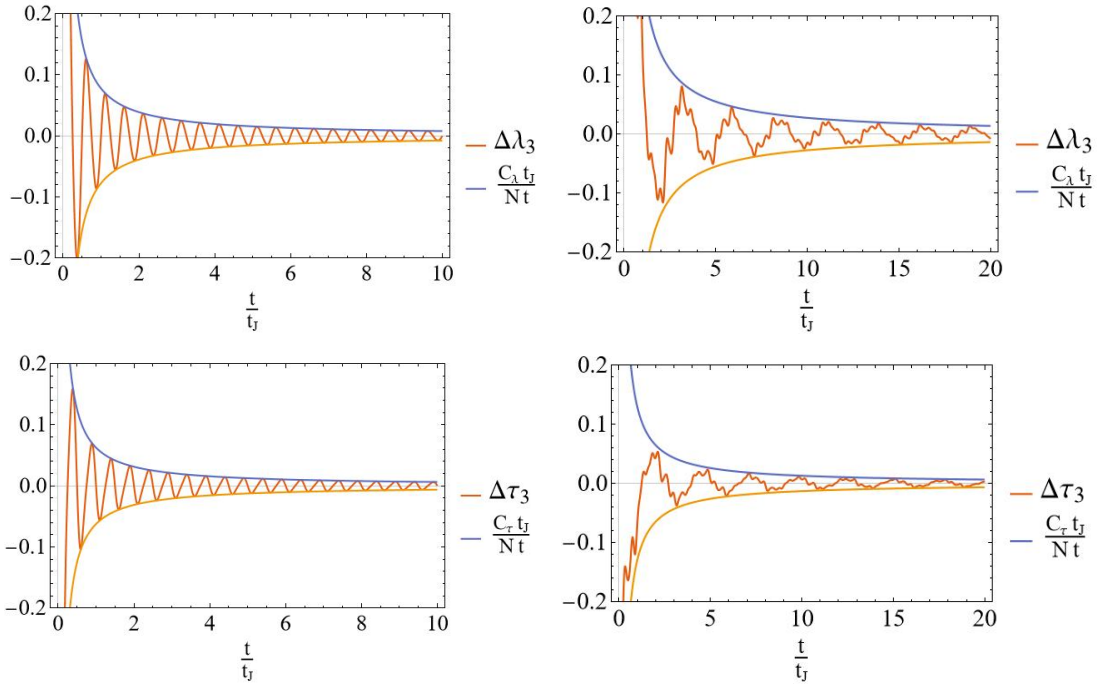

Figure 3.4: The approximate normalized fluctuations of $\overline{\lambda}_3(t)$ and $\overline{\tau}_3(t)$ considering only lowest order terms are plotted for the XXZ ring. The bounding hyperbolas estimate the size of the late-time fluctuations, as in Eq.(3.32).

3.4 Physical relevance of the long-time averaged channel

Consider a qubit network that consists of $N_{\rm CL}$ clusters, each containing N qubits, where we assume $N_{\rm CL} \gg N$. For simplicity, each cluster is assumed to have the same connectivity. The spin-averaged dynamical map for the Ith cluster is

$$\langle \Lambda_{\rm I}(t) \rangle = \frac{1}{N} \sum_{i=1}^{N} \Lambda_{\rm I_i}(t)\,. \tag{3.1}$$

Suppose at some very early time there are no interactions and the state of the network is entirely uncorrelated. Interactions within each individual cluster are turned on via a quenching mechanism, but that not all clusters are quenched at the same time. Let the time-scale for over which the cluster quenching is (uniformly) staggered be longer than that set by the interaction time-scale within each cluster. The time-dependent Hamiltonians considered (and initial states) are such that the conditions for phase covariance are satisfied for each cluster. For example, this scenario can be modeled by a

Hamiltonian of the form

$$H(t) = \sum_{\mathrm{I}=1}^{N_{\mathrm{CL}}} \Big(h_{\mathrm{I}} \sum_{i=1}^{N} Z_{\mathrm{I_i}} + J\theta\big(t - t_{\mathrm{I}}\big) \sum_{i,j} \big(X_{\mathrm{I_i}} X_{\mathrm{I_j}} + Y_{\mathrm{I_i}} Y_{\mathrm{I_j}} + Z_{\mathrm{I_i}} Z_{\mathrm{I_j}} \big) \Big) \tag{3.2}$$

where $\theta(t)$ is the Heaviside step function, and t_{I} are the various quench times associated with the clusters. If the timing of the quench varies over a time-scale longer than that set by J, and the large number of clusters ensures that all oscillation scales of the single-cluster Hamiltonian are smoothly sampled, then the clusters will be at varying points in their evolution and the average map at late times will be given by

$$\lim_{N_{\mathrm{CL}} \to \infty} \frac{1}{N_{\mathrm{CL}}} \sum_{\mathrm{I}} \langle \Lambda_{\mathrm{I}}(t) \rangle = \frac{1}{t} \int_0^t dt' \langle \Lambda_{\mathrm{K}}(t') \rangle = \overline{\Lambda}_N(t)\,. \tag{3.3}$$

In fact, as long as there are many clusters with any given initial state, which experience the quench at offset times, one can imagine a further average over steady channels with different initial states to match the full complexity of the initial system of size $\gg N$. That is, one could average over the initial states appearing in the steady channels.

Under such a quenching scenario, even for relatively small clusters, we obtain average dynamical maps that approach a steady-channel, denoted as $\overline{\Lambda}_N^{\infty}$, in the limit $t \to \infty$. We are then able to construct distributions of channels that have the steady channel as their average. By studying the approach to the steady channel, we able to constrain the second moment of the distributions.

3.5 Phase-covariance on average from disordered Hamiltonians

While in the staggered quench example above we imposed that each cluster had the same Hamiltonian and an initial state from the phase-covariant set, the regime of applicability of the phase-covariant steady channel is actually larger. In this section we show that constrained Hamiltonian disorder, or noise, can be rather naturally consistent with phase-covariant, average reduced dynamics. We show this by considering ensembles of qubit pairs, which serve as a simple model of the paradigm set forth at the end of the previous section.

3.5.1 An ensemble with non-phase-covariant elements

To begin we start with a physical setting where distributions of maps that are not necessarily phase-covariant appear. We consider a Hamiltonian that governs the time evolution of $N_{\rm CL}$ pairs of spins, where each pair evolves independently, and conserves the total excitation number $Q = \sum Z_i$. This can be compactly written as

$$\begin{aligned} H &= \sum_{i=1}^{2N_{\rm CL}} h_i Z_i + \sum_{i=1}^{2N_{\rm CL}} \frac{J_{i(i+1)}}{2} \left[\frac{1+(-1)^{i+1}}{2}\right] [X_i X_{i+1} + Y_i Y_{i+1}] \\ &= \sum_{i=1}^{2N_{\rm CL}} \frac{1+(-1)^{i+1}}{2} H_{\rm XX}^{i,i+1} = H_{\rm XX}^{1,2} + H_{\rm XX}^{3,4} + ... + H_{\rm XX}^{2N-1,2N_{\rm CL}} \,. \end{aligned} \tag{3.4}$$

The $2N_{\rm CL}$ qubits are taken to be in a completely uncorrelated initial state. For each pair, we allow this example to break both phase-covariant conditions from Eq.(3.2). First, allowing $h_i \neq h_j$ means that the interaction term will not commmute with the free Hamiltonian. In addition, we do not impose any restriction on the initial state.

As the Hamiltonian is block diagonal in the qubit pairs, we can determine both the 1-spin and 2-spin dynamical maps obtained for a single pair. The 2-qubit maps describe unitary evolution, and this example may be viewed as an generalization of the noisy qubit models proposed in [70] to a larger system size. However, at the single-spin level the evolution is non-unitary and richer than what can be found with noisy Hamiltonians alone.

To write the single-spin dynamical map, it is convenient to decompose the unitary evolution in terms of

$$\mathcal{U}_{lk}^{ij} \equiv \frac{1}{4}{\rm tr}\left[\left(\sigma_1^i \otimes \sigma_2^j\right) e^{-i(H_{\rm XX}^{1,2})t} \left(\sigma_1^l \otimes \sigma_2^k\right) e^{i(H_{\rm XX}^{1,2})t}\right] . \tag{3.5}$$

The Hamiltonian parameters enter in the unitary evolution in the following combinations:

$$\begin{aligned} h_{12} &= \frac{h_1+h_2}{2} \,, \qquad \omega_{12} = {\rm sgn}(\Delta_{12})\sqrt{\Delta_{12}^2 + J_{12}^2} \\ \Delta_{12} &= h_1 - h_2 \,, \qquad \tan\phi_{12} = \frac{J_{12}}{\Delta_{12}} \,. \end{aligned} \tag{3.6}$$

Further details can be found in Appendix B.2. Then the evolution of the first spin in the first pair, for example, is given by

$$\rho_1(t) = {\rm tr}_2\left[e^{-i(H_{\rm XX}^{1,2})t}\rho_1(0)\otimes\rho_2(0)e^{i(H_{\rm XX}^{1,2})t}\right] = {\rm tr}_2\left[\mathcal{U}(t)\rho(0)\right] \equiv \Lambda_1(t,0)\rho_1(0) \,. \tag{3.7}$$

Using the Bloch parameterization for the second spin (which provides the initial environment state for the first spin) as $\rho_2 = \frac{1}{2}(1 + x_2 X_2 + y_2 Y_2 + z_2 Z_2)$, and defining partial components

$$\Lambda_1^{ijk} = \mathcal{U}_{jk}^{i0}\,, \tag{3.8}$$

the dynamical map is

$$\Lambda_1(t,0) = \begin{bmatrix} 1 & 0 & 0 & 0 \\ 0 & \Lambda_1^{xx0} & \Lambda_1^{xy0} & \left(x_2\Lambda_1^{xzx} + y_2\Lambda_1^{xzy}\right) \\ 0 & \Lambda_1^{yx0} & \Lambda_1^{yy0} & \left(x_2\Lambda_1^{yzx} + y_2\Lambda_1^{yzy}\right) \\ z_2\Lambda_1^{z0z} & \left(x_2\Lambda_1^{zxx} + y_2\Lambda_1^{zxy}\right) & \left(x_2\Lambda_1^{zyx} + y_2\Lambda_1^{zyy}\right) & \Lambda_1^{zz0} \end{bmatrix}. \tag{3.9}$$

The dynamical map is non-unital so long as $z_2(0) \neq 0$.

The dynamical map $\Lambda_2(t,0)$ for the second spin can be obtained directly from Eq.(3.9). From the Hamiltonian it is easy to see that we need only exchange the values of h_i, so $\Lambda_2(t,0)$ is directly obtained by exchanging the initial states and sending $\Delta_{12} \to -\Delta_{12}$. In terms of map components, this is accomplished by

$$\Lambda_2^{ijk}(t,\Delta_{12}) = \mathcal{U}_{kj}^{0i}(t,\Delta_{12}) = \mathcal{U}_{jk}^{i0}(t,-\Delta_{12}) = \Lambda_1^{ijk}(t,-\Delta_{12})\,. \tag{3.10}$$

The dynamical maps associated to the second qubit pair are obtained through the replacement $12 \to 34$ in the initial states, h_i and $J_{i,i+1}$. In this way we obtain an ensemble of non-unital 1-qubit dynamical maps and unitary 2-qubit dynamical maps.

Given the collection of disjoint qubit pairs, and the associated 2-qubit unitary channels, it is possible to construct their ensemble averages. Both averages will be non-unitary, since convex combinations of unitary channels may be non-unitary. This provides a useful means to efficiently simulated non-unitary evolution [90]. If each pair is assumed to be in the same uncorrelated 2-qubit state, the following non-unitary ensemble averaged 2-qubit dynamical map may be defined

$$\overline{\mathcal{U}}(t)\left[\rho_1(0)\otimes\rho_2(0)\right] = \frac{1}{N_{\mathrm{CL}}}\sum_{\text{clusters}}\left(e^{-i\left(H_{\mathrm{XX}}^{i,i+1}\right)t}\rho_1(0)\otimes\rho_2(0)e^{i\left(H_{\mathrm{XX}}^{i,i+1}\right)t}\right). \tag{3.11}$$

At this point we have a physical representation of the sort of noisy Hamiltonians that have appeared in numerous works. Now conceptually we may view the the previous ensemble as an instantiation of some noise distribution over Hamiltonian parameters.

Therefore in the limit of large N_{CL} the network average is equivalent to

$$\overline{\mathcal{U}}(t)\left[\rho_1(0)\otimes\rho_2(0)\right] = \langle e^{-iH_{\mathrm{XX}}t}\rho_1(0)\otimes\rho_2(0)e^{iH_{\mathrm{XX}}t}\rangle_{\mathrm{disorder}} \tag{3.12}$$

where we have dropped the superscripts on H_{XX} to emphasis the conceptual difference with the network of clusters.

Now instead of considering a disorder distribution directly over the parameters in the Hamiltonian, we consider the distributions directly over its eigenvalues and eigenvectors. That is, we take the fundamental parameters to be those on the left hand side of Eq.(3.6), e.g. h (from h_{12}), ω, and ϕ, rather than $(h_1, h_2, J_\perp)$. This approach allows for a closer connection to the dynamical map components. For example, the following component

$$\Lambda_1^{xzy} \propto \sin\phi\,, \tag{3.13}$$

which is compactly expressed in terms of the mixing angle ϕ from H_{XX} eigendecomposition. Notice that such a component vanishes if the noise distribution is an even function of ϕ, where $\tan\phi = \frac{J}{\Delta}$. The other dynamical map components that break phase-covariance also vanish under the same assumption. We understand this as the phase-covariant constraints in Eq.(3.2) being satisfied on average.

We can apply a similar procedure to other non-phase-covariant maps. In particular, for more general non-unital quantum channels with non-zero shift in the x and y direction ($\tau_1 \neq 0$ and $\tau_2 \neq 0$), the invariant state can have coherences and therefore cannot be represented as a Gibbs state in the computational basis. However, ensembles of such general non-unital maps can be generated such that the shift in the x and y directions are eliminated, resulting in a Gibbs-like state for the ensemble-averaged map. We will demonstrate this with an example.

3.5.2 Phase-covariance via disorder averaging

We begin by considering independent Gaussian distributions for h and ω,

$$p_h(h) = \frac{1}{\sqrt{2\pi\sigma_h^2}}e^{-\frac{(h-B)^2}{2\sigma_h^2}} \quad , \quad p_\omega(\omega) = \frac{1}{\sqrt{2\pi\sigma_\omega^2}}e^{-\frac{(\omega-\Omega)^2}{2\sigma_\omega^2}} \tag{3.14}$$

and two different examples of probability distributions over ϕ,

$$p_{\mathrm{G}}(\phi) = \frac{1}{\sqrt{2\pi\sigma_\phi^2}} e^{-\frac{\phi^2}{2\sigma_\phi^2}} \quad , \quad p_{\mathrm{T}}(\phi) = \frac{\tanh[a_\phi \phi]^2}{\left(\pi - \frac{2}{a_\phi}\tanh\left[\frac{a_\phi \pi}{2}\right]\right)} , \tag{3.15}$$

where for $p_{\mathrm{T}}(\phi)$ the range is restricted to be $-\pi/2 \leq \phi \leq \pi/2$. Both distributions have $\langle\phi\rangle = 0$ to ensure that the 1-qubit dynamical maps are phase-covariant. We consider multiple ϕ-distributions as the average values of τ_3 and λ_3 are strongly tied to this choice. Certain ϕ-distributions restrict the range of allowed average values of map parameters, and we see from Figure 3.5 that the Gaussian distribution cannot generate large enough τ_3 to be compatible all examples from Section 3.3.

Using these distributions, the partial components of the effective focal dynamical map are

$$\begin{aligned}
\overline{\Lambda}_1^{xx0} &= \overline{\Lambda}_1^{yy0} = \left(\cos\Omega t \cos 2Bt - e^{-\frac{\pi^2}{2\varphi^2}} \sin\Omega t \sin 2Bt\right) e^{-\frac{(\sigma_\omega^2 + 4\sigma_h^2)t^2}{2}} \\
\overline{\Lambda}_1^{yx0} &= -\overline{\Lambda}_1^{xy0} = \left(\cos\Omega t \sin 2Bt + e^{-\frac{\pi^2}{2\varphi^2}} \sin\Omega t \cos 2Bt\right) e^{-\frac{(\sigma_\omega^2 + 4\sigma_h^2)t^2}{2}} \\
\overline{\Lambda}_1^{z0z} &= 1 - \overline{\Lambda}_1^{zz0} = \frac{1}{4}\left(1 - e^{-\frac{2\pi^2}{\varphi^2}}\right)\left(1 - \cos(2\Omega t) e^{-2\sigma_\omega^2 t^2}\right) .
\end{aligned} \tag{3.16}$$

Figure 3.5 shows the non-unitary phase-covariant parameters of the map $\overline{\Lambda}_1(t,0)$. For plotting purposes we have defined the dimensionless quantity $\chi = \frac{\Omega}{2\pi}t$.

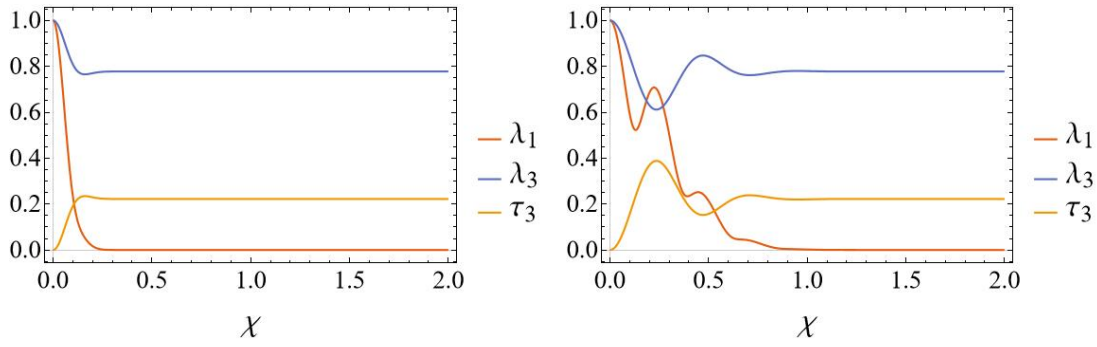

Figure 3.5: The non-unitary parameters of $\overline{\Lambda}_1(t,0)$ are plotted for $\sigma_h = \sigma_\omega = 1$, $\varphi = 3$, and the traced out qubit has $z = 1$. For large enough Ω, revivals appear in the non-unitary parameters. In either case, the x and y components of the focal Bloch vector fully decohere before $\zeta = 1$.

We have introduced the additional truncated distribution over ϕ to demonstrate that disorder distributions can capture the larger values of τ_3 found above. For example, in

the truncated hyperbolic tangent distribution the maximum allowed value of τ_3 is found to be

$$\lim_{a_\phi \to 0} \frac{1}{\pi - \frac{2}{a_\phi}\tanh[a_\phi \pi/2]} \int_{-\pi/2}^{\pi/2} \sin^2[\phi] \tanh^2[a_\phi \phi] d\phi = \frac{6+\pi^2}{2\pi^2} \approx 0.8\,. \tag{3.17}$$

3.6 Phase-covariant dynamics from channel ensembles

In the final section of this work we construct measures over phase-covariant channels that capture key features of the long-time averaged channels derived from XXZ networks. However, the time-evolving ensemble can be considered on its own, characterized by its thermodynamic properties without reference to a particular Hamiltonian. From the Gaussian examples considered in Section 4, we are motivated to considered a phase-covariant measure consisting of truncated Gaussian distributions over the non-unitary parameters. We use the physical constraints from Section 2 to fix the mean (μ) and scale (σ) parameters.

3.6.1 Phase-covariant measures

The key point in defining a measure over channels is determining the domain of integration. This depends on the constraints imposed by complete positivity, which are especially simple in the case of phase-covariant qubit channels. Then, a phase-covariant measure may be defined by supplying a joint probability distribution $p_N(\lambda_1, \tau_3, \lambda_3; t)$ which satisfies the normalization condition

$$\begin{aligned} 1 &= \int_{\Gamma_{\rm PC}} p_N(\lambda_1, \tau_3, \lambda_3; t) d\lambda_1 d\tau_3 d\lambda_3 \\ &= \int_0^1 \int_{-(1-\lambda_3)}^{1-\lambda_3} \int_{-\frac{1}{2}\sqrt{(1+\lambda_3)^2-\tau_3^2}}^{\frac{1}{2}\sqrt{(1+\lambda_3)^2-\tau_3^2}} p_N(\lambda_1, \tau_3, \lambda_3; t) d\lambda_1 d\tau_3 d\lambda_3 \\ &+ \int_{-1}^0 \int_{-(1+\lambda_3)}^{1+\lambda_3} \int_{-\frac{1}{2}\sqrt{(1+\lambda_3)^2-\tau_3^2}}^{\frac{1}{2}\sqrt{(1+\lambda_3)^2-\tau_3^2}} p_N(\lambda_1, \tau_3, \lambda_3; t) d\lambda_1 d\tau_3 d\lambda_3\,, \end{aligned} \tag{3.1}$$

where the order of integration follows from the form of the constraints in Eq.(3.6). For more general quantum systems it may not be possible to determine the boundary of integration, but restricting the reduced dynamics to be G-covariant potentially makes the problem tractable for larger quantum channel.

The above measure allows us to define the average dynamical map,

$$\langle \Lambda_N \rangle(t) = \int_{\Gamma_{\rm PC}} p_N(\lambda_1, \tau_3, \lambda_3; t) \Lambda(\lambda_1, \tau_3, \lambda_3) d\lambda_1 d\tau_3 d\lambda_3 \,. \tag{3.2}$$

We choose to introduce time-dependence into the probability distribution, instead of directly into the dynamical map, as the time-dependence of the dynamical map becomes quite complicated for large clusters.

This form of the map ensemble can be usefully compared to prior explorations of random open system dynamics, and to compare the phase-covariant class to the larger class of channels.

We compare the distribution of eigenvalues for a non-unital phase-covariant ensemble to those of the more general class of dynamical maps, treated for example in [77]. To do so, it is helpful to diagonalize the phase-covariant channel and define

$$D_{\Lambda_{\rm PC}} = \begin{bmatrix} 1 & 0 & 0 & 0 \\ 0 & \lambda_1 e^{i\theta} & 0 & 0 \\ 0 & 0 & \lambda_1 e^{-i\theta} & 0 \\ 0 & 0 & 0 & \lambda_3 \end{bmatrix}, \tag{3.3}$$

where $\mu_\pm = \lambda_1 e^{\pm i\theta}$. Note that τ_3 does not appear in the eigenvalues but only in the eigenvectors. The dynamical map parameters (restricted by complete positivity) are uniformly sampled and plotted on the left panels of Figures 6 and 7.

To make a comparison with the more general class of dynamical maps in [77], we consider a minimal breaking of the phase-covariance through the introduction of a new parameter λ_2,

$$\Lambda_{\rm PC} \xrightarrow[\rm PC]{\rm Break} \begin{bmatrix} 1 & 0 & 0 & 0 \\ 0 & \lambda_1 \cos\theta & -\lambda_2 \sin\theta & 0 \\ 0 & \lambda_1 \sin\theta & \lambda_2 \cos\theta & 0 \\ \tau_3 & 0 & 0 & \lambda_3 \end{bmatrix}. \tag{3.4}$$

The eigenvalues of the non-phase-covariant map are

$$\mu_\pm = \frac{(\lambda_1 + \lambda_2)\cos\theta \pm \sqrt{(\lambda_1 + \lambda_2)^2 \cos^2\theta - 4\lambda_1\lambda_2}}{2}. \tag{3.5}$$

The dynamical map parameters are uniformly sampled (again restricting to complete positivity) and the eigenvalues of the non-phase-covariant ensemble are plotted on the

right panels of Figures 6 and 7. This simple breaking of phase covariance introduces additional structure seen in Figure 6 (right), several of which match those in Figure 1 of the slightly more general treatment of [77]. For example, there is agreement in the empty parts of the plane, and the apparent 'repulsion' of the points away from the real axis. Note also that a significant number of $\mu_\pm$ eigenvalues become real when phase covariance is broken.

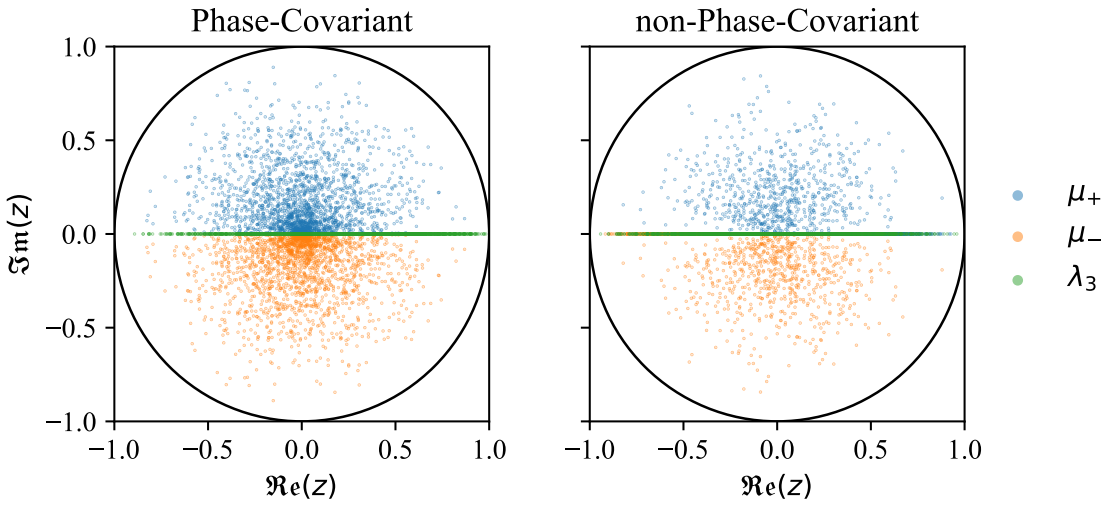

Figure 3.6: The distribution of eigenvalues, $\mu_\pm$, λ_3, for a non-unital phase-covariant ensemble (left) and non-unital non-phase-covariant ensemble (right) in the complex plane.

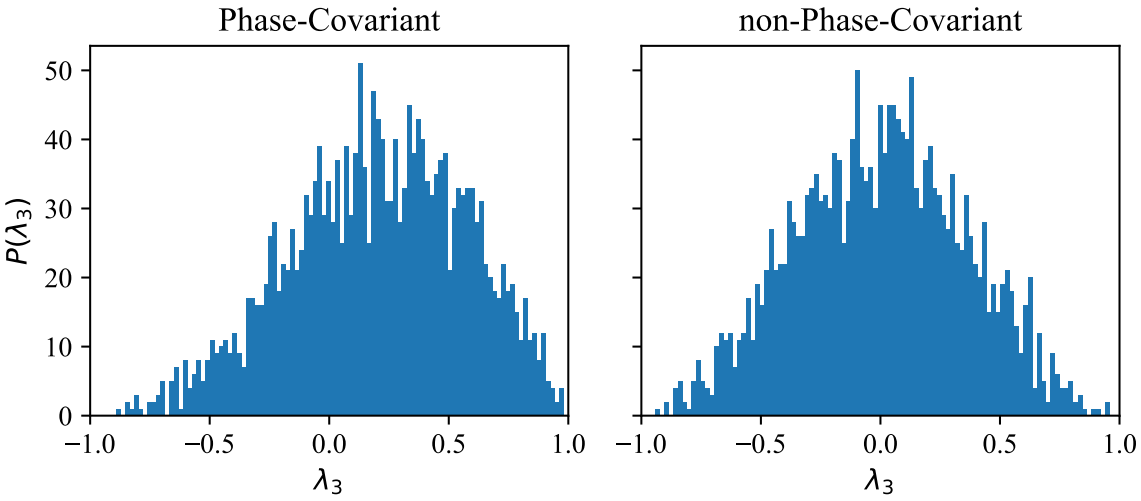

Figure 3.7: Plotted are histograms of the distribution of the eigenvalue, λ_3, for a non-unital phase-covariant ensemble (left) and non-unital non-phase-covariant ensemble (right).

Finally, we end by defining the uniform distribution over phase-covariant channels

$$vol\Big(\Gamma_{\mathrm{PC}}\Big) = vol\Big(\Gamma^{+}_{\mathrm{PC}}\Big) + vol\Big(\Gamma^{-}_{\mathrm{PC}}\Big) = \Big(\frac{16}{9} - \frac{\pi}{6}\Big) + \frac{\pi}{6} = \frac{16}{9} \tag{3.6}$$

where we have separated the integral into two regions based on the sign of λ_3. The positive region has a larger volume than that of the negative region, which is confirmed in Figure 7 (left). Therefore when sampling the phase-covariant channels using a uniform distribution, we expect there to be a bias towards positive λ_3. Our results are consistent with, although scaled differently from, those found in [81].

3.6.2 Example distribution: Truncated-Gaussians

There are of course many other non-uniform distributions to use to define a phase-covariant measure, and making an appropriate choice allows one to more easily capture the behavior of the long time average channels determined in Section 2. Although a time-dependent uniform distribution could be used, this is a more difficult to define from the data gathered from the average and late-time fluctuations. Ostensibly, the results of Section 4 indicate that using truncated Gaussian distributions could be a fruitful approach. We consider phase-covariant measures defined in this way for the remainder of this section.

A truncated Gaussian distribution over a single random variable (X) is given by

$$p_{\mathrm{TG}}(X;\vec{\eta}) = \frac{e^{-\frac{(X-\mu)^2}{2\sigma^2}}}{\mathcal{N}(\vec{\eta})} \tag{3.7}$$

where $\vec{\eta}$ stands in for the parameters of the distribution and $\mathcal{N}$ is the normalization factor

$$\mathcal{N}(\vec{\eta}) = \int_a^b e^{-\frac{(X-\mu)^2}{2\sigma^2}} dX\,. \tag{3.8}$$

There are four total parameters associated to a two-sided truncated Gaussian, the mean parameter (μ) , the scale parameter (σ), and the end points of the interval that define the truncation. For our purposes the end points of each distribution are set by the complete-positivity constraints. For example the truncated Gaussian associated with λ_3 may take values between -1 and 1, while the other distributions have intervals depending on the values of λ_3.

The remaining parameters we set through the use of the physical constraints found in the previous section. For example the scale parameter (assumed real) takes the form

$$\sigma = \frac{C}{N}\frac{t_{\mathrm{ref}}}{t}\,, \tag{3.9}$$

where the constant C is $O(1)$. We define the mean of each parameter by

$$\begin{aligned} \mu_1(N) &= \overline{\lambda}_1^{\infty}(N) = 0 \\ \mu_\lambda(N) &= \overline{\lambda}_3^{\infty}(N) \\ \mu_\tau(N) &= \overline{\tau}_3^{\infty}(N)\,, \end{aligned} \tag{3.10}$$

where we have seen that $\mu_\lambda \approx a_0$ and $\mu_\tau \approx (1-a_0)\overline{z}$ are approximations that are valid for a non-empty set of initial states. Notice that these parameters do not correspond to the mean and variance of the truncated Gaussians, and in general they will be larger than these values.

In order to construct instances of these distributions and how they change over time we use the following procedure. First, we choose a sampling time, set by the time-scale $t_{\mathrm{ref}} = t_J = \frac{2\pi}{J_\perp}$. We then sample the distribution $p_{\mathrm{TG}}(\lambda_3, \vec{\eta}_3)$ at each time step, where the scale parameter is changed according to Eq.(3.9). In this way we obtain an ordered list of values that λ_3 during each time-step. From these values of λ_3, we may construct the distribution $p_{\mathrm{TG}}(\tau_3, \vec{\eta}_\tau)$, as recall the end-point parameters for a given time-step depend explicitly on obtained values of λ_3. The procedure then carries on in the same

manner as for λ_3, a successive list of values for τ_3 are generated for each time-step. Finally, using the outcomes of the previous steps a list of values for λ_1 may be generated from the distribution $p_{\mathrm{TG}}(\lambda_1, \vec{\eta}_1)$. Figure 8 illustrates the results of this procedure. One could define a smaller sampling time, as it is clear that the sampling procedure does not capture the smaller scale fluctuations. However, these fluctuations do not carry additional physical information about the convergence toward the steady channel, for single-qubit dynamics, at least.

Care must be taken into the above procedure, as the endpoints for the distribution over τ_3 depends explicitly on the sign of λ_3. One way around the potential issues is to simply take the τ_3-interval to be set by the sign of the late-time limit of λ_3. This guarantees that at late-enough times, no positivity breaking occurs. Of course one may just consider the sign of λ_3 in the above procedure and take care to use the correct interval for τ_3 at a given time-step.

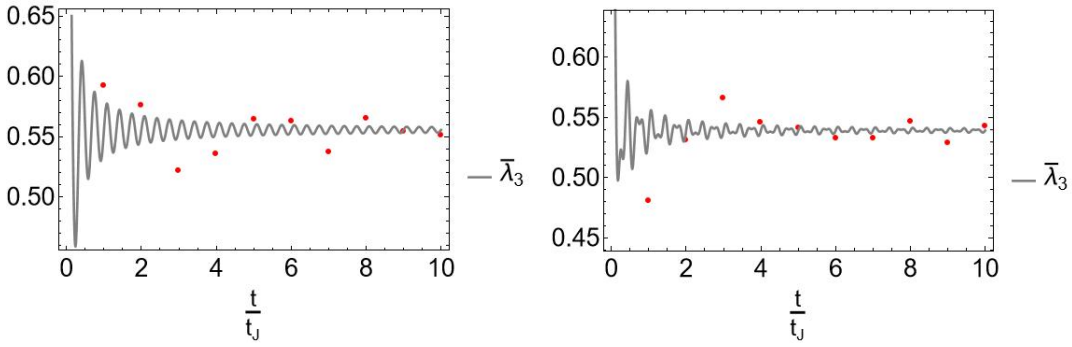

Figure 3.8: The time and network averaged $\lambda_3(t)$ are plotted for the completely-connected XXZ-cluster with $N = 3$ and $N = 5$, assuming each is in their respective hierarchical initial states. Additionally, there are instantiations of the time-dependent truncated Gaussians plotted, given by the red dots within each plot. As expected, at small $\frac{t}{t_J}$ the distribution fails to capture the dynamics, but better approximates the dynamics as $\frac{t}{t_J} \to \infty$.

3.7 Conclusions

In this work we have defined phase-covariant ensembles in two different ways. The first approach was to construct ensembles directly from a time-independent Hamiltonian, and consider the individual reduced dynamics for all possible subsystems of the smallest size. We constructed examples where each dynamical map in the ensemble was phase-covariant, and examples where only the network averaged reduced dynamics was phase-covariant.

From these examples, we are able to conjecture the form of the map parameters in terms of the initial state and connectivity, as shown in Eq.(3.25) and Eq.(3.26) for completely connected maps and Eq.(3.28) and Eq.(3.29) for one-dimensional rings with only nearest neighbor interactions. While we are unable to conjecture the general form of the long-time average for the ring connectivity, we do see that in general only the translation symmetry should be imposed.

The resulting time-independent, phase-covariant channels generate a notion of thermalization associated with each Hamiltonian and initial state, since under many repeated applications of the steady channel, every single-spin state will be driven toward the Gibbs state associated with $\beta_* = \log\left[\frac{2}{1-\overline{a}_*^\infty}\right]$, where $\overline{a}_*^\infty = \frac{\overline{\tau}_3^\infty}{1-\overline{\lambda}_3^\infty}$. The repeated application of such maps has also found a role in the simulation of open quantum systems [91], although so far restricted to systems described by stationary Lindblads. Our results may open up a similar route to efficient simulation of a broader class of open systems. This is especially interesting as quantum simulators may have an exponential advantage for simulating open-system evolution [92]. The procedure in Section 5 could be used in this direction.

The phase-covariant dynamics of 1-qubit subsystems do not seem to differ based on the integrable vs. non-integrable nature of the spin-chain Hamiltonian considered. In principle, such a characterization should be crucially important in determining the nature of a random distribution over channels, similar to how it constrains the form of random unitary dynamics in various large systems. It will be interesting to expand this study to both larger subsystems and more explicit breaking of phase-covariance.

Chapter 4
Emergent Quantum Subsystems

4.1 Preamble

This chapter is a reprint of [93]. In this chapter we explore the idea of quantum subsystem emergence. We find this to be an important aspect of any effective theory of open system, as the subsystems found in nature are not arbitrary and often the boundaries found are set by dynamical features, such as the form of the metric etc. But what mechanisms can be responsible for the appearance of physical subsystems? We further explore the ideas developed in [94–96], where they leveraged the geometry of the space of unitary operators to deduce a subsystem structure. Here we explore further the action principle that determines the metric or geometry over the space of unitary operators of a quantum system.

4.2 Introduction

Although the notion of emergent gravity has been studied from a variety of perspectives[1], a simpler but still illuminating question to consider is the emergence of locality. A formal structure to pose that question, at least for toy systems described by large, finite-dimensional quantum systems, was recently suggested by Freedman and Zini [103–105]. They introduced functionals of geometry on the evolutionary operators of high-dimensional quantum systems and asked whether the geometries that minimize those functionals correspond to dynamics of a many-body quantum system with a notion of local interactions. The tools to answer this question are inner products on the Lie algebra $\mathfrak{su}(N)$, corresponding to left-invariant metrics on the associated manifold of the

[1] A non-exhaustive list of examples includes [97–102].

Lie group $SU(N)$ [106–108]. Those inner products, or metrics, can be used to construct probability distributions over Hamiltonians that give preference to different classes of dynamics on a Hilbert space of dimension N.

Here, we expand in two technical ways on the examples considered in the original statement of this program [103]. First, we consider a new set of geometrically motivated loss functionals which have critical points corresponding to a qubit structure decomposition. Reference [103] labeled critical points of that type as KAQ since they 'know about qubits'. Motivated by the critical point structure of the Ricci scalar, we consider loss functions built from higher-order curvature terms. The exact equations of motion for such actions already exist in the literature [109–112]. Secondly, we provide a construction for classes of KAQ metrics that generalize those recovered in [103] and originally found in [113]. We use this construction as an ansatz for critical points of our loss functionals. In this way we are able to determine potential KAQ critical points in the space of our ansatz metrics, which then may be checked against the equations of motion. We do not need to search in the full space of left-invariant metrics, we only need to search in the exponentially reduced space of our ansatz KAQ metrics. Although still numerically intensive, this is a promising approach to apply to systems larger than those we treat in this article.

In the rest of this section, we lay out in more detail the statement of the problem and the tools to be used, including the new loss functionals. Section 4.3 then describes in detail the parameterizations of KAQ metrics we find useful. In Section 4.4 we present the equations of motion that must be solved to find critical points and apply the parameterizations to find new critical points, presented in Section 4.5. We conclude with implications and further directions in Section 4.6.

4.2.1 Distributions over Hamiltonians

Rather than searching for some dynamics that picks out a specific Hamiltonian, it is natural to ask for a distribution over Hamiltonians that assigns a higher likelihood to a particular class with interesting behavior. A simple and familiar choice for a distribution over dynamics of a quantum system of dimension N is the Gaussian Unitary Ensemble [114, 115], where each independent real number of the $N \times N$ Hermitian matrix that defines the Hamiltonian, H, is independently drawn from a Gaussian distribution. Equivalently,

$$\rho_{\mathrm{GUE}}\Big(H\Big) \propto e^{-\mathrm{tr}\Big(H^2\Big)} \,. \tag{4.1}$$

This distribution is invariant under unitary transformations, $H \to UHU^\dagger$ (as is clear from the cyclic property of the trace). It does not give preference to Hamiltonians that have the many-body local structure typical of spin systems frequently observed in nature, where the many entries in the large matrix H that correspond to interactions among nearly all the degrees of freedom would be suppressed. A different distribution that would support a many-body local structure when $N = 2^d$ would, for example, have a basis constructed from Pauli words for qubits, $\otimes_{i=1}^{d} \sigma_i^{(J)}$, where each $\sigma^{(J)}$ is any of the Pauli matrices or the 2×2 identity. A choice of weights assigned to operators in this basis could define a distribution favoring some subset of operators, for example words of shorter length (measured by the number of non-identity Pauli matrices).

To formalize distributions that are different from GUE, consider the set of inner products on the space of operators, which for quantum systems with Hilbert space of dimension N is the algebra $\mathfrak{g} = \mathfrak{su}(N)$. The Lie algebra comes equipped with the Lie bracket, but the bracket itself does not assign an inner product. The GUE arises from the most symmetric choice of metric, given by the Killing form $K : \mathfrak{g} \times \mathfrak{g} \to \mathbb{C}$, which defines a map that is invariant under a basis change. Using K defines the Killing-Cartan metric for X, Y elements of the algebra

$$\delta(X, Y) \equiv \mathrm{tr}\Big(\mathrm{ad}X * \mathrm{ad}Y\Big)\,, \tag{4.2}$$

where $\mathrm{ad}X$ is the map defined by $\mathrm{ad}X(Y) = [X, Y]$ for all Y. General inner products on the algebra correspond to left-invariant metrics on the group manifold for $G = SU(N)$, while the Killing-Cartan metric is special in that it is both left and right invariant i.e. bi-invariant. Although from the manifold point of view one can imagine more complex metrics that depend on some choice of coordinates, the set of left-invariant metrics is sufficient for constructing a larger class of distributions over Hamiltonians. The more general distributions over Hamiltonians can be written

$$\rho_{\mathrm{FZ}}(H) \propto e^{-g(H,H)} \tag{4.3}$$

where g is a strictly left-invariant metric over $SU(N)$. To construct a left-invariant metric, one need only supply its value over the Lie algebra. This is equivalent to supplying the Lie algebra with an inner product i.e.

$$\langle \cdot, \cdot \rangle : \mathfrak{g} \times \mathfrak{g} \to \mathbb{C} \tag{4.4}$$

which may be propagated to the rest of the Lie group through use of the differential of left-multiplication [106]. Defining the metric in this way guarantees that it is indeed left-invariant. For a left-invariant metric to be bi-invariant, its associated inner product must be $\mathrm{ad}_{\mathfrak{g}}$ invariant i.e.

$$\langle [\mathcal{O}, A], [\mathcal{O}, B] \rangle = \langle A, B \rangle \tag{4.5}$$

holds for all $\mathcal{O}, A, B \in \mathfrak{su}(N)$. In Section 4.3 we construct several classes of strictly left-invariant metrics, and one may demonstrate they are strictly left-invariant by finding any particular $\mathcal{O}$ for which Eq.4.5 fails to hold.

In fact the Killing-Cartan geometry is the only bi-invariant geometry over SU(N) (up to overall scale) and so considering strictly left-invariant geometries allows for more structure. Left-invariant metrics can be distinguished using their principal axes, which correspond to the elements of the orthonormal basis (X_a) of an associated inner product. These operators are orthonormal in the sense that $\langle X_a, X_b \rangle = \delta_{ab}$ where δ_{ab} is the Kronecker delta and the indices take values between 1 and $4^d - 1$. In general, the orthonormal basis of an inner product produces a non-holonomic or non-coordinate basis over the manifold since the structure constants $(C^c{}_{ab}\ )$ are non-zero. Recall that the structure constants of a basis are given by

$$[X_a, X_b] = \sum_c C^c{}_{ab} X_c \,. \tag{4.6}$$

Therefore, one may not use the standard formulas from general relativity when computing curvature functionals. For example, in a non-holonomic basis the Christoffel connection picks up a term proportional to the structure constants. See Appendix C.1 for all relevant formula of the curvature functionals expressed in a non-holonomic basis.

4.2.2 Many-body dynamics via preferred geometries

Although one can construct any distribution over Hamiltonians by hand, it is interesting to ask if there may be a geometrical means of picking out interesting classes, which perhaps could be dynamically realized as a spontaneous symmetry breaking process that fragments a large "single-particle" quantum system into an ensemble of small quantum systems interacting in a way that resembles local, many-body physics. Freedman and Zini [103–105] considered a family of functionals of the group geometry, parameterized by the metric and the structure constants, and explored whether the minima of these functionals select out KAQ metrics.

Here, we explore this idea a bit further by looking at functionals $\mathcal{L}[g]$ that are natural on the group manifold, defined by the set of two-derivative curvature tensors

$$\begin{aligned}\mathcal{L}[g] &= R + \alpha R^2 + \beta R_{ab}R^{ab} + \gamma R_{abcd}R^{abcd} \\ &= R + \alpha\mathcal{R}_0 + \beta\mathcal{R}_2 + \gamma\mathcal{R}_4\,.\end{aligned} \tag{4.7}$$

The critical points of just the Ricci scalar, R, were first studied by [113], and the same results were recovered by [103]. The larger class of functionals in Eq.(4.7) is especially tractable to study since the conditions for a metric to be a critical point are already known [112, 116]. We return to this in Section 4.4. While [103] used numerical techniques to find all critical points of some loss functionals and then determine if they corresponded to KAQ or non-KAQ metrics, we take a different approach and instead explore whether or not KAQ metrics occur as critical points (and ideally minima) of an expanded set of loss functions. To do so, we next introduce parameterizations of KAQ metrics, including generalizations of those that correspond to the KAQ critical points found in [113] for $\mathcal{L}[g] = R$. This allows us to explore the structure and properties of the KAQ metrics in more detail, although with the drawback that we cannot determine the relative frequency of KAQ vs non-KAQ minima.

4.3 KAQ parameterization schemes

Among the $\binom{N+1}{2}$ distinct metrics on $SU(N)$, only some will have a structure that is compatible with a tensor product decomposition into d qubit operators when $N = 2^d$. This notion can be expanded to apply to tensor decompositions of more general large N spaces that can include factors of dimension other than two (qudits) [104, 105]. The KAQ property of a metric g is decoded from its (possibly non-unique) principle axes. An observable E_a is said to be a principle axis of the metric if

$$g^a{}_b E_a = \lambda_b E_b \tag{4.8}$$

that is E_a is an eigenvector of the tensor $g^a{}_b = g_{cb}\delta^{ca}$, where δ_{ab} is the Killing-Cartan metric. The location of indices in the previous equation matter; they are chosen so that we may compute eigenvectors. Later on we compute only the components of tensors in an orthonormal basis of the metric, therefore placement of indices becomes essentially irrelevant. In Eq.4.8 the index placement is relevant, as we require a tensor that maps vectors to vectors.

The principal axis $\{E_a\}$ need only be orthogonal, hence the need for a distinct from an orthonormal basis which are denoted by $\{X_a\}$. A left-invariant (but not bi-invariant) metric is said to be KAQ if $\mathbf{a}$ basis of principal axis exist such that

$$\begin{aligned} \Phi[E_a] &= \sigma_1^{(a_1)} \otimes ... \otimes \sigma_d^{(a_d)} \\ [E_a, E_b] &= \mathcal{P}^c{}_{ab} E_c \end{aligned} \tag{4.9}$$

where Φ is a Lie algebra isomorphism i.e. a bijective linear map which preserves commutation relations and the tensors $\mathcal{P}^c{}_{ab}$ are the structure constants of $\mathfrak{s}\Big(\mathfrak{u}(2)^{\otimes d}\Big)$, the Lie algebra $\mathfrak{u}(2)^{\otimes d}$ with the generator $\mathbb{1}^{\otimes d}$ removed. While our definition is slightly different than that given in [103], they are in fact equivalent. Taking a given Pauli word to a linear combination requires using unitary conjugation which will not affect commutation relations. It is important to stress that the metric will typically have many possible bases of principle axes, and only one needs to satisfy the KAQ condition. Furthermore, among that restricted set of KAQ metrics, not all will generate many-body local dynamics by suppressing the contributions from Pauli words with length close to d.

The degeneracy pattern of metric determines the freedom there is in choosing a KAQ basis. In the case of no degenerate eigenvalues, the metric is KAQ iff all principal axes already align with some Pauli word basis. This is clearly a special case. More generally, a degenerate eigenspace may be decomposed into a basis that aligns with Pauli words, although some "decoding" may be required. Decoding here means that the degenerate principal axes are mixed using an element of $SO(4^d - 1)$ which is not an inner automorphism of $\mathfrak{su}(2^d)$. Such transformations keep distinct degenerate axis orthogonal, but they do not preserve commutation relations. Later in this section we give an explicit example of such a decoding process, where we demonstrate that Gell-Mann matrices may serve the role of a KAQ basis for certain metrics.

An obvious structure to make use of in searching for KAQ metrics is the $\mathfrak{so}(2^d)$ subalgebra of $\mathfrak{su}(2^d)$, which one might expect contains a set of axes decodable to the length-one Pauli words, the single-qubit operators [117]. In the case of $\mathfrak{su}(4)$, the construction is simple: if one starts with the natural basis of Gell-mann matrices, the single-qubit operators can be recovered by identifying linear combinations of matrices in the sub-algebra that have a tensor product form and then making a rotation to align those linear combinations with length-one Pauli words. On the other hand, the other obvious subalgebra decomposition, $\mathfrak{sp}(2^{d-1})$, contains degenerate subspaces that must align with Pauli word basis, and others which may require decoding. Operationally, we consider this case in detail below to illuminate the relationship between known critical

points of the Ricci scalar, which carry this subgroup structure, and critical points with KAQ structure.

In order to construct parameterizations of KAQ metrics, which can then be used as ansatze for critical metrics, we use the fact that a left-invariant metric over a Lie group is entirely specified by an inner product over the corresponding Lie algebra. In this way instead of referring to the metric, one may just as well refer to an orthonormal basis of the associated inner product. For excellent reviews of the Lie algebra and geometric background needed for these constructions, see [106–108].

4.3.1 Riemannian geometry of compact symmetric Lie algebras

Consider first the Killing-Cartan geometry naturally available to SU(4). It is the unique (up to scale) bi-invariant geometry over the special unitary group, and describes color dynamics (in 0+1 dimensions) mediated by 15 gluons. The generalized Gell-Mann matrices, G_a provide an orthonormal basis, where we use the definitions provided in [118]. However, we include an additional factor of i in our construction of generalized Gell-Mann matrices therefore taking them to be anti-Hermitian operators. This is more in keeping with standard notation in differential geometry. We further consider a non-standard normalization

$$\mathrm{tr}\Big(G_a^\dagger G_b\Big) = \frac{1}{2}\delta_{ab}\,, \tag{4.10}$$

which will enter the structure constants

$$[G_a, G_b] = K^c{}_{ab} G_c\,. \tag{4.11}$$

Denoting K_a as the matrix of structure constants with entries $K^c{}_{ab}$ in the Gell-Mann basis we then have

$$\mathrm{tr} K_a K_b = -4\delta_{ab} \tag{4.12}$$

and bi-invariance implies that $K_a^{\mathrm{T}} = -K_a$ i.e. the structure constants are totally anti-symmetric. This equation is negative definite due to the compactness of the special unitary group. The normalization choice here leads to a convenient normalization later on in the loss functionals, where the Ricci scalar takes the value $R = 15 = N^2 - 1$ when evaluated over the Killing-Cartan geometry.

The Killing-Cartan geometry serves the role of a simple fiducial metric, as well as the assumed unstable starting point for spontaneous symmetry breaking. Instead of studying a more complicated left-invariant metric directly, one may look at the linear

transformation (ω) relating one of its orthonormal bases to that of the Killing-Cartan geometry [113]. The transformation ω is required to fix the determinant, which we impose in order to use the equations of motion referenced in Section 4.4. The linear transformation is related to the metric when expressed in the Gell-Mann basis as $g = \omega^{-2}$. One may check such transformation certainly maps Gell-Mann letters to an orthonormal basis of g.

Assume we have related a new orthonormal basis to the Gell-Mann matrices by a special linear transformation $\tilde{G}_a = \sum_a \omega_{ab} G_b$. Then the structure constants are related by

$$\tilde{K}_a = \sum_b \omega_{ab} [\omega^{-1} K_b \omega] \,, \tag{4.13}$$

where K_b is the matrix with kjth entry K^k_{bj}. For these calculations the location of an index (up or down) is unimportant, as the metric is always an identity matrix. The preceding equation makes explicit the matrix multiplication that must be performed to determine the new structure constants. That is, the transformation law may be written equivalently as

$$\tilde{K}^c{}_{ad} = \tilde{K}_{cad} = \sum_{bef} \omega_{ab} \omega^{-1}_{ce} K_{ebf} \omega_{fd} \,. \tag{4.14}$$

The utility is that now curvature functions may be expressed in terms of Killing-Cartan tensor networks, where the total anti-symmetry can be leveraged.

We shall end with a final bit of notation, which simplifies the construction of KAQ metrics. As the metrics are considered over the Lie algebra, it is helpful to use the adjoint representation (ad$\mathfrak{g}$). Here observables themselves become operators acting over $\mathfrak{g}$. For example, we can define kets from the Gell-mann matrices $G_a \in \mathfrak{su}(2^d)$, denoted $|G_a\rangle$. We then define dual vectors with respect to the Killing-Cartan metric i.e.

$$\langle G_b| \equiv 2\mathrm{tr}\left[G_b^\dagger(\cdot)\right] \,. \tag{4.15}$$

Defined in this way $\{|G_a\rangle\}$ is an orthonormal basis of $\mathfrak{g}$, with inner product $\langle G_a|G_b\rangle = \delta_{ab}$. Projectors are defined in the standard way

$$\Pi_a = |G_a\rangle\langle G_a| \,, \tag{4.16}$$

and the action of the observables becomes (4.11)

$$\mathrm{ad}G_a|G_b\rangle = K_a|G_b\rangle = |[G_a, G_b]\rangle = \sum_c K_{cab}|G_c\rangle\,. \tag{4.17}$$

We also obtain a matrix representation for the action of any metric over $\mathfrak{g}$. For example the linear transformation ω takes the form

$$\omega = \sum_{ab} \omega_{ab}|G_a\rangle\langle G_b| \tag{4.18}$$

where $\omega_{ab} = \omega_{ba}$ and $\omega_{ab} \in \mathbb{R}$.

4.3.2 Jensen geometries over SU(4)

In [113] the author searched for the critical points of the Ricci scalar curvature (R) in the space of left-invariant metrics with fixed determinant. It was shown that for unimodular Lie algebras ($\mathrm{tr}\,[C_a] = 0$), Einstein metrics are precisely the critical points of R. While the proof was not constructive for general unimodular Lie groups, by specializing the author was able to construct several classes of Einstein metrics, now called Jensen metrics. These were found over symmetric Lie algebras i.e. those Lie algebras with at least one Cartan decomposition. The Cartan decomposition plays a crucial role in forming the ansatz metric used in [113] to find Einstein metrics. Further exploring the algebraic structures of these decompositions is an interesting point we return to later. We find it useful to first explore the algebraic properties of Jensen metric through explicit constructions of two classes relevant for this work.

Further assuming that the manifold is compact guarantees the existence of a strictly left-invariant Einstein metric. The Lie algebra $\mathfrak{su}(4)$ is compact and symmetric. Thus it may be Cartan decomposed into a subalgebra and its orthogonal complement with respect to the Killing-Cartan form, allowing for non-trivial Ricci critical metrics. There are two inequivalent ways to do this, corresponding to the two non-isomorphic subalgebras $\mathfrak{so}(4)$, and $\mathfrak{sp}(2)$ the compact symplectic Lie algebra.

The heart of the Cartan decomposition is to break the Lie algebra into the subalgebra and the orthogonal complement with respect to the Killing-Cartan form. That is, given a subalgebra $\mathfrak{R} \subset \mathfrak{g}$ we decompose $\mathfrak{g}$ as

$$\mathfrak{g} = \mathfrak{R} \oplus \mathfrak{M} \tag{4.19}$$

where $\delta(A, B) = 0$ for all $A \in \mathfrak{K}$ and $B \in \mathfrak{M}$. We say the pair $(\mathfrak{g}, \mathfrak{K})$ forms a Cartan decomposition if the following are satisfied

$$[\mathfrak{K}, \mathfrak{K}] \subseteq \mathfrak{K}\,, \quad [\mathfrak{K}, \mathfrak{M}] \subseteq \mathfrak{M} \ \text{, and} \quad [\mathfrak{M}, \mathfrak{M}] \subseteq \mathfrak{K}\,. \tag{4.20}$$

The commutation relations above are equivalent to the existence of a certain kind of Lie algebra isomorphism, known as the Cartan involution (θ). Explicitly a Cartan involution is a Lie algebra automorphism $\theta : \mathfrak{g} \to \mathfrak{g}$ such that [119]

$$\theta = \begin{bmatrix} \mathbb{1}_r & 0 \\ 0 & -\mathbb{1}_m \end{bmatrix} \tag{4.21}$$

where $r = \dim\mathfrak{K}$ and $m = \dim\mathfrak{M}$. In what follows we construct the two types of Jensen metrics that exist for $\mathfrak{su}(4)$. To do so, we construct the transformation ω, which takes an orthonormal basis of the Killing-Cartan metric to an orthonormal basis of the given critical metric. These transformations are generated by the symmetric, traceless operator

$$B = \begin{bmatrix} \frac{1}{r}\mathbb{1}_r & \mathbf{0} \\ \mathbf{0} & -\frac{1}{m}\mathbb{1}_m \end{bmatrix} \tag{4.22}$$

yielding the linear transformation

$$\omega = \exp \tau B\,. \tag{4.23}$$

The metric corresponding to $\omega(\tau)$ is a non-trivial critical point of the Ricci scalar iff

$$\tau = \frac{rm}{2(r+m)} \ln \frac{2r+m}{2r-m}\,. \tag{4.24}$$

These metrics are KAQ due to the following. First, the subalgebras which are pulled out for these two Cartan decompositions are generated by known sets of Pauli-words. This in conjunction with the large degeneracy in the Cartan blocks that ensures a KAQ basis may be defined. We do this explicitly in the next section.

Before moving to our more general sets of KAQ parameterizations, it is worth explaining the algebraic structures we leverage. To begin we simply note that the Jensen metrics have a reduced symmetry structure compared to the Killing-Cartan metric. Using the form of Jensen metrics, defined by Eq.(4.22)-Eq.(4.24), and the commutation relations, one may show that the Jensen metrics are only bi-invariant with respect to $\mathfrak{K}$.

Thus since Jensen metrics are not ad$\mathfrak{g}$ invariant, they cannot support GUE dynamics. However the ad$\mathfrak{R}$ invariance allows for the creation of Gaussian ensembles over smaller sets of matrices. For example the $\mathfrak{so}(4)$ Jensen metric gives dynamics via the Ricci scalar where the GUE spontaneously breaks down to a model which approximates a lower dimensional Gaussian orthogonal ensemble (GOE),

$$\rho = \rho_{\mathrm{GUE}}(H^{(N^2-1)}) \rightarrow \rho \approx \rho_{\mathrm{GOE}}(H^{(N(N-1)/2)}) \,. \tag{4.25}$$

It does not exactly yield the GOE as there is a non-negligible probability for observables outside of the $\mathfrak{so}(4)$ subalgebra to contribute to the Hamiltonian. Similarly, the $\mathfrak{sp}(2)$ Jensen metrics generate an approximate Gaussian Symplectic Ensemble (GSE).

But there are other known examples of Einstein metrics over SU(N), which have more varied structure than Jensen metrics. Most of these metrics are naturally reductive like the Jensen metrics. Naturally reductive metrics are more general than Jensen metrics, but they remain ad$\mathfrak{R}$ invariant. The more varied structure is obtained by decomposing the Lie algebra further, isolating certain algebraic structures of $\mathfrak{R}$. Given a Lie algebra with an orthogonal (but not necessarily Cartan) decomposition, one further decomposes it as

$$\mathfrak{g} = \mathfrak{R} \oplus \mathfrak{M} = \mathfrak{C} \oplus \mathfrak{I}_1 \oplus ... \oplus \mathfrak{I}_q \oplus \mathfrak{M} \tag{4.26}$$

where $\mathfrak{C}$ is the center of $\mathfrak{R}$ ($[\mathfrak{C}, \mathfrak{R}]$=0) and $\mathfrak{I}_i (i > 0)$ are simple ideals satisfying

$$[\mathfrak{R}, \mathfrak{I}_i] \subset \mathfrak{I}_i \,. \tag{4.27}$$

Using this decomposition, a general form of naturally reductive metrics is given in [120],

$$\langle \, | \, \rangle = \langle \, | \, \rangle_{\mathfrak{C}} + \lambda_1 \mathbb{1}_{\mathfrak{I}_1} + ... + \lambda_q \mathbb{1}_{\mathfrak{I}_q} + \mu \mathbb{1}_{\mathfrak{M}} \tag{4.28}$$

where $\langle \, | \, \rangle_{\mathfrak{C}}$ is a general inner product over $\mathfrak{C}$, and λ_i and μ are non-negative. The authors used these parameterization to find examples of naturally reductive (non-Jensen) Einstein metrics, which are also critical points of R. The critical points of R found in [103–105] were only of Jensen type. We find evidence later for why the non-Jensen type critical points were not found during the evolutionary search done by Freedman and Zini.

It has recently been shown that non-naturally reductive Einstein metrics exist over $SU(N)$ [121], but we do not yet know how large the overlap is with KAQ metrics. With that said, we shall also consider metric parameterizations which are non-naturally reductive. We motivate our construction by considering metrics with a reduced bi-

invariance compared with the Jensen metrics. That is we consider metrics which are bi-invariant with respect to a Cartan subalgebra of $\mathfrak{R}$. Explicitly we decompose the Lie algebra as

$$\mathfrak{g} = \mathfrak{R} \oplus \mathfrak{M} = \mathfrak{R}_0 \oplus \mathfrak{R}_1 \oplus ... \oplus \mathfrak{R}_q \oplus \mathfrak{M} \tag{4.29}$$

where $\mathfrak{R}_0$ is a Cartan subalgebra of $\mathfrak{R}$, and $\mathfrak{R}_i$ are subspaces satisfying

$$[\mathfrak{R}_0, \mathfrak{R}_i] \subset \mathfrak{R}_i \,. \tag{4.30}$$

Using this decomposition we define the following metrics

$$\langle \, | \, \rangle = \langle \, | \, \rangle_{\mathfrak{R}_0} + \lambda_1 \mathbb{1}_{\mathfrak{R}_1} + ... + \lambda_q \mathbb{1}_{\mathfrak{R}_q} + \mu \mathbb{1}_{\mathfrak{M}} \tag{4.31}$$

where $\lambda_i, \mu > 0$. It is simple to show these metrics are indeed ad$\mathfrak{R}_0$ invariant using the preceding commutation relations.

4.3.3 Cipher classes

In this section we introduce our KAQ parameterizations, which we break into cipher classes. These classes are distinguished by the existence of non-isomorphic KAQ bases. A given cipher class will have a basis of principal axes that is mixed between Gell-Mann letters and Pauli words. The smallest of these classes are the untranslated KAQ (UKAQ) metrics. These metrics have a KAQ basis consisting entirely of Gell-Mann letters. Such metrics are the most difficult to decode the KAQ property. The next biggest class are the partially translated KAQ metrics (PKAQ), followed by the fully translated KAQ metrics (FKAQ). The FKAQ metrics only have KAQ bases consisting entirely of Pauli words, thus they require no decoding when checking the KAQ property. We have the inclusion relation

$$\mathbf{U}\text{KAQ} \subset \mathbf{P}\text{KAQ} \subset \mathbf{F}\text{KAQ} \,. \tag{4.32}$$

For what follows we assume the basis principal axes maps to pure tensor Pauli words i.e.

$$\Phi \left[\tilde{E}_a \right] = \sigma_{a_1} \otimes ... \otimes \sigma_{a_d} \tag{4.33}$$

where $\tilde{E}_a$ represents the bases of principal axes post possible decoding process. It is useful to introduce some additional notation for the generalized Gell-Mann matrices,

splitting them into three groups

$$\{G_a\} = \{\{iA_l\}, \{iS_l\}, \{iD_p\}\} \tag{4.34}$$

which are the anti-symmetric matrices, the off-diagonal symmetric matrices, and the diagonal matrices respectively. For a generic N these indices take values in

$$\begin{aligned} 1 \leq l \leq \binom{N}{2} \\ 1 \leq p \leq N-1 \end{aligned} \tag{4.35}$$

How we label the Gell-Mann matrices follows the notation from [118], although we use a different overall normalization.

4.3.3.1 Untranslated KAQ metrics

We consider first the class of untranslated KAQ metrics (UKAQ). As a natural example, we use generalizations of the $\mathfrak{so}(4)$ Jensen metrics that are considerably less degenerate. To begin the construction we choose an orthonormal basis of the Killing-Cartan metric. We define generalized $\mathfrak{so}(4)$ Jensen metrics as those with an orthonormal basis compatible with the involution $\theta[X] = -X^{\mathrm{T}}$, i.e. an orthonormal basis constructed from eigenvectors of θ. Notice that

$$\begin{aligned} \theta[A_l] &= A_l \\ \theta[S_l] &= -S_l \\ \theta[D_p] &= -D_p \end{aligned} \tag{4.36}$$

thus Gell-Mann letters are a good fiducial basis that can be used to construct generalized $\mathfrak{so}(4)$ Jensen metrics.

Now notice that the eigen-spectra of Gell-Mann letters do not match those of the Pauli words. Therefore it is impossible to relate these bases through unitary conjugation i.e. inner automorphism. But in order to serve as a basis of principal axes, a Lie algebra homomorphism to Pauli words must exist. See also [117, 122]. Having ruled out the existence of an inner automorphism (unitary conjugation) that accomplishes the translation to Pauli words, the only remaining isomorphisms are the outermorphisms. But the only non-trivial outermorphism of $\mathfrak{su}(n)$ is complex conjugation. Complex conjugation combined with unitary conjugation can never match the eigen-spectra of

Gell-Mann letters and Pauli words.

Therefore we need to be able to decode the Gell-Mann matrices for the constructed metrics to be KAQ. It is straightforward to show that they may serve as **a** basis of principal axis, so long as we assume certain degeneracy patterns exist in the metric. To elucidate this concept, we construct the following dictionary that translates Gell-Mann letters to Pauli words

$$\begin{aligned}
(A_1 + A_6) &= \frac{1}{2}\Big(\mathbb{1}_1 \otimes Y_2\Big), \quad (A_1 - A_6) = \frac{1}{2}\Big(Z_1 \otimes Y_2\Big) \\
(A_2 + A_5) &= \frac{1}{2}\Big(Y_1 \otimes \mathbb{1}_2\Big), \quad (A_2 - A_5) = \frac{1}{2}\Big(Y_1 \otimes Z_2\Big) \\
(A_3 + A_4) &= \frac{1}{2}\Big(Y_1 \otimes X_2\Big), \quad (A_3 - A_4) = \frac{1}{2}\Big(X_1 \otimes Y_2\Big).
\end{aligned} \tag{4.37}$$

We may further construct Pauli words from $\mathfrak{M}$

$$\begin{aligned}
(S_1 + S_6) &= \frac{1}{2}\Big(\mathbb{1}_1 \otimes X_2\Big), \quad (S_1 - S_6) = \frac{1}{2}\Big(Z_1 \otimes X_2\Big) \\
(S_2 + S_5) &= \frac{1}{2}\Big(X_1 \otimes \mathbb{1}_2\Big), \quad (S_2 - S_5) = \frac{1}{2}\Big(X_1 \otimes Z_2\Big) \\
(S_3 + S_4) &= \frac{1}{2}\Big(X_1 \otimes X_2\Big), \quad (S_4 - S_3) = \frac{1}{2}\Big(Y_1 \otimes Y_2\Big) \\
\left(D_1 - \sqrt{\frac{1}{3}}D_2 + \sqrt{\frac{2}{3}}D_3\right) &= \frac{1}{2}\Big(\mathbb{1}_1 \otimes Z_2\Big) \\
\left(D_1 + \sqrt{\frac{1}{3}}D_2 - \sqrt{\frac{2}{3}}D_3\right) &= \frac{1}{2}\Big(Z_1 \otimes Z_2\Big) \\
\left(0D_1 + \sqrt{\frac{4}{3}}D_2 + \sqrt{\frac{1}{3}}D_3\right) &= \frac{1}{2}\Big(Z_1 \otimes \mathbb{1}_2\Big).
\end{aligned} \tag{4.38}$$

Therefore it is possible for Gell-Mann letters to form a KAQ basis, so long as the metric has appropriate degeneracy patterns. These degeneracies are required to be able to translate Gell-Mann letters to Pauli words using more general maps than inner automorphisms. As an example consider A_1 and A_6. Their weights must be the same to construct the words E_1 and E_2. It is these considerations that lead us to the following

UKAQ metrics

$$\begin{aligned}\omega_{\text{UKAQ}}(\vec{r},\vec{m}) = e^{r_1}\Big(|A_1\rangle\langle A_1| + |A_6\rangle\langle A_6|\Big) + e^{r_2}\Big(|A_2\rangle\langle A_2| + |A_5\rangle\langle A_5|\Big) \\ + e^{r_3}\Big(|A_3\rangle\langle A_3| + |A_4\rangle\langle A_4|\Big) + e^{m_1}\Big(|S_1\rangle\langle S_1| + |S_6\rangle\langle S_6|\Big) \\ + e^{m_2}\Big(|S_2\rangle\langle S_2| + |S_5\rangle\langle S_5|\Big) + e^{m_3}\Big(|S_3\rangle\langle S_3| + |S_4\rangle\langle S_4|\Big) \\ + e^{-\Delta}\Big(|D_1\rangle\langle D_1| + |D_2\rangle\langle D_2| + |D_3\rangle\langle D_3|\Big),\end{aligned} \tag{4.39}$$

where we fix the determinant by setting $\Delta = \frac{2}{3}\sum_i(r_i + m_i)$. Now we may see that the UKAQ parameterization is compatible with a many-body structure. A physically interesting structure arises when

$$\begin{aligned} r_i &> 0 \\ m_i &< 0 \\ \Delta &\geq 0\,, \end{aligned} \tag{4.40}$$

where a many-body structure exists if an inner automorphism Φ_{MBP} exists mapping $\mathfrak{R}$ to the set of 1-string Pauli words. The inner automorphism for this example is constructed by the unitary

$$U_{\text{MBP}} = \exp\left[\frac{i\pi}{4} Y_1 \otimes Y_2\right] \tag{4.41}$$

which maps computational states to Bell states. Therefore, with a few assumptions about the singular values, we have shown that many-body KAQ metrics exist which generalize the $\mathfrak{so}(4)$ Jensen metrics. For further exploration in the more complex loss functionals, we make the simplifying assumption that $m_i = -\Delta$ and $r_2 = r_3$. This results in a class of $\text{ad}\mathfrak{R}_0$ invariant metrics

$$\begin{aligned}\Omega_{\text{UKAQ}}(t,s) = e^{\frac{t}{6}}\Big(|A_1\rangle\langle A_1| + |A_6\rangle\langle A_6|\Big) + e^{\frac{s}{6}}\Big(|A_2\rangle\langle A_2| + |A_5\rangle\langle A_5| + |A_3\rangle\langle A_3| + |A_4\rangle\langle A_4|\Big) \\ + e^{-\frac{t+2s}{27}}\Big(|S_1\rangle\langle S_1| + |S_6\rangle\langle S_6| + |S_2\rangle\langle S_2| + |S_5\rangle\langle S_5| + |S_3\rangle\langle S_3| + |S_4\rangle\langle S_4| \\ + |D_1\rangle\langle D_1| + |D_2\rangle\langle D_2| + |D_3\rangle\langle D_3|\Big)\end{aligned} \tag{4.42}$$

where $\mathfrak{R}_0$=span(A_1, A_6). Notice that $\Omega_{\text{UKAQ}}(t,t)$ corresponds to the class of $\mathfrak{so}(4)$ Jensen metrics, and all metrics off of this line are non-Jensen. We note this as over $\mathfrak{R}$ the metric contains two unequal weights whenever $t \neq s$.

4.3.3.2 Partially translated KAQ metrics

The partially translated or PKAQ metrics have a KAQ basis which is mixed between Gell-Mann letters and Pauli words. They will be simpler to decode than UKAQ metrics, but still require some work. A natural class of PKAQ metric structures appear from a generalization of the $\mathfrak{sp}(2)$ Jensen metrics. The KAQ basis in this case must be compatible with the involution $\theta[X] = \mathcal{J}X^{\mathrm{T}}\mathcal{J}$ where the matrix $\mathcal{J}$ is defined as

$$\mathcal{J} = \begin{bmatrix} 0 & \mathbb{1}_{2^{d-1}} \\ -\mathbb{1}_{2^{d-1}} & 0 \end{bmatrix} \tag{4.43}$$

A critical difference appearing for this choice of θ is that most Gell-Mann matrices are not eigenvectors. For example

$$\begin{aligned} \theta[A_1] &= -A_6 \\ \theta[A_6] &= -A_1 \end{aligned} \tag{4.44}$$

thus $\Big(A_1 - A_6\Big)$ is an eigenvector of θ that lives in $\mathfrak{R}$ and $\Big(A_1 + A_6\Big)$ is an eigenvector of θ that lives in $\mathfrak{M}$. So we must use an orthonormal basis of the Killing-Cartan metric that is mixed between Gell-Mann letters and Pauli words to be compatible with θ. Using the same dictionary, but a different Cartan decomposition, the Pauli words in $\mathfrak{R}$ are

$$\begin{aligned} (S_1 - S_6) &= \frac{1}{2}\Big(Z_1 \otimes X_2\Big), \quad (A_1 - A_6) = \frac{1}{2}\Big(Z_1 \otimes Y_2\Big) \\ (S_2 + S_5) &= \frac{1}{2}\Big(X_1 \otimes \mathbb{1}_2\Big), \quad (A_2 + A_5) = \frac{1}{2}\Big(Y_1 \otimes \mathbb{1}_2\Big) \\ (S_3 + S_4) &= \frac{1}{2}\Big(X_1 \otimes X_2\Big), \quad (S_4 - S_3) = \frac{1}{2}\Big(Y_1 \otimes Y_2\Big) \\ (A_3 + A_4) &= \frac{1}{2}\Big(Y_1 \otimes X_2\Big), \quad (A_3 - A_4) = \frac{1}{2}\Big(X_1 \otimes Y_2\Big) \\ D_1 - \sqrt{\frac{1}{3}}D_2 + \sqrt{\frac{2}{3}}D_3 &= \frac{1}{2}\Big(\mathbb{1}_1 \otimes Z_2\Big) \\ 0D_1 + \sqrt{\frac{4}{3}}D_2 + \sqrt{\frac{2}{3}}D_3 &= \frac{1}{2}\Big(Z_1 \otimes \mathbb{1}_2\Big), \end{aligned} \tag{4.45}$$

and the Pauli words constructed from $\mathfrak{M}$ are

$$\begin{aligned}
(S_1 + S_6) &= \frac{1}{2}\Big(\mathbb{1}_1 \otimes X_2\Big), \quad (A_1 + A_6) = \frac{1}{2}\Big(\mathbb{1}_1 \otimes Y_2\Big) \\
(S_2 - S_5) &= \frac{1}{2}\Big(X_1 \otimes Z_2\Big), \quad (A_2 - A_5) = \frac{1}{2}\Big(Y_1 \otimes Z_2\Big) \\
D_1 &+ \sqrt{\frac{1}{3}} D_2 - \sqrt{\frac{2}{3}} D_3 = \frac{1}{2}\Big(Z_1 \otimes Z_2\Big).
\end{aligned} \tag{4.46}$$

Each word constructed from the same pair of Gell-Mann letters living in different Cartan blocks must be pre-translated into the Killing-Cartan basis to be compatible with θ. For each of these pre-translated words, we may assign an independent weight in the metric. Only the pairs (S_3, S_4) and (A_3, A_4) have the same weights, as we do not require them to be translated to achieve the Cartan decomposition. We are thus lead to the following parameterization for generalized $\mathfrak{sp}(2)$ metrics

$$\begin{aligned}
\omega_{\mathrm{PKAQ}}(r_i, m_\alpha) = {} & e^{r_1}|Z_1X_2\rangle\langle Z_1X_2| + e^{r_2}|Z_1Y_2\rangle\langle Z_1Y_2| + e^{r_3}|X_1\rangle\langle X_1| + e^{r_4}|Y_1\rangle\langle Y_1| \\
& + e^{r_5}\Big(|S_3\rangle\langle S_3| + |S_4\rangle\langle S_4|\Big) + e^{r_6}\Big(|A_3\rangle\langle A_3| + |A_4\rangle\langle A_4|\Big) \\
& + e^{r_7}|Z_2\rangle\langle Z_2| + e^{r_8}|Z_1\rangle\langle Z_1| + e^{m_1}|X_2\rangle\langle X_2| + e^{m_2}|Y_2\rangle\langle Y_2| \\
& + e^{m_3}|X_1Z_2\rangle\langle X_1Z_2| + e^{m_4}|Y_1Z_2\rangle\langle Y_1Z_2| + e^{-\Delta}|Z_1Z_2\rangle\langle Z_1Z_2|
\end{aligned} \tag{4.47}$$

where again Δ is chosen such that $\det\Big(\omega_{\mathrm{PKAQ}}\Big) = 1$. Here we clearly see that a few principle axes are still untranslated, but there is far less translation to be done than in the UKAQ example. Note as well that there are many other ways to construct a PKAQ parameterization that are not compatible with the Cartan involution.

Again we take a simpler PKAQ parameterization for further investigation. We reduce to two parameters as this is the minimal number necessary to search for non-Jensen type critical points. We take the following non-naturally reductive $\mathrm{ad}\mathfrak{R}_0$ invariant parameterization

$$\begin{aligned}
\Omega_{\mathrm{PKAQ}}(t, s) = {} & e^{-\frac{3t+2s}{25}}\Big(|X_2\rangle\langle X_2| + e^{m_2}|Y_2\rangle\langle Y_2| + |X_1Z_2\rangle\langle X_1Z_2| + |Y_1Z_2\rangle\langle Y_1Z_2| + |Z_1Z_2\rangle\langle Z_1Z_2|\Big) \\
& + e^{\frac{t}{10}}\Big(|Z_1X_2\rangle\langle Z_1X_2| + |Z_1Y_2\rangle\langle Z_1Y_2| + |X_1\rangle\langle X_1| + |Y_1\rangle\langle Y_1| + |Z_2\rangle\langle Z_2| + |Z_1\rangle\langle Z_1|\Big) \\
& + e^{\frac{s}{10}}\Big(|S_3\rangle\langle S_3| + |S_4\rangle\langle S_4| + |A_3\rangle\langle A_3| + |A_4\rangle\langle A_4|\Big)
\end{aligned} \tag{4.48}$$

which is bi-invariant with respect to $\mathfrak{R}_0$=span(Z_1, Z_2). When $t = s$ the parametrization

reduces to that of $\mathfrak{sp}(2)$ Jensen metrics, therefore any critical points found along the line $t = s$ in the $t - s$ plane are Jensen metrics for the given parameterization. Otherwise the other metrics in the $t - s$ plane are all non-Jensen.

4.3.3.3 Fully translated KAQ metrics

The final cipher class we consider is the class of fully translated KAQ (FKAQ) metrics. These metrics have no degeneracy, therefore to know about qubits the principal axes must already agree with a set of Pauli words. We use the following parameterization for FKAQ metrics

$$\begin{aligned}\omega_{\mathrm{FKAQ}}(w_i, W_\alpha) = {} & e^{w_1}|X_1\rangle\langle X_1| + e^{w_2}|Y_1\rangle\langle Y_1| + e^{w_3}|Z_1\rangle\langle Z_1| \\ & + e^{w_4}|X_2\rangle\langle X_2| + e^{w_5}|Y_2\rangle\langle Y_2| + e^{w_6}|Z_2\rangle\langle Z_2| \\ & + e^{W_1}|X_1X_2\rangle\langle X_1X_2| + e^{W_2}|X_1Y_2\rangle\langle X_1Y_2| + e^{W_3}|X_1Z_2\rangle\langle X_1Z_2| \\ & + e^{W_4}|Y_1X_2\rangle\langle Y_1X_2| + e^{W_5}|Y_1Y_2\rangle\langle Y_1Y_2| + e^{W_6}|Y_1Z_2\rangle\langle Y_1Z_2| \\ & + e^{W_7}|Z_1X_2\rangle\langle Z_1X_2| + e^{W_8}|Z_1Y_2\rangle\langle Z_1Y_2| + e^{-\Delta}|Z_1Z_2\rangle\langle Z_1Z_2|\end{aligned} \tag{4.49}$$

where we have assumed that all the principal axes are pure tensor. We have reduced the number of parameters by choosing a set of lab frames for the qubits, i.e. a choice of xyz-axes. But notice that this choice has no effect on the shape of the curvature functionals, changing the definition of axis or even meronomic frame comes only at the cost of performing an inner automorphism. The parameter Δ is chosen such that ω_{FKAQ} has unit determinant. In this class no decoding needs to be done, only the commutation relations need to be checked to confirm the KAQ property.

Again we reduce the number of independent weights to simplify the search. First we consider a naturally reductive example based upon a penalty metric [123–126]. We

define the biased penalty metric

$$\begin{aligned}\Omega_{\mathrm{BP}}(t,s) = e^{\frac{t}{6}}\Big(|X_1\rangle\langle X_1| + |Y_1\rangle\langle Y_1| + |Z_1\rangle\langle Z_1|\Big) + e^{\frac{s}{6}}\Big(|X_2\rangle\langle X_2| + |Y_2\rangle\langle Y_2| + |Z_2\rangle\langle Z_2|\Big)\\ +e^{-\frac{(t+s)}{18}}\Bigg(|X_1X_2\rangle\langle X_1X_2| + |X_1Y_2\rangle\langle X_1Y_2| + |X_1Z_2\rangle\langle X_1Z_2|\\ + |Y_1X_2\rangle\langle Y_1X_2| + |Y_1Y_2\rangle\langle Y_1Y_2| + |Y_1Z_2\rangle\langle Y_1Z_2|\\ + |Z_1X_2\rangle\langle Z_1X_2| + |Z_1Y_2\rangle\langle Z_1Y_2| + |Z_1Z_2\rangle\langle Z_1Z_2|\Bigg).\end{aligned} \tag{4.50}$$

Motivated by the construction in [127] we define a class of non-naturally reductive class of metrics, referred to as Abelian breakdown (AB)

$$\begin{aligned}\omega_{\mathrm{AB}}(t_i) = e^{-\Delta}\Big(|Z_1\rangle\langle Z_1| + |Z_2\rangle\langle Z_2| + |Z_1Z_2\rangle\langle Z_1Z_2|\Big)\\ + e^{t_1}\Big(|X_1\rangle\langle X_1| + |X_1Z_2\rangle\langle X_1Z_2|\Big) + e^{t_2}\Big(|Y_1\rangle\langle Y_1| + |Y_1Z_2\rangle\langle Y_1Z_2|\Big)\\ + e^{t_3}\Big(|X_2\rangle\langle X_2| + |Z_1X_2\rangle\langle Z_1X_2|\Big) + e^{t_4}\Big(|Y_2\rangle\langle Y_2| + |Z_1Y_2\rangle\langle Z_1Y_2|\Big)\\ + e^{t_5}\Big(|X_1X_2\rangle\langle X_1X_2| + |Y_1Y_2\rangle\langle Y_1Y_2|\Big) + e^{t_6}\Big(|X_1Y_2\rangle\langle X_1Y_2| + |Y_1X_2\rangle\langle Y_1X_2|\Big).\end{aligned} \tag{4.51}$$

The name is chosen as all degenerate eigenspaces form Abelian subalgebras. We may reduce to two parameters for further investigation

$$\begin{aligned}\Omega_{\mathrm{AB}}(t,s) = e^{-\frac{8t+4s}{30}}\Big(|Z_1\rangle\langle Z_1| + |Z_2\rangle\langle Z_2| + |Z_1Z_2\rangle\langle Z_1Z_2|\Big)\\ + e^{\frac{t}{10}}\Big(|X_1\rangle\langle X_1| + |Y_1\rangle\langle Y_1| + |X_2\rangle\langle X_2| + |Y_2\rangle\langle Y_2|\\ + |X_1Z_2\rangle\langle X_1Z_2| + |Y_1Z_2\rangle\langle Y_1Z_2| + |Z_1X_2\rangle\langle Z_1X_2| + |Z_1Y_2\rangle\langle Z_1Y_2|\Big)\\ + e^{\frac{s}{10}}\Big(|X_1X_2\rangle\langle X_1X_2| + |Y_1X_2\rangle\langle Y_1X_2| + |X_1Y_2\rangle\langle X_1Y_2| + |Y_1Y_2\rangle\langle Y_1Y_2|\Big).\end{aligned} \tag{4.52}$$

Notice that when $t = s$, a 1-dimensional space of naturally reductive metrics is obtained. But none of the contained naturally reductive metrics are Jensen metrics. To see this note that while the 3 dimensional subspace does form a subalgebra, the final commutation relation $[\mathfrak{M},\mathfrak{M}] \in \mathfrak{R}$ does not hold.

4.4 Equations of motion

We turn our attention now to the loss functionals we consider in this work, which may only depend on the metric and structure constants. We consider loss functionals derived from curvature functionals which are essentially tensor networks of the Christoffel connection. These classes of loss functionals contain structure constant networks not appearing in [103–105] at the same order in "perturbation" (defined by the number of structure constants in the contraction). We find it appealing to construct the loss functional from curvature functionals as

I $R[g]$ is the lowest order term in many natural classes of such actions.

II $R[g]$ always has two distinct classes of KAQ critical metrics.

A larger, natural class of loss functionals is

$$\begin{aligned}\mathcal{L}[g] &= R + \alpha R^2 + \beta R_{ab}R^{ab} + \gamma R_{abcd}R^{abcd} \\ &= R + \alpha\mathcal{R}_0 + \beta\mathcal{R}_2 + \gamma\mathcal{R}_4\,.\end{aligned} \tag{4.53}$$

An additional improvement on the pure Ricci theory is that this loss functional contains order parameters, allowing for the appearance of quantum subsystems through spontaneous symmetry breaking. The results of [112, 116] provide the equations of motion that must be satisfied in order for g to be a critical metric of the loss functional $\mathcal{L}[g;\alpha,\beta,\gamma]$, over a compact manifold while enforcing a fixed volume element. The last point is why the determinant of the metric must be fixed for our purposes.

Performing the variation of these functionals (in an orthonormal basis of the metric) yields the following "stress-energy" tensors

$$\begin{aligned}
T_{ij} &= R_{ij} - \frac{1}{2}R\delta_{ij} \\
T^{(0)}_{ij} &= 2RR_{ij} + 2\nabla^k\nabla_k(R\delta_{ij}) - 2\nabla_i\nabla_j R - \frac{1}{2}R^2\delta_{ij} \\
T^{(2)}_{ij} &= 2R_{ikjl}R^{kl} + \nabla^k\nabla_k R_{ij} + \frac{1}{2}\nabla^k\nabla_k(R\delta_{ij}) - \nabla_i\nabla_j R - \frac{1}{2}R_{kl}R^{kl}\delta_{ij} \\
T^{(4)}_{ij} &= 2R_{iklm}R_j{}^{klm} + 4R_{ikjl}R^{kl} + 4\nabla^k\nabla_k R_{ij} - 2\nabla_i\nabla_j R - 4R_{ik}R^k{}_j - \frac{1}{2}R_{klmn}R^{klmn}\delta_{ij}
\end{aligned}$$

It is important to note that using our definition of R_{ijkl} (see Appendix A), leads to different indicies being contracted in the Riemann-Ricci terms than those found in [112].

Muto [111] proved that a given metric is a critical point iff

$$\mathcal{T}_{ij} = T_{ij} + \alpha T^{(0)}_{ij} + \beta T^{(2)}_{ij} + \gamma T^{(4)}_{ij} = \Lambda \delta_{ij} \tag{4.54}$$

where Λ is a real constant depending on the parameters of the problem, namely m, r, and the coupling constants. Note to reduce the calculation, we may move all the terms already proportional to the metric to the RHS. Further, as we are considering homogeneous spaces the covariant derivatives of the Ricci scalar vanish. The "stress-energy" tensors simplify to

$$\begin{aligned}
T_{ij} &= R_{ij} \\
T^{(0)}_{ij} &= 2RR_{ij} + 2R\nabla_k\nabla_k(\delta_{ij}) \\
T^{(2)}_{ij} &= 2R_{ikjl}R_{kl} + \nabla_k\nabla_k(R_{ij}) + \frac{1}{2}R\nabla_k\nabla_k(\delta_{ij}) \\
T^{(4)}_{ij} &= 2R_{iklm}R_{jklm} + 4R_{ikjl}R_{kl} + 4\nabla_k\nabla_k(R_{ij}) - 4R_{ik}R_{kj},
\end{aligned}$$

where, as we are working in an orthonormal basis, we are free to lower all the indices. Summation over repeated indices is still implied. The last simplification available is to compute the terms involving the covariant Laplacian. The Laplacian of the metric vanishes

$$\nabla_k\nabla_k(\delta_{ij}) = -\nabla_k(\Gamma_{lki}\delta_{lj} + \Gamma_{lkj}\delta_{il}) = \nabla_k(\Gamma_{ikj} + \Gamma_{jki}) = 0 \tag{4.55}$$

which is equivalent to metric compatibility of the connection. We need to also compute the Laplacian of the Ricci tensor, but notice if we take a particular choice of the coupling constants the contribution from this term cancel. This particular combination is in fact the Gauss-Bonnet term yielding the loss functional

$$\mathcal{L}_{\mathrm{GB}}(\gamma) = R + \gamma(\mathcal{R}_0 - 4\mathcal{R}_2 + \mathcal{R}_4)\,. \tag{4.56}$$

We should emphasis that the Gauss-Bonnet term is not topological in this theory; the dimension of the space is $4^d - 1 \geq 15$, thus clearly never 4. The equations of motion for the chosen loss functional are

$$\mathcal{T}_{ij} = R_{ij} + \gamma\Big(2RR_{ij} + 2R_{iklm}R_{jklm} - 4R_{iljk}R_{lk} - 4R_{ik}R_{kj}\Big) = \Lambda_{\mathrm{GB}}\delta_{ij}\,. \tag{4.57}$$

where indeed we see the $\nabla^2 R_{ij}$ term vanishes. In the next section we provide much

evidence that the Gauss-Bonnet functional has the Killing-Cartan geometry as an unstable critical point. We suspect that the general class of loss functionals contained in Eq.4.53 are concave about the Killing-Cartan geometry for the same reason as found in [103], who examined the behavior of individual diagrams contributing to the functionals (see their Appendix C and our Appendix C.2).

And while ostensibly we have made a restrictive choice of coupling constants, by using a graphical method developed in Appendix C.2 we in fact see that the loss functional in Eq.(4.56) has general properties of the larger family, as no special cancellations appear in the graphs. As further evidence we may also contrast the Gauss-Bonnet loss functional with those introduced by Freedman and Zini. Besides the Ricci scalar, they considered non-Gaussian functionals for example the Euclidean integral

$$F[G;\kappa] = \int_{\mathbb{R}^{3(4^n-1)}} dy_1 dy_2 dy_3 e^{\left[-\kappa \sum_{i=1}^{3} g_{ab} y_i^a y_i^b + C_{abc} y_1^a y_2^b y_3^c\right]}. \tag{4.58}$$

The use of three integration variables is necessary to construct a non-vanishing scalar from the structure constants. Considering perturbed Gaussian integrals allows for a systematic approach to the perturbative calculation. In this way a series of trivalent tensor networks is obtained that determines the loss functional at a given order in perturbation parameter κ.

Now consider the graphical representation of the types of terms is given in Appendix C.2. The diagrams help illuminate a few important points of comparison between the loss functionals in Eq. (4.53) compared to Eq. (4.58). First, the family of curvature terms depends on diagrams with only at most four structure constants in the contraction. In contrast, the perturbed Gaussian of [103] contains a series out to infinite order, which was computed up to terms of order six for the analysis. At the level of fourth order terms, the Gauss-Bonnet combination does not induce any special cancellation between diagrams appearing in $\mathcal{R}_0$, $\mathcal{R}_2$, and $\mathcal{R}_4$. The individual curvature terms contain somewhat symmetric combinations of diagrams with a different relationship from that imposed by Eq. (4.58). This family of loss-functionals is well-suited to a geometrically illuminating study that may be able to connect KAQ structure to other known and interesting classes of metrics, including the naturally reductive metrics.

4.5 Results for SU(4)

The equations of motion allow us to search for solutions in the space of each 2-parameter KAQ metrics defined in Section 4.3. These parameterizations include both naturally and non-naturally reductive metrics. To yield a solution, a given ω must generate a diagonal stress energy tensor satisfying

$$\mathcal{T}_i \equiv \mathcal{T}_{ii} = \Lambda_{\mathrm{GB}} \tag{4.59}$$

where $1 \leq i \leq 15$ and Λ_{GB} is real. Thus for a given parameterization, we first determine the number of independent $\mathcal{T}_i$. By setting $s = at$, we simultaneously plot the independent $\mathcal{T}_i$, allowing us to vary a and check if any critical points appear for non-zero values of t.

By making contour plots of the loss function, we systematically find potential critical points and check if they are indeed true critical points. Further, while we do not have access to the second variation of the loss functional, we still obtain information about the second derivative by comparing contour plots which agree along the line $t = s$. Doing so affords us a glimpse at the stability of the loss functional around certain Jensen type critical points. The straightforward but lengthy evaluation of the second variation could be performed to fully check stability.

4.5.1 FKAQ critical points

Here we collect our results for the two FKAQ parameterizations given in Section 4.3. These include the naturally reductive parameterization Ω_{BP} defined in Eq.(4.50) and the non-naturally reductive parameterization Ω_{AB} defined in Eq.(4.52). Using two parameterizations allows us to compare the type of critical metrics that appear in the naturally reductive vs. non-naturally reductive cases.

We show results with the help of two types of figures. First, to demonstrate the technique, we plot the equations of motion for an example, at fixed values of the weighting parameters in the metric (s, t). But, to visualize the space of solutions in the weighting parameters, we show contour plots of the loss functionals for varying s, t. It is important to stress that not all critical points that appear in these plots are critical in the space of left-invariant metrics. All that can be learned from these plots is whether they are critical in the considered parameterization space. In order to determine true criticality we always appeal to the equations of motion.

4.5.1.1 Biased penalty metric

There are only three independent $\mathcal{T}_i$ for the biased penalty metric ansatz, Ω_{BP} from Eq.(4.50). The equations that must be satisfied are

$$\begin{aligned}\mathcal{T}_1 = e^{\frac{1}{9}(-7a-10)t}\Big(&-3\gamma e^{\frac{at}{3}} + 18.75\gamma e^{\frac{4}{9}(a+1)t} + 9\gamma e^{\frac{2}{3}(a+2)t} - 1.125\gamma e^{\frac{1}{9}(2a+11)t} + 1.125\gamma e^{\frac{1}{9}(8a+5)t} \\ &+0.375\gamma e^{\frac{1}{9}(10a+13)t} + 0.75e^{\frac{5}{9}(a+1)t} + 0.25e^{\frac{1}{9}(7a+13)t} - 1.125\gamma e^{t/3}\Big) \\ &=\Lambda_{\mathrm{GB}},\end{aligned}$$

$$\begin{aligned}\mathcal{T}_4 = e^{\frac{1}{9}(-10a-7)t}\Big(&-1.125\gamma e^{\frac{at}{3}} + 18.75\gamma e^{\frac{4}{9}(a+1)t} + 1.125\gamma e^{\frac{1}{9}(5a+8)t} - 1.125\gamma e^{\frac{1}{9}(11a+2)t} \\ &+0.375\gamma e^{\frac{1}{9}(13a+10)t} + 9\gamma e^{\frac{2}{3}(2at+t)} + 0.75e^{\frac{5}{9}(a+1)t} + 0.25e^{\frac{1}{9}(13a+7)t} \\ &-3\gamma e^{t/3}\Big) = \Lambda_{\mathrm{GB}},\end{aligned}$$

$$\begin{aligned}\mathcal{T}_7 = e^{-\frac{10}{9}(a+1)t}\Big(&2\gamma e^{\frac{2at}{3}} + 1.5\gamma e^{\frac{1}{3}(a+1)t} + 51.5\gamma e^{\frac{8}{9}(a+1)t} + 3\gamma e^{\left(a+\frac{4}{3}\right)t} - 18.75\gamma e^{\frac{1}{9}(4a+7)t} \\ &-0.75\gamma e^{\frac{1}{9}(5a+11)t} - 18.75\gamma e^{\frac{1}{9}(7a+4)t} - 0.75\gamma e^{\frac{1}{9}(11a+5)t} + 3\gamma e^{\frac{4at}{3}+t} \\ &-0.5e^{\frac{1}{9}(5a+8)t} - 0.5e^{\frac{1}{9}(8a+5)t} + 2e^{at+t} + 2\gamma e^{2t/3}\Big) \\ &=\Lambda_{\mathrm{GB}}.\end{aligned} \tag{4.60}$$

With only three independent diagonal elements, this parameterization is only slightly more complicated than the Jensen type. For Jensen metrics there are only 2 independent $\mathcal{T}_i$. Recall that we want to find non-Jensen type critical points, as for larger number of qubits Jensen metrics are highly non-local and do not give a typical many-body structure.

In Figure 4.1 we plot the set of $\mathcal{T}_i$ for two different values of a. The left plot shows that for most values of a (here 0.1), the only solution that appears is the trivial non-KAQ solution $s = at = 0$. But for special values of a, non-trivial solutions do appear. We unsurprisingly find Jensen type critical points for $a = 1$, which is expected due to the simplicity of the equations of motion. Figure 4.2 however, shows an example of a non-Jensen type critical points, of which several exist.

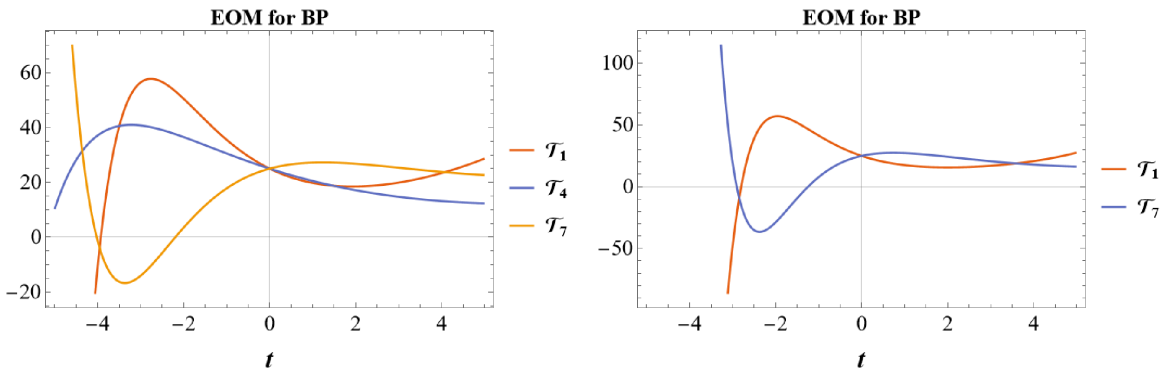

Figure 4.1: Here the equations of motion (Eq.4.56) are plotted for the biased penalty metric ansatz Ω_{BP} (Eq.4.50), which includes a Gauss-Bonnet with $\gamma = 1$. The left plot shows the line $t = s$, and for the biased penalty metric these are Jensen-type. In fact we find an additional solution (relative to pure Ricci scalar) for $t < 0$. The second plot demonstrates that for most a strictly left-invariant solutions do not exist.

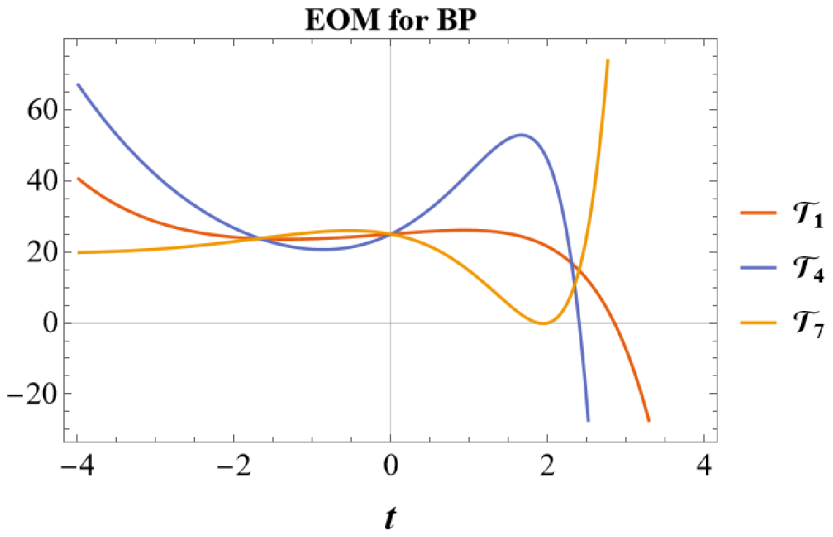

Figure 4.2: Here the equations of motion for Ω_{BP} are plotted for $a \approx -2.06$. We see that there is a non-Jensen type solution for $t \approx -1.67$.

In Fig 4.3 we present a holistic view of the critical points that appear through the use of contour plots of the loss functional. We see that even for the Ricci scalar, non-Jensen naturally reductive critical points are present. The shapes of the contour near the origin show why evolutionary searches performed in [103] likely missed out on the more structured critical points. Evolutionary searches begin with the choice of an initial parent point. The natural choice here is the Killing-Cartan metric, or a randomly selected nearby point. The search then casts a small net around the parent point, and the loss

functions is computed for each of these points. The point with the lowest value serves as the new parent point in the following step. The topography of these plots demonstrates that such a method can fail to find the saddle points, instead settling on the Jensen-type critical point(s).

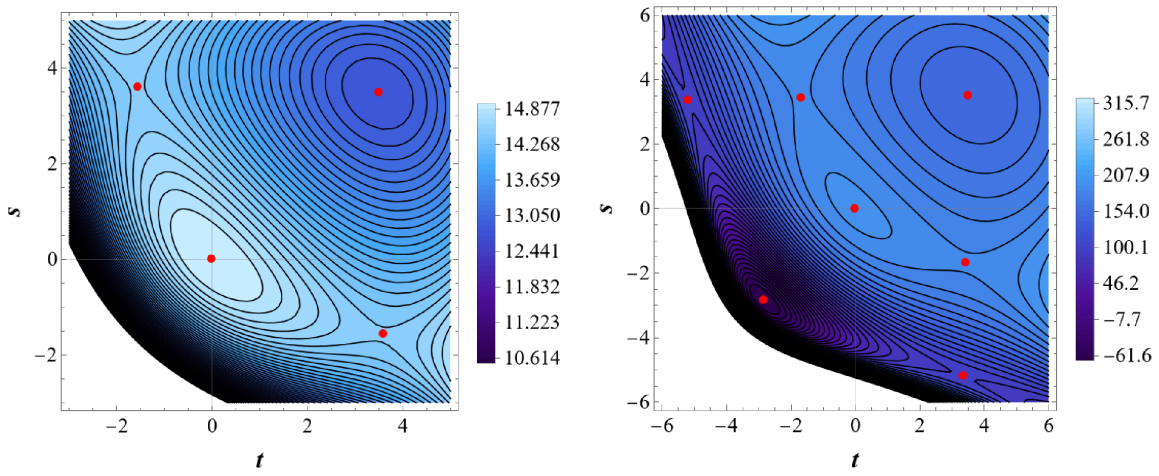

Figure 4.3: Contours of the loss functional are plotted for Ω_{BP}, Eq.(4.50), with $\gamma = 0$ (the Ricci scalar only) and $\gamma = 1$. All red points marked on the plots are critical in the space of left-invariant metrics with fixed determinant. Critical points residing on the line $t = s$ are Jensen type, while all others are non-Jensen appealing to the form of $\Omega_{\mathrm{BP}}(t, s)$.

4.5.1.2 Abelian breakdown metric

Moving to the non-naturally reductive FKAQ parameterization, Ω_{AB} from Eq.(4.52), we plot the set of independent $\mathcal{T}_i$ in Fig 4.4, where there are 4 such elements. We find solutions only for $a = 1$, the potential meeting point in the left plot never actually becomes a crossing. In this case the solution is naturally reductive but not of Jensen type, even though the corresponding critical metric only has two distinct weights, as the weights do not distinguish blocks that belong to a Cartan decomposition.

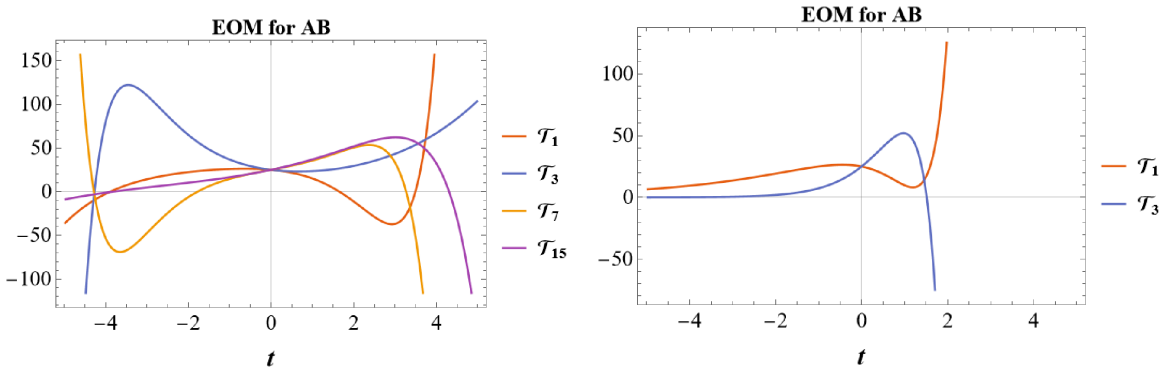

Figure 4.4: Plotted are the equations of motion for the Abelian breakdown metric ansatz, Ω_{AB} of Eq.(4.52), which is non-naturally reductive. Again, we have taken $\gamma = 1$ for the amplitude of the Gauss-Bonnet term. The first plot shows the behavior for a typical a; no non-trivial solutions exist. The second plot shows the existence of a non-Jensen type critical point for $a = 1$ and $t \approx 1.45$.

We have plotted contour plots in Fig 4.5, where we find only one non-trivial solution. Comparing to the biased penalty example we may make two comments. First, there are far fewer critical points along these directions in the space of left-invariant metrics. Further, the critical point we obtained is rather interesting. The KAQ critical metric puts distinct weight on Cartan subalgebra distinguishing it from the remaining observables. While a small step, it is evidence that curvature-based loss functionals may support KAQ critical points with many-body local structure.

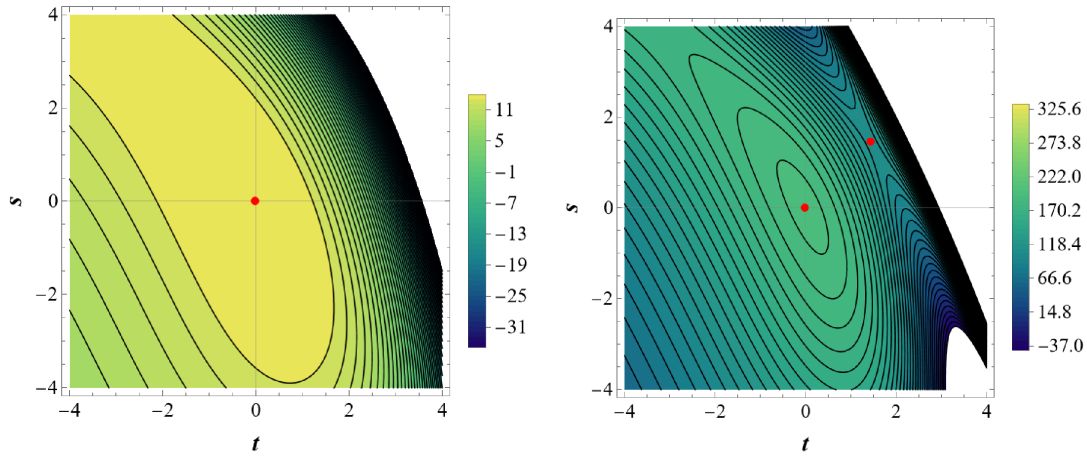

Figure 4.5: Contours of the loss functional $\mathcal{L}_{\text{GB}}$ is plotted for Ω_{AB}, Eq.(4.52), with $\gamma = 0$ (the Ricci scalar only) and $\gamma = 1$. The red points marked on the plots are critical points in the space of left-invariant metrics with fixed determinant. As explained in Section 4.3.3.3, no metric in this class, regardless of parameter values, is of the Jensen type.

4.5.2 UKAQ critical points

Turning to our UKAQ parametrization, Ω_{UKAQ} from Eq.(4.42), we may perform the same search for critical points. The equations of motions are much more complex for this example, where there are 6 independent $\mathcal{T}_i$. While certain choices of a reduce the number of independent $\mathcal{T}_i$, only for $a = 1$ do we obtain non-trivial solutions to the equations of motion.

By comparing Figure 4.3 and Figure 4.6 we obtain some evidence about the preference of naturally reductive metric. Notice that these figures exactly agree on the line $t = s$, so we can see how the value of the functional changes in naturally reductive vs. non-naturally reductive direction. We see that Figure 4.3 clearly contains more true critical metrics, and that the only critical metrics contained within Figure 4.6 are naturally reductive as well. This provides some evidence that naturally reductive metrics may be favored over non-naturally reductive metrics when weighed by curvature based functionals.

Some understanding about the stability of the Jensen type critical points common to both examples can be obtained by comparing these figures. The Jensen type critical point with $s, t < 0$ appears to be a stable critical point, where as the solution for positive t and s is clearly a saddle point. Although there are many different cross sections one must consider to truly determine the stability.

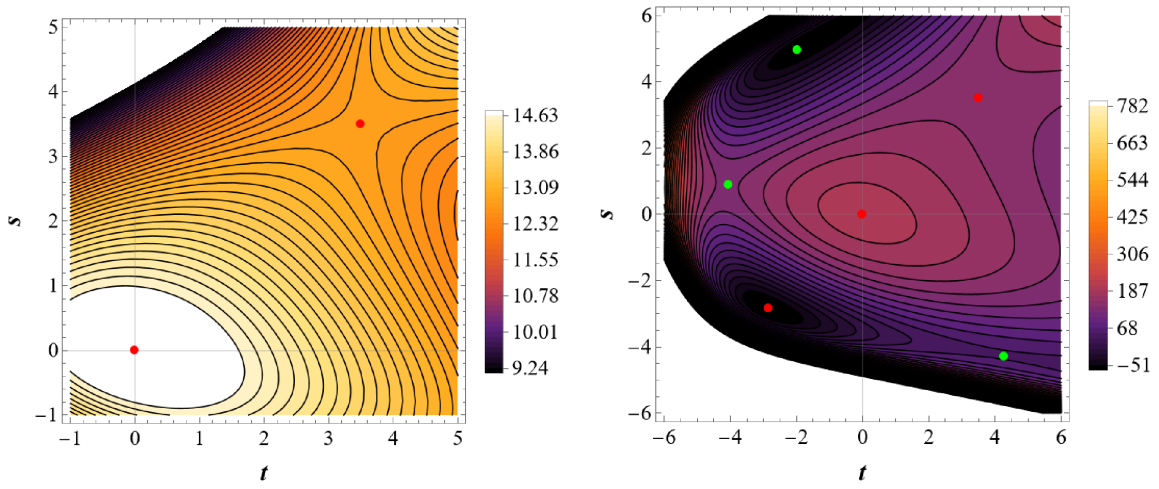

Figure 4.6: Contours of the loss functionals are plotted for the Ω_{UKAQ} parameterization, Eq.(4.42). The red points located along the line $t = s$ are critical points in the space of left-invariant metrics. All other points (green) are only critical in the considered parameterization space.

We do not fully understand the propensity towards Jensen metrics in our examples.

It could simply be a preference for naturally reductive metrics. There is however another possibility. At such a low dimension (two qubits) the Jensen metrics and penalty metrics are essentially the same. So, the loss functions investigated here may simply be favoring penalty structures. It would be enlightening to study $\mathfrak{su}(8)$ to illuminate this point.

4.5.3 PKAQ critical points

For the final parameterization, we investigate Ω_{PKAQ} defined in Eq.(4.48). We only find Jensen-type critical points, and note that this direction seems the least fruitful in the search for critical metrics.

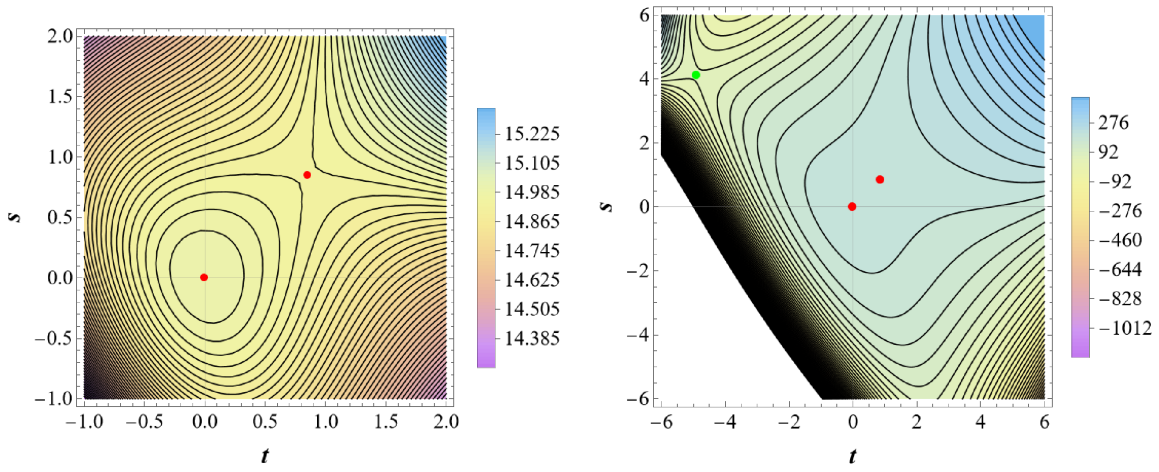

Figure 4.7: Contours are plotted for the Ω_{PKAQ} parameterization, Eq.(4.48). The red points indicate true critical points, which are all Jensen type. The green point, in the second plot, is only critical in the parameterization space.

4.6 Conclusions

In this work we have found critical points of curvature-based loss functionals that are KAQ and include metrics which are compatible with many-body physics. All of the critical points we have found are naturally reductive, although we cannot rule out the existence of non-naturally reductive KAQ metrics. From the examples we tried we found no $\text{ad}\mathfrak{R}_0$ invariant critical metrics which were not Jensen. We also have found that most critical points are saddle points, with the potential for a few stable Jensen critical points.

While we have only analyzed detailed examples for $\mathfrak{su}(4)$, it is straightforward, although numerically intensive, to generalize these constructions to larger N. What we have presented is evidence that the KAQ ansatz is a useful tool both for finding critical

metrics among the large set of left-invariant metrics and for better understanding the structure of KAQ critical points. Even going to $\mathfrak{su}(8)$ would be helpful in determining more about the structure of the critical points of curvature-based loss functionals. For example with three qubits, penalty metrics are not Jensen, allowing for more exploration in what exactly drives the value of the loss function; the algebraic properties of the principal axes or structure of the weights?

These constructions for KAQ metrics we provide may also be used to explore a much broader family of functionals depending on curvature tensors. However, as this construction cannot find non-KAQ minima, we cannot study the relative frequency of KAQ vs non-KAQ. Ideally, one would like functionals with only KAQ minima, or related structure for $N \neq 2^d$.

Chapter 5
Conclusions

In this work we presented analytic descriptions of several types of open qubit systems, and along the way we derived several results that can aid in the development of open effective theories. Among these results, we have found that time-dependent environmental landscapes have a dramatic effect on the form of an effective master equation, making necessary the use of a non-time-local kernel in the master equation. From these results we determined that an effective approach constructed from quantum channels may be more fruitful, and is much simpler in principle to develop. Along these lines we explored an ensemble approach to an effective theory, by studying the ensemble of phase-covariant dynamics that appears in qubit networks interacting under XXZ-Hamiltonians. We found that the long-time dynamics may be approximated using a phase-covariant ensemble of channels, needing only some information about the symmetry of the interaction governing the network dynamics, and information about how fluctuations scale with time and system size. Finally, we have explored a model for the spontaneous emergence of qubits from featureless quantum systems. We found that natural geometrically motivated loss functionals have a plethora of KAQ minima, and show promise to contain minima that are both many-body and local.

There are several routes towards future work from what was presented in this dissertation. Most relevant for understanding open quantum cosmology, is more sophisticated studies of the dynamic environmental landscape. Perhaps most glaring, can we understand the role phase-covariance breaking plays in the models we set forth. At the moment it is not clear if the features we derived, namely the eternal non-time-local nature of the dynamics, persist for different configurations of system and environments. Another interesting model to consider is the spreading of time-non-locality from local phase-covariance breaking, that is introduced phase-covariance breaking locally in a spin-network and determine what the time-local nature of the dynamical map near and

far from the phase-covariance breaking site. A final consideration past our simple model is to consider a mosaic environment where degrees of freedom may activate and deactivate. By taking the times of activation and deactivation to be random an interesting, and perhaps solvable model in some instances, emerges. The interesting question to ask what typical duration of environmental degrees of freedom yield time-local vs. non-time-local dynamics.

The random ensembles of quantum channels and certain generalizations of phase-covariant ensembles are another promising direction of research. The first obvious direction is to consider larger sized dynamical maps, taking the minimal step to 2-qubit dynamical maps can provide useful information. As two-point correlation functions find vast uses in modern physics, and they can be probed in certain models to understand certain phase-transitions. Therefore it seems plausible that some features of these kinds of transitions in say spin-chains could be discerned from features or late-time behavior of the dynamical map.

Further, by exploring larger dynamical maps we can ponder another potential connection to thermodynamics. From random matrix theory it is well known that integrable models, that is the most symmetric theories, fully resist thermalization in the thermodynamic limit. An idea we can investigate is whether the G-covariance of a given dynamical map relates at all to these thermodynamic notions. For example we see that phase-covariance at the level of qubit maps is ostensibly uninteresting in these regards. The integrable vs. thermalizing nature of the full Hamiltonian is obfuscated in the 1-qubit dynamical maps. However this does not mean that for larger maps phase-covariance still hides these features. In principle one can imagine that a certain size of group relative to the size of the dynamical map may allow for interesting thermodynamic features to appear.

And the most open is the possible extension of the KAQ metrics. From the work done so far it looks promising to explore the set of KAQ Einstein metrics, which are critical points of the Ricci scalar. The appeal of this approach is that the search for critical points is much less numerically intensive than that of the high order curvature terms. Ultimately one is interested in taking a large N limit for these theories and showing (or not) that in these scenarios many-body local Hamiltonians are favored then there non-local counterparts.

Appendix A
Effective Master Equations

A.1 Derivation of the maximally entangling parameter space

Following [57, 58], we find the essential non-local properties of U by changing to the Bell basis using the unitary operator,

$$Q = \frac{1}{\sqrt{2}} \begin{bmatrix} 1 & 0 & 0 & i \\ 0 & i & 1 & 0 \\ 0 & i & -1 & 0 \\ 1 & 0 & 0 & -i \end{bmatrix} . \tag{A.1}$$

The choice of Bell states is made so that the entanglement quadratic form $\hat{Ent}$ maps to the identity matrix. The operator $\hat{Ent}$ is defined as,

$$Det I_{\mathrm{C}}(|\psi\rangle) = \psi_{00}\psi_{11} - \psi_{01}\psi_{10} = |\psi\rangle^T \hat{Ent} |\psi\rangle \,, \tag{A.2}$$

where I_{C} is the Choi isomorphism $I_{\mathrm{C}} : \mathcal{H} \to Mat(2, \mathbb{C})$, and one sees upon further inspection that $\hat{Ent} = -\frac{1}{2} Y_{\mathrm{S}} \otimes Y_{\mathrm{E}}$ and $Q^T(\hat{Ent})Q = \frac{1}{2}\mathbb{1}_{\mathrm{S}} \otimes \mathbb{1}_{\mathrm{E}}$. At the level of observables Q takes the subalgebra of local observables $\mathfrak{su}(2)_{\mathrm{S}} \oplus \mathfrak{su}(2)_{\mathrm{E}}$ to the generators of 4D rotations on the Bell space $\mathfrak{so}(4)_{\mathrm{Bell}}$.

The time evolution operator is expressed in the Bell basis as,

$$U_{\text{Bell}}(t) = \begin{bmatrix} \cos\omega_+ t & 0 & 0 & e^{i\phi_+}\sin\omega_+ t \\ 0 & \cos\omega_- t & -e^{i\phi_-}\sin\omega_- t & 0 \\ 0 & e^{-i\phi_-}\sin\omega_- t & \cos\omega_- t & 0 \\ -e^{-i\phi_+}\sin\omega_+ t & 0 & 0 & \cos\omega_+ t \end{bmatrix} \tag{A.3}$$

The non-local properties of the time evolution in the reduction frame are determined by the eigenvalues of $U_{\text{Bell}}^T U_{\text{Bell}}$ found to be,

$$\begin{aligned} u_+ &= \cos^2\omega_+ t + (\cos 2\phi_+ + i\sqrt{\sin^2 2\phi_+ + \sin^2\phi_+})\sin^2\omega_+ t \\ u_- &= \cos^2\omega_+ t + (\cos 2\phi_+ - i\sqrt{\sin^2 2\phi_+ + \sin^2\phi_+})\sin^2\omega_+ t \\ v_+ &= \cos^2\omega_- t + (\cos 2\phi_- + i\sqrt{\sin^2 2\phi_- + \sin^2\phi_-})\sin^2\omega_- t \\ v_- &= \cos^2\omega_- t + (\cos 2\phi_- - i\sqrt{\sin^2 2\phi_- + \sin^2\phi_-})\sin^2\omega_- t \end{aligned} . \tag{A.4}$$

Assume we are given a linear combination of these eigenvalues $au_+ + bu_- + cv_+ + dv_-$ such that $a, b, c, d \geq 0$ and $a + b + c + d = 1$. For this combination to be real we must have $a = b$ and $c = d$. Setting $a = \cos^2\varphi$ and $c = \sin^2\varphi$ we have,

$$\begin{aligned} 0 &= \cos^2\varphi(\cos^2\omega_+ t + \cos 2\phi_+ \sin^2\omega_+ t) + \sin^2\varphi(\cos^2\omega_- t + \cos 2\phi_- \sin^2\omega_- t) \\ &= \cos^2\varphi(|\alpha_+|^2(t) - \beta_+^2(t)) + \sin^2\varphi(|\alpha_-|^2(t) - \beta_-^2(t)) \end{aligned} \tag{A.5}$$

A little bit of algebra and we find,

$$\cos^2\varphi\beta_+^2(t) + \sin^2\varphi\beta_-^2(t) = \frac{1}{2}. \tag{A.6}$$

This condition may only be satisfied iff the largest of $\beta_+^2(t)$ and $\beta_-^2(t)$ is greater than or equal to $\frac{1}{2}$, or equivalently $\text{Max}(\phi_+, \phi_-) \geq \frac{\pi}{4}$. That is maximally entangled states may only be generated when U has large enough off diagonal components, which we see becomes one of the conditions that non-invertibilities appear in the reduced dynamics.

A.2 Divisibility in channels

In this appendix we establish the divisibility of the dynamical map family $\mathcal{D}_+$. For simplicity we assume that $\vec{r}_E(0) = \vec{0}$ although the results derived apply even if $\vec{r}_{\text{E}}(0) = x_{\text{E}}(0)\hat{x}$. We are interested in when the map $\Phi(\tau_2, \tau_1)$ fails to be completely positive, and

how this depends on τ_2 and ϕ. To that end, the dynamical map has the structure,

$$\Lambda(t) = \begin{bmatrix} 1 & 0 & 0 & 0 \\ 0 & \Lambda_{xx}(t) & \Lambda_{xy}(t) & 0 \\ 0 & \Lambda_{yx}(t) & \Lambda_{yy}(t) & 0 \\ 0 & 0 & 0 & \Lambda_{zz}(t) \end{bmatrix} \tag{A.7}$$

with determinant $\mathrm{Det}\Lambda = \Lambda_{zz}^2$ and inverse,

$$\Lambda^{-1}(t) = \begin{bmatrix} 1 & 0 & 0 & 0 \\ 0 & \frac{\Lambda_{yy}(t)}{\Lambda_{zz}(t)} & -\frac{\Lambda_{xy}(t)}{\Lambda_{zz}(t)} & 0 \\ 0 & -\frac{\Lambda_{yx}(t)}{\Lambda_{zz}(t)} & \frac{\Lambda_{xx}(t)}{\Lambda_{zz}(t)} & 0 \\ 0 & 0 & 0 & \frac{1}{\Lambda_{zz}(t)} \end{bmatrix}, \tag{A.8}$$

and the (possibly singular) interweaving map is,

$$\Phi(\tau_2,\tau_1) = \begin{bmatrix} 1 & 0 & 0 & 0 \\ 0 & \frac{\Lambda_{xx}(\tau_2)\Lambda_{yy}(\tau_1)-\Lambda_{xy}(\tau_2)\Lambda_{yx}(\tau_1)}{\Lambda_{zz}(\tau_1)} & \frac{-\Lambda_{xx}(\tau_2)\Lambda_{xy}(\tau_1)+\Lambda_{xy}(\tau_2)\Lambda_{xx}(\tau_1)}{\Lambda_{zz}(\tau_1)} & 0 \\ 0 & \frac{\Lambda_{yx}(\tau_2)\Lambda_{yy}(\tau_1)-\Lambda_{yy}(\tau_2)\Lambda_{yx}(\tau_1)}{\Lambda_{zz}(\tau_1)} & \frac{\Lambda_{yy}(\tau_2)\Lambda_{xx}(\tau_1)-\Lambda_{yx}(\tau_2)\Lambda_{xy}(\tau_1)}{\Lambda_{zz}(\tau_1)} & 0 \\ 0 & 0 & 0 & \frac{\Lambda_{zz}(\tau_2)}{\Lambda_{zz}(\tau_1)} \end{bmatrix}. \tag{A.9}$$

N.B. that the map $\Phi(\tau_2,\tau_1)$ can have a restricted domain, where instead of the Bloch ball the interweaving map only acts on the image of $\Lambda(\tau_1)$.

The criterion in [6] asserts that $\Phi(\tau_2,\tau_1)$ is completely positive if,

$$\begin{aligned} &\left[\frac{\Lambda_{xx}(\tau_2)\Lambda_{yy}(\tau_1)-\Lambda_{xy}(\tau_2)\Lambda_{yx}(\tau_1)}{\Lambda_{zz}(\tau_1)} \pm \frac{\Lambda_{yy}(\tau_2)\Lambda_{xx}(\tau_1)-\Lambda_{yx}(\tau_2)\Lambda_{xy}(\tau_1)}{\Lambda_{zz}(\tau_1)}\right]^2 \\ &\leq \left[1 \pm \frac{\Lambda_{zz}(\tau_2)}{\Lambda_{zz}(\tau_1)}\right]^2 . \end{aligned} \tag{A.10}$$

The + inequality is saturated at all times, so the components of Λ satisfy the relation (recall $\Lambda_{yx}(t) = -\Lambda_{xy}(t)$),

$$\Lambda_{xx}(\tau_2)\Lambda_{yy}(\tau_1) + 2\Lambda_{xy}(\tau_2)\Lambda_{xy}(\tau_1) + \Lambda_{yy}(\tau_2)\Lambda_{xx}(\tau_1) = \Lambda_{zz}(\tau_2) + \Lambda_{zz}(\tau_1)\,. \tag{A.11}$$

Thus Φ is completely positive if,

$$(\Lambda_{xx}(\tau_2)\Lambda_{yy}(\tau_1) - \Lambda_{yy}(\tau_2)\Lambda_{xx}(\tau_1))^2 \leq (\Lambda_{zz}(\tau_2) - \Lambda_{zz}(\tau_1))^2 . \tag{A.12}$$

We already see that if $\tau_n = \frac{n\pi}{2\omega}$, then $\Phi(\tau_n, \tau_1)$ is CP as the above inequality reduces to a CP condition satisfied by $\Lambda(\tau_1)$. Therefore, special times τ_2 exist where the dynamics is CP divisible. This condition is not dependent on what particular values are chosen for ω and ϕ. However for other values of τ_2, the CP inequality will fail to be satisfied for certain values of τ_1. The size of this interval is not dependent on ω, but depends on ϕ and τ_2.

Appendix B
Quantum Channel Ensembles

B.1 N-qubit Fourier modes

In this appendix we lay out the symmetries that are useful in computing exact dynamical maps. The first of these symmetries is the charge, or equivalently the excitation number, operator

$$Q_N = \sum_i Z_i \,. \tag{B.1}$$

Throughout the article the excitation number is labeled as q, but note this is not the eigenvalue of Q_N. Each block with a given value of q has dimension $m = \binom{N}{q}$, simply the number of ways to pick q qubits to be excited.

Hamiltonians satisfying $[H, Q_N] = 0$ will be block diagonal in any excitation eigenbasis. Since Q_N is already diagonal in the computational basis, block diagonalizing the Hamiltonian at most requires a permutation matrix that reorders computational basis states by excitation number. For this article we chose $\mathcal{P}_N$ so that the computational states within the same q-blocks are ordered based on their binary representation. For example when $N = 3$, in the $q = 1$ block the computational state $|001\rangle$ comes before $|100\rangle$. The next symmetry available to the models we consider is the translation operator (T_N). The translation action on computational basis states is

$$T_N |a_1 a_2 ... a_N\rangle = |a_N a_1 ... a_{N-1}\rangle \tag{B.2}$$

and the adjoint action on Pauli matrices is

$$T_N \sigma_i^\alpha T_N^\dagger = \sigma_{i+1}^\alpha \,. \tag{B.3}$$

where a tensor product of the Pauli with the identity operator on all other spins is

implied. Since $[Q_N, T_N] = 0$ the translation operator is block diagonal in any excitation-ordered computational basis. Further noting that $T_N^N = \mathbb{1}$, it is not hard to see that its eigen-spectrum consists entirely of N^{th} roots of unity. Combining these results we may label the eigenstates of T_N as

$$\begin{aligned} T_N|\mathcal{F}_q^a;k\rangle &= e^{i\frac{2\pi a}{N}}|\mathcal{F}_q^a;k\rangle \\ Q_N|\mathcal{F}_q^a;k\rangle &= \Big(2q-N\Big)|\mathcal{F}_q^a;k\rangle \end{aligned} \tag{B.4}$$

where q is the excitation number, and k is a label that removes any remaining degeneracy of the eigenstates. In a given q-block, Fourier modes corresponding to subgroups of the cyclic group $\mathbb{Z}_N$ may appear, which happens when N is a composite integer. In the remainder of this appendix we give constructions of the Fourier modes for $N \leq 6$.

B.1.1 3-qubits

$$|\mathcal{F}_0^0;0\rangle = |111\rangle \quad |\mathcal{F}_3^0;0\rangle = |000\rangle \tag{B.5}$$

$$\begin{aligned} |\mathcal{F}_1^0;0\rangle &= \frac{1}{\sqrt{3}}\Big(|011\rangle + |101\rangle + |110\rangle\Big) \\ |\mathcal{F}_1^1;0\rangle &= \frac{1}{\sqrt{3}}\Big(|011\rangle + e^{\frac{2\pi i}{3}}|101\rangle + e^{\frac{4\pi i}{3}}|110\rangle\Big) \\ |\mathcal{F}_1^2;0\rangle &= \frac{1}{\sqrt{3}}\Big(|011\rangle + e^{\frac{4\pi i}{3}}|101\rangle + e^{\frac{2\pi i}{3}}|110\rangle\Big) \end{aligned} \tag{B.6}$$

$$\begin{aligned} |\mathcal{F}_2^0;0\rangle &= \frac{1}{\sqrt{3}}\Big(|001\rangle + |010\rangle + |100\rangle\Big) \\ |\mathcal{F}_2^1;0\rangle &= \frac{1}{\sqrt{3}}\Big(|001\rangle + e^{\frac{2\pi i}{3}}|010\rangle + e^{\frac{4\pi i}{3}}|100\rangle\Big) \\ |\mathcal{F}_2^2;0\rangle &= \frac{1}{\sqrt{3}}\Big(|001\rangle + e^{\frac{4\pi i}{3}}|010\rangle + e^{\frac{2\pi i}{3}}|100\rangle\Big) \end{aligned} \tag{B.7}$$

B.1.2 4-qubits

$$|\mathcal{F}_0^0;0\rangle = |1111\rangle \quad |\mathcal{F}_4^0;0\rangle = |0000\rangle \tag{B.8}$$

$$
\begin{aligned}
|\mathcal{F}_1^0;0\rangle &= \frac{1}{\sqrt{4}}\Big(|0111\rangle + |1011\rangle + |1101\rangle + |1110\rangle\Big)\\
|\mathcal{F}_1^1;0\rangle &= \frac{1}{\sqrt{4}}\Big(|0111\rangle + i|1011\rangle - |1101\rangle - i|1110\rangle\Big)\\
|\mathcal{F}_1^2;0\rangle &= \frac{1}{\sqrt{4}}\Big(|0111\rangle - |1011\rangle + |1101\rangle - |1110\rangle\Big)\\
|\mathcal{F}_1^3;0\rangle &= \frac{1}{\sqrt{4}}\Big(|0111\rangle - i|1011\rangle - |1101\rangle + i|1110\rangle\Big)
\end{aligned}
\tag{B.9}
$$

$$
\begin{aligned}
|\mathcal{F}_3^0;0\rangle &= \frac{1}{\sqrt{4}}\Big(|0001\rangle + |0010\rangle + |0100\rangle + |1000\rangle\Big)\\
|\mathcal{F}_3^1;0\rangle &= \frac{1}{\sqrt{4}}\Big(|0001\rangle + i|0010\rangle - |0100\rangle - i|1000\rangle\Big)\\
|\mathcal{F}_3^2;0\rangle &= \frac{1}{\sqrt{4}}\Big(|0001\rangle - |0010\rangle + |0100\rangle - |1000\rangle\Big)\\
|\mathcal{F}_3^3;0\rangle &= \frac{1}{\sqrt{4}}\Big(|0001\rangle - i|0010\rangle - |0100\rangle + i|1000\rangle\Big)
\end{aligned}
\tag{B.10}
$$

$$
\begin{aligned}
|\mathcal{F}_2^0;0\rangle &= \frac{1}{\sqrt{4}}\Big(|0011\rangle + |0110\rangle + |1001\rangle + |1100\rangle\Big)\\
|\mathcal{F}_2^1;0\rangle &= \frac{1}{\sqrt{4}}\Big(|0011\rangle + i|0110\rangle - |1001\rangle - i|1100\rangle\Big)\\
|\mathcal{F}_2^2;0\rangle &= \frac{1}{\sqrt{4}}\Big(|0011\rangle - |0110\rangle + |1001\rangle - |1100\rangle\Big)\\
|\mathcal{F}_2^3;0\rangle &= \frac{1}{\sqrt{4}}\Big(|0011\rangle - i|0110\rangle - |1001\rangle + i|1100\rangle\Big)\\
|\mathcal{F}_2^0;1\rangle &= \frac{1}{\sqrt{2}}\Big(|0101\rangle + |1010\rangle\Big)\\
|\mathcal{F}_2^2;1\rangle &= \frac{1}{\sqrt{2}}\Big(|0101\rangle - |1010\rangle\Big)
\end{aligned}
\tag{B.11}
$$

B.2 Glossary of dynamical maps

In this Appendix we present the exact formulae for the dynamical maps considered in this work. We have the following form of phase-covariant maps

$$
\Lambda(t) = \begin{bmatrix}
1 & 0 & 0 & 0\\
0 & \Lambda_{xx}(t) & \Lambda_{xy}(t) & 0\\
0 & \Lambda_{yx}(t) & \Lambda_{yy}(t) & 0\\
\Lambda_{z0}(t) & 0 & 0 & \Lambda_{zz}(t)
\end{bmatrix}
\tag{B.12}
$$

where for the Hamiltonians considered, the various components all may be decomposed as

$$\begin{aligned}
\Lambda_{xx}(t) &= \alpha(t)\cos 2ht - \beta(t)\sin 2ht = \lambda_1(t)\cos\left(2ht+\phi(t)\right) \\
\Lambda_{yx}(t) &= \beta(t)\cos 2ht + \alpha(t)\sin 2ht = \lambda_1(t)\sin\left(2ht+\phi(t)\right) \\
\Lambda_{zz}(t) &= \lambda_3(t) \\
\Lambda_{z0}(t) &= \tau_3(t)\,,
\end{aligned} \tag{B.13}$$

with the remaining components determined by the relations $\Lambda_{yy} = \Lambda_{xx}$ and $\Lambda_{xy} = -\Lambda_{yx}$. To perform the minimum amount of computations, we only provide explicit formulas for τ_3, λ_3, α, and β for each model.

B.2.1 Completely-connected XXZ-network

We present the exact dynamical map components for the completely-connected and homogeneous XXZ-network. We present all the non-unitary parameters defined in Eq.(B.13).

B.2.1.1 4-qubits

For 4-qubits the Hamiltonian has the block diagonal structure

$$\mathcal{P}_4 H_{\mathrm{XXZ}} \mathcal{P}_4^\dagger = H^0_{\mathrm{XXZ}} \oplus H^1_{\mathrm{XXZ}} \oplus H^2_{\mathrm{XXZ}} \oplus H^3_{\mathrm{XXZ}} \oplus H^4_{\mathrm{XXZ}} \tag{B.14}$$

The only non-trivial diagonalization occurs in the $q = 2$ block. Restricting to this sector, we now invoke the translation symmetry of the model

$$\Gamma_4 H^2_{\mathrm{XXZ}} \Gamma_4^\dagger = H^{2,0}_{\mathrm{XXZ}} \oplus H^{2,1}_{\mathrm{XXZ}} \oplus H^{2,2}_{\mathrm{XXZ}} \oplus H^{2,3}_{\mathrm{XXZ}} \tag{B.15}$$

where Γ_4 is a unitary transformation that diagonalizes T_4. The $a = 1, 3$ blocks are singlets, while $a = 0, 2$ are doublets (see Eq.(B.11)). Only for $a = 0$ do the Fourier modes mix, although the mixing angle is parameter independent. But obviously the eigenvalues depend on the Hamiltonian paramters. We find the non-unitary parameters

of the dynamical map to be

$$\begin{aligned}\lambda_{3,i}(t,4) =&\left(\frac{7}{16}+\frac{1}{4}\cos 2J_\perp t+\frac{5}{16}\cos 4J_\perp t\right)\\ &+\left(\frac{1}{16}-\frac{1}{12}\cos 2J_\perp t+\frac{1}{48}\cos 4J_\perp t\right)\sum_{\substack{k<l\\k,l\neq i}} z_k z_l\end{aligned} \tag{B.16}$$

$$\begin{aligned}\tau_{3,i}(t,4) =&\left(\frac{3}{16}-\frac{1}{12}\cos 2J_\perp t-\frac{5}{48}\cos 4J_\perp t\right)\sum_{k\neq i} z_k\\ &-\left(\frac{3}{16}-\frac{1}{4}\cos 2J_\perp t+\frac{1}{16}\cos 4J_\perp t\right)\prod_{k\neq i} z_k\end{aligned} \tag{B.17}$$

$$\begin{aligned}\alpha_i(t,4) =&\left(\frac{3}{16}\cos\left(3J_\perp+J_\parallel\right)t+\frac{1}{16}\cos 3(J_\perp-J_\parallel)t\right.\\ &+\frac{3}{32}\cos\left(J_\perp+3J_\parallel\right)t+\frac{1}{4}\cos\left(J_\perp+J_\parallel\right)t\\ &\left.+\frac{3}{8}\cos\left(J_\perp-J_\parallel\right)t+\frac{1}{32}\cos\left(5J_\perp-J_\parallel\right)t\right)\\ &+\left(\frac{3}{16}\cos\left(3J_\perp+J_\parallel\right)t+\frac{1}{16}\cos 3(J_\perp-J_\parallel)t\right.\\ &-\frac{1}{32}\cos\left(J_\perp+3J_\parallel\right)t-\frac{1}{12}\cos\left(J_\perp+J_\parallel\right)t\\ &\left.-\frac{1}{8}\cos\left(J_\perp-J_\parallel\right)t-\frac{1}{96}\cos\left(5J_\perp-J_\parallel\right)t\right)\sum_{\substack{k<l\\k,l\neq i}} z_k z_l\end{aligned} \tag{B.18}$$

$$
\begin{aligned}
\beta_i(t,4) = &\left(\frac{3}{16}\sin\left(3J_\perp + J_\parallel\right)t - \frac{1}{16}\sin 3(J_\perp - J_\parallel)t \right. \\
&+ \frac{1}{32}\sin\left(J_\perp + 3J_\parallel\right)t + \frac{1}{12}\sin\left(J_\perp + J_\parallel\right)t \\
&\left. - \frac{1}{8}\sin\left(J_\perp - J_\parallel\right)t - \frac{1}{96}\sin\left(5J_\perp - J_\parallel\right)t \right) \sum_{k\neq i} z_k \\
&+ \left(\frac{3}{16}\sin\left(3J_\perp + J_\parallel\right)t - \frac{1}{16}\sin 3(J_\perp - J_\parallel)t \right. \\
&- \frac{3}{32}\sin\left(J_\perp + 3J_\parallel\right)t - \frac{1}{4}\sin\left(J_\perp + J_\parallel\right)t \\
&\left. + \frac{3}{8}\sin\left(J_\perp - J_\parallel\right)t + \frac{1}{32}\sin\left(5J_\perp - J_\parallel\right)t \right) \prod_{k\neq i} z_k
\end{aligned}
\tag{B.19}
$$

B.2.1.2 5-qubits

As the exact diagonalization is more complicated for the 5-qubit network, we shall go through the steps more explicitly than the 4-qubit case. Again we may change to the canonical excitation basis

$$
\mathcal{P}_5 H_{\mathrm{XXZ}} \mathcal{P}_5^\dagger = H^0_{\mathrm{XXZ}} \oplus H^1_{\mathrm{XXZ}} \oplus H^2_{\mathrm{XXZ}} \oplus H^3_{\mathrm{XXZ}} \oplus H^4_{\mathrm{XXZ}} \oplus H^5_{\mathrm{XXZ}} \,. \tag{B.20}
$$

As with the ring topology, we further go to the basis of translation eigenstates. Again the only excitation number blocks that are not diagonalized trivially at this stage are

$$
\Gamma_5 H^2_{\mathrm{XXZ}} \oplus H^3_{\mathrm{XXZ}} \Gamma_5^\dagger = \bigoplus_{a=0}^{4} H^{2,a}_{\mathrm{XXZ}} \oplus H^{3,a}_{\mathrm{XXZ}} \,. \tag{B.21}
$$

And as for the ring-topology, we obtain a set of ten 2×2 matrices that require further computation to diagonalize. The $q = 2$ blocks are found to be

$$
\begin{aligned}
H^{2,0}_{\mathrm{XXZ}} &= \begin{bmatrix} -h - J_{\parallel} + 2J_{\perp} & 4J_{\perp} \\ \\ 4J_{\perp} & -h - J_{\parallel} + 2J_{\perp} \end{bmatrix} \\
H^{2,1}_{\mathrm{XXZ}} &= \begin{bmatrix} -h - J_{\parallel} + \left(\frac{\sqrt{5}-1}{2}\right) J_{\perp} & -J_{\perp} e^{-\frac{6\pi i}{5}} \\ \\ -J_{\perp} e^{\frac{6\pi i}{5}} & -h - J_{\parallel} - \left(\frac{\sqrt{5}+1}{2}\right) J_{\perp} \end{bmatrix} \\
H^{2,2}_{\mathrm{XXZ}} &= \begin{bmatrix} -h - J_{\parallel} - \left(\frac{\sqrt{5}+1}{2}\right) J_{\perp} & -J_{\perp} e^{-\frac{2\pi i}{5}} \\ \\ -J_{\perp} e^{\frac{2\pi i}{5}} & -h - J_{\parallel} + \left(\frac{\sqrt{5}-1}{2}\right) J_{\perp} \end{bmatrix}
\end{aligned}
\tag{B.22}
$$

With the remaining blocks determined by the relations $H^{2,2}_{\mathrm{XXZ}} = \left(H^{2,3}_{\mathrm{XXZ}}\right)^T$ and $H^{2,1}_{\mathrm{XXZ}} = \left(H^{2,4}_{\mathrm{XXZ}}\right)^T$. The matrix representations for the $q = 3$ block are obtained through the replacement $h \to -h$, affecting only the eigenvalues and not the form of the associated eigenvectors. Again to due to large degree of symmetry of the model, the eigenvectors are parameter independent. The resulting map parameter functions are:

$$
\begin{aligned}
\lambda_{3,i}(t,5) =& \left(\frac{7}{15} + \frac{1}{3}\cos 3J_{\perp}t + \frac{1}{5}\cos 5J_{\perp}t\right) \\
&+ \left(\frac{8}{225} - \frac{1}{18}\cos 3J_{\perp}t + \frac{1}{50}\cos 5J_{\perp}t\right) \sum_{\substack{k<l \\ k,l\neq i}} z_k z_l
\end{aligned}
\tag{B.23}
$$

$$
\begin{aligned}
\tau_{3,i}(t,5) =& \left(\frac{2}{15} - \frac{1}{12}\cos 3J_{\perp}t - \frac{1}{20}\cos 5J_{\perp}t\right) \sum_{k\neq i} z_k \\
&- \left(\frac{4}{75} - \frac{1}{12}\cos 3J_{\perp}t + \frac{3}{100}\cos 5J_{\perp}t\right) \sum_{\substack{k<l<j \\ k,l,j\neq i}} z_k z_l z_j
\end{aligned}
\tag{B.24}
$$

$$
\begin{aligned}
\alpha_i(t,5) =& \left(\frac{157}{600} + \frac{1}{12}\cos 3J_\perp t + \frac{3}{100}\cos 5J_\perp t + \frac{3}{50}\cos{(3J_\perp + 2J_\parallel)}t \right. \\
&+ \frac{1}{40}\cos 4(J_\perp - J_\parallel)t + \frac{1}{100}\cos{(7J_\perp - 2J_\parallel)}t \\
&+ \frac{9}{50}\cos 2(J_\perp - J_\parallel)t + \frac{1}{4}\cos{(J_\perp + 2J_\parallel)}t \\
&\left. + \frac{1}{10}\cos{(J_\perp + 4J_\parallel)}t \right) \\
&- \left(\frac{157}{1800} + \frac{1}{36}\cos 3J_\perp t + \frac{1}{100}\cos 5J_\perp t - \frac{1}{40}\cos 4(J_\perp - J_\parallel)t \right. \\
&\left. - \frac{1}{10}\cos{(J_\perp + 4J_\parallel)}t \right) \sum_{\substack{k<l \\ k,l\neq i}} z_k z_l \\
&+ \left(\frac{157}{600} + \frac{1}{12}\cos 3J_\perp t + \frac{3}{100}\cos 5J_\perp t + \frac{1}{10}\cos{(J_\perp + 4J_\parallel)}t \right. \\
&- \frac{1}{4}\cos{(J_\perp + 2J_\parallel)}t - \frac{3}{50}\cos{(3J_\perp + 2J_\parallel)}t \\
&- \frac{1}{100}\cos{(7J_\perp - 2J_\parallel)}t - \frac{9}{50}\cos 2(J_\perp - J_\parallel)t \\
&\left. + \frac{1}{40}\cos 4(J_\perp - J_\parallel)t \right) \sum_{\substack{j<k<l<m \\ j,k,l,m\neq i}} z_j z_k z_l z_m
\end{aligned}
\tag{B.25}
$$

$$
\begin{aligned}
\beta_i(t,5) =& \left(\frac{3}{100}\sin{(3J_\perp + 2J_\parallel)}t - \frac{1}{40}\sin 4(J_\perp - J_\parallel)t \right. \\
&- \frac{1}{200}\sin{(7J_\perp - 2J_\parallel)}t - \frac{9}{100}\sin 2(J_\perp - J_\parallel)t \\
&\left. + \frac{1}{8}\sin{(J_\perp + 2J_\parallel)}t + \frac{1}{10}\sin{(J_\perp + 4J_\parallel)}t \right) \sum_{k\neq i} z_k \\
&- \left(\frac{3}{100}\sin{(3J_\perp + 2J_\parallel)}t + \frac{1}{40}\sin 4(J_\perp - J_\parallel)t \right. \\
&- \frac{1}{200}\sin{(7J_\perp - 2J_\parallel)}t - \frac{9}{100}\sin 2(J_\perp - J_\parallel)t \\
&\left. + \frac{1}{8}\sin{(J_\perp + 2J_\parallel)}t - \frac{1}{10}\sin{(J_\perp + 4J_\parallel)}t \right) \sum_{\substack{k<l<j \\ j,k,l\neq i}} z_j z_k z_l
\end{aligned}
\tag{B.26}
$$

B.2.1.3 6-qubits

Repeating the procedures of the previous sections we may block diagonalize the 6-qubit XXZ-network. Going to the Fourier basis we have the remaining blocks to diagonalize

$$\Gamma_6\Big(H^2_{\rm XXZ}\oplus H^3_{\rm XXZ}\oplus H^4_{\rm XXZ}\Big)\Gamma_6^\dagger=\bigoplus_{a=0}^{5}H^{2,a}_{\rm XXZ}\oplus H^{3,a}_{\rm XXZ}\oplus H^{4,a}_{\rm XXZ} \tag{B.27}$$

which provides more of a challenge than the previous examples as now 4×4 blocks and 3×3 blocks appear. But the example still retains a degree of simplicity, as the eigenvectors do not contain any parameter dependence. The computation may be further reduced by noting that once $H^{2,a}_{\rm XXZ}$ is diagonalized, a similar transformation may be used to diagonalize $H^{4,a}_{\rm XXZ}$. As for the size of the various blocks we have for $q=2$

$$\begin{aligned}{\rm dim}H^{2,0}_{\rm XXZ}={\rm dim}H^{2,2}_{\rm XXZ}={\rm dim}H^{2,4}_{\rm XXZ}=3\\ {\rm dim}H^{2,1}_{\rm XXZ}={\rm dim}H^{2,3}_{\rm XXZ}={\rm dim}H^{2,5}_{\rm XXZ}=2\end{aligned} \tag{B.28}$$

where the same holds for $q=4$. All of these blocks create superpositions amongst the Fourier modes except $H^{2,3}_{\rm XXZ}$, which is comprised of two singlet states $|\mathcal{F}^3_2,0\rangle$ and $|\mathcal{F}^3_2,1\rangle$. The same conclusion applies for $q=4$. For $q=3$ we have

$$\begin{aligned}{\rm dim}H^{3,0}_{\rm XXZ}={\rm dim}H^{3,3}_{\rm XXZ}=4\\ {\rm dim}H^{3,1}_{\rm XXZ}={\rm dim}H^{3,2}_{\rm XXZ}={\rm dim}H^{3,4}_{\rm XXZ}={\rm dim}H^{3,5}_{\rm XXZ}=3\end{aligned} \tag{B.29}$$

and there are mixtures created among all the Fourier modes except $|\mathcal{F}^2_3,0\rangle$ and $|\mathcal{F}^4_3,0\rangle$.

$$\begin{aligned}\lambda_{3,i}(t,6)=&\left(\frac{59}{144}+\frac{5}{32}\cos 2J_\perp t+\frac{5}{16}\cos 4J_\perp t+\frac{35}{288}\cos 6J_\perp t\right)\\ &+\left(\frac{1}{24}-\frac{1}{32}\cos 2J_\perp t-\frac{1}{40}\cos 4J_\perp t+\frac{7}{480}\cos 6J_\perp t\right)\sum_{\substack{k<l\\ k,l\neq i}}z_kz_l\\ &-\left(\frac{1}{48}-\frac{1}{32}\cos 2J_\perp t+\frac{1}{80}\cos 4J_\perp t-\frac{1}{480}\cos 6J_\perp t\right)\sum_{\substack{j<k<l,m\\ j,k,l,m\neq i}}z_jz_kz_lz_m\end{aligned} \tag{B.30}$$

$$\begin{aligned}\tau_{3,i}(t,6) =&\left(\frac{17}{144}-\frac{1}{32}\cos 2J_\perp t-\frac{1}{16}\cos 4J_\perp t-\frac{7}{288}\cos 6J_\perp t\right)\sum_{k\neq i} z_k\\ &-\left(\frac{1}{24}-\frac{1}{32}\cos 2J_\perp t-\frac{1}{40}\cos 4J_\perp t+\frac{7}{480}\cos 6J_\perp t\right)\sum_{\substack{k<l<j\\ k,l,j\neq i}} z_k z_l z_j\\ &+\left(\frac{5}{48}-\frac{5}{32}\cos 2J_\perp t+\frac{1}{16}\cos 4J_\perp t-\frac{1}{96}\cos 6J_\perp t\right)\prod_{j\neq i} z_j\end{aligned} \tag{B.31}$$

The expressions for $\alpha(t)$ and $\beta(t)$ are lengthy, therefore we shall express our results using the partial components. The remaining non-zero partial components are obtained using the permutation symmetry, for example $\alpha_i^{zz000}=\alpha_i^{z0z00}=\alpha_i^{00zz0}$, etc. We find

$$\begin{aligned}\alpha_i^{00000}(t,6) =&\frac{5}{96}\cos\left(J_\perp+5J_\parallel\right)t+\frac{1}{96}\cos 5(J_\perp-J_\parallel)t\\ &+\frac{3}{16}\cos\left(J_\perp+3J_\parallel\right)t+\frac{25}{288}\cos 3(J_\perp-J_\parallel)t\\ &+\frac{1}{288}\cos\left(9J_\perp-3J_\parallel\right)t+\frac{1}{48}\cos\left(5J_\perp+J_\parallel\right)t\\ &+\frac{3}{32}\cos\left(3J_\perp+J_\parallel\right)t+\frac{5}{32}\cos\left(J_\perp+J_\parallel\right)t\\ &+\frac{5}{16}\cos\left(J_\perp-J_\parallel\right)t+\frac{1}{32}\cos\left(5J_\perp-J_\parallel\right)t\\ &+\frac{1}{96}\cos\left(7J_\perp-J_\parallel\right)t+\frac{5}{144}\cos 3(J_\perp+J_\parallel)t\end{aligned} \tag{B.32}$$

$$\begin{aligned}\alpha_i^{zz000}(t,6) =&\frac{5}{96}\cos\left(J_\perp+5J_\parallel\right)t+\frac{1}{96}\cos 5(J_\perp-J_\parallel)t\\ &+\frac{3}{80}\cos\left(J_\perp+3J_\parallel\right)t-\frac{1}{240}\cos\left(5J_\perp+J_\parallel\right)t\\ &-\frac{3}{160}\cos\left(3J_\perp+J_\parallel\right)t-\frac{1}{32}\cos\left(J_\perp+J_\parallel\right)t\\ &+\frac{5}{288}\cos 3(J_\perp-J_\parallel)t+\frac{1}{1440}\cos\left(9J_\perp-3J_\parallel\right)t\\ &-\frac{1}{16}\cos\left(J_\perp-J_\parallel\right)t-\frac{1}{160}\cos\left(5J_\perp-J_\parallel\right)t\\ &-\frac{1}{480}\cos\left(7J_\perp-J_\parallel\right)t+\frac{1}{144}\cos 3(J_\perp+J_\parallel)t\end{aligned} \tag{B.33}$$

$$
\begin{aligned}
\alpha_i^{zzzz0}(t,6) =& \frac{5}{96}\cos{(J_\perp+5J_\parallel)t} + \frac{1}{96}\cos{5(J_\perp-J_\parallel)t} \\
&-\frac{9}{80}\cos{(J_\perp+3J_\parallel)t} - \frac{5}{96}\cos{3(J_\perp-J_\parallel)t} \\
&-\frac{1}{480}\cos{(9J_\perp-3J_\parallel)t} + \frac{1}{240}\cos{(5J_\perp+J_\parallel)t} \\
&+\frac{3}{160}\cos{(3J_\perp+J_\parallel)t} + \frac{1}{32}\cos{(J_\perp+J_\parallel)t} \\
&+\frac{1}{16}\cos{(J_\perp-J_\parallel)t} + \frac{1}{160}\cos{(5J_\perp-J_\parallel)t} \\
&+\frac{1}{480}\cos{(7J_\perp-J_\parallel)t} - \frac{1}{48}\cos{3(J_\perp+J_\parallel)t}
\end{aligned} \tag{B.34}
$$

$$
\begin{aligned}
\beta_i^{z0000}(t,6) =& \frac{5}{96}\sin{(J_\perp+5J_\parallel)t} - \frac{1}{96}\sin{5(J_\perp-J_\parallel)t} \\
&+\frac{9}{80}\sin{(J_\perp+3J_\parallel)t} - \frac{5}{96}\sin{3(J_\perp-J_\parallel)t} \\
&-\frac{1}{480}\sin{(9J_\perp-3J_\parallel)t} + \frac{1}{240}\sin{(5J_\perp+J_\parallel)t} \\
&+\frac{3}{160}\sin{(3J_\perp+J_\parallel)t} + \frac{1}{32}\sin{(J_\perp+J_\parallel)t} \\
&-\frac{1}{16}\sin{(J_\perp-J_\parallel)t} - \frac{1}{160}\sin{(5J_\perp-J_\parallel)t} \\
&-\frac{1}{480}\sin{(7J_\perp-J_\parallel)t} + \frac{1}{48}\sin{3(J_\perp+J_\parallel)t}
\end{aligned} \tag{B.35}
$$

$$
\begin{aligned}
\beta_i^{zzz00}(t,6) =& \frac{5}{96}\sin{(J_\perp+5J_\parallel)t} - \frac{1}{96}\sin{5(J_\perp-J_\parallel)t} \\
&-\frac{3}{80}\sin{(J_\perp+3J_\parallel)t} + \frac{5}{288}\sin{3(J_\perp-J_\parallel)t} \\
&+\frac{1}{1440}\sin{(9J_\perp-3J_\parallel)t} - \frac{1}{240}\sin{(5J_\perp+J_\parallel)t} \\
&-\frac{3}{160}\sin{(3J_\perp+J_\parallel)t} - \frac{1}{32}\sin{(J_\perp+J_\parallel)t} \\
&+\frac{1}{16}\sin{(J_\perp-J_\parallel)t} + \frac{1}{160}\sin{(5J_\perp-J_\parallel)t} \\
&+\frac{1}{480}\sin{(7J_\perp-J_\parallel)t} - \frac{1}{144}\sin{3(J_\perp+J_\parallel)t}
\end{aligned} \tag{B.36}
$$

$$
\begin{aligned}
\beta_i^{zzzzz}(t,6) =& \frac{5}{96}\sin\left(J_\perp + 5J_\parallel\right)t - \frac{1}{96}\sin 5(J_\perp - J_\parallel)t \\
&- \frac{3}{16}\sin\left(J_\perp + 3J_\parallel\right)t + \frac{25}{288}\sin 3(J_\perp - J_\parallel)t \\
&+ \frac{1}{288}\sin\left(9J_\perp - 3J_\parallel\right)t + \frac{1}{48}\sin\left(5J_\perp + J_\parallel\right)t \\
&+ \frac{3}{32}\sin\left(3J_\perp + J_\parallel\right)t + \frac{5}{32}\sin\left(J_\perp + J_\parallel\right)t \\
&- \frac{5}{16}\sin\left(J_\perp - J_\parallel\right)t - \frac{1}{32}\sin\left(5J_\perp - J_\parallel\right)t \\
&- \frac{1}{96}\sin\left(7J_\perp - J_\parallel\right)t - \frac{5}{144}\sin 3(J_\perp + J_\parallel)t
\end{aligned}
\tag{B.37}
$$

B.2.2 Ring-connected XXZ-network

Turning to the more difficult model, the homogeneous XXZ-ring. Due to the more complicated structure of this model we only investigate the XXZ model for $N = 4$, and use the XXX model for $N = 5$, where we only present the computations for $\lambda_3(t)$ and $\tau_3(t)$.

B.2.2.1 4-qubits

For 4-qubits the Hamiltonian has the block diagonal structure

$$
\mathcal{P}_4 H_{\mathrm{XXZ}} \mathcal{P}_4^\dagger = H^0_{\mathrm{XXZ}} \oplus H^1_{\mathrm{XXZ}} \oplus H^2_{\mathrm{XXZ}} \oplus H^3_{\mathrm{XXZ}} \oplus H^4_{\mathrm{XXZ}} \tag{B.38}
$$

The only non-trivial diagonalization occurs in the q=2 block. Restricting to this sector, we may reduce it to smaller blocks by invoking the translation symmetry

$$
\Gamma_4 H^2_{\mathrm{XXZ}} \Gamma_4^\dagger = H^{2,0}_{\mathrm{XXZ}} \oplus H^{2,1}_{\mathrm{XXZ}} \oplus H^{2,2}_{\mathrm{XXZ}} \oplus H^{2,3}_{\mathrm{XXZ}} \tag{B.39}
$$

where Γ_4 is a unitary transformation that diagonalizes T_4. The $a = 1, 3$ blocks are singlets, while $a = 0, 2$ are both doublets. Mixing only occurs within the $a = 0$ block, which in this case does depend on the parameters of the Hamiltonian. Theses stationary states of $H^{2,2}_{\mathrm{XXZ}}$ are determined to be

$$
\begin{aligned}
|E_2^0; 0\rangle &= \cos\frac{\phi_\times}{2}|\mathcal{F}_2^0; 0\rangle + \sin\frac{\phi_\times}{2}|\mathcal{F}_2^0; 1\rangle \\
|E_2^0; 1\rangle &= \sin\frac{\phi_\times}{2}|\mathcal{F}_2^0; 0\rangle - \cos\frac{\phi_\times}{2}|\mathcal{F}_2^0; 1\rangle \\
\omega_\pm &= J_\parallel \pm \mathrm{sgn}\Big(J_\parallel\Big) J_\times
\end{aligned}
\tag{B.40}
$$

where the Hamiltonian dependent parameters we have introduced are

$$\begin{aligned} J_\times &= \sqrt{J_\parallel^2 + 8J_\perp^2} \\ \phi_\times &= -\tan^{-1} 2^{\frac{3}{2}} \frac{J_\perp}{J_\parallel}\,. \end{aligned} \tag{B.41}$$

$$\begin{aligned} \lambda_{3,i}(t,4) = &\Big(\frac{7}{16} + \frac{1}{4}\cos 2J_\perp t + \frac{1}{16}\cos 4J_\perp t + \frac{1}{4}\cos J_\parallel t \cos J_\times t \\ &+ \frac{1}{4}\cos\phi_\times \sin J_\parallel t \sin J_\times t\Big) \\ &+ \Big(\frac{1}{16} + \cos 4J_\perp t - \frac{1}{8}\cos J_\parallel t \cos J_\times t \\ &- \frac{1}{8}\cos\phi_\times \sin J_\parallel t \sin J_\times t\Big)\Big(z_{i-1}z_{i+2} + z_{i+1}z_{i+2}\Big) \\ &- \Big(\frac{3}{16} - \frac{1}{4}\cos 2J_\perp t + \frac{1}{16}\cos 4J_\perp t\Big)\Big(z_{i-1}z_{i+1}\Big) \end{aligned} \tag{B.42}$$

$$\begin{aligned} \tau_{3,i}(t,4) = &\Big(\frac{1}{16} - \frac{1}{4}\cos 2J_\perp t - \frac{1}{16}\cos 4J_\perp t + \frac{1}{4}\cos J_\parallel t \cos J_\times t \\ &+ \frac{1}{4}\cos\phi_\times \sin J_\parallel t \sin J_\times t\Big)\prod_{k\neq i} z_k \\ &+ \Big(\frac{3}{16} - \frac{1}{16}\cos 4J_\perp t - \frac{1}{8}\cos\phi_\times \sin J_\parallel t \sin J_\times t \\ &- \frac{1}{8}\cos J_\parallel t \cos J_\times t\Big)(z_{i-1} + z_{i+1}) \\ &+ \Big(\frac{3}{16} - \frac{1}{4}\cos 2J_\perp t + \frac{1}{16}\cos 4J_\perp t\Big) z_{i+2} \end{aligned} \tag{B.43}$$

As seen in the previous section, the expression for $\alpha(t)$ and $\beta(t)$ are more cumbersome than the other non-unitary parameters. Therefore we again split them into their partial components. For the ring topology we only need to consider the reflection symmetry to generate additional partial components as will be clear in the following equations. We find

$$\begin{aligned} \alpha_i^{000}(t,4) = &\frac{1}{4} + \frac{1+3\cos 2J_\parallel t}{16}\cos^2 J_\perp t + \frac{1+3\cos 2J_\perp t}{16}\cos J_\parallel t \cos J_\times t \\ &- \frac{\sqrt{2}}{8}\sin\phi_\times \sin 2J_\perp t \cos J_\parallel t \sin J_\times t \\ &- \frac{\big(1+\cos\phi_\times \sin J_\perp t \sin J_\times t\big)}{8}\sin^2 J_\parallel t \end{aligned} \tag{B.44}$$

$$\begin{aligned}\alpha_i^{0zz}(t,4) = \frac{\cos^2 J_\perp t}{8}\Big(\cos 2J_\parallel t - \cos J_\parallel t\cos J_\times t + \cos\phi_\times \sin J_\parallel t \sin J_\times t\Big)\\ + \frac{\sqrt{2}}{16}\sin\phi_\times \cos J_\parallel t \sin 2J_\perp t \sin J_\times t = \alpha_i^{zz0}(t,4)\end{aligned} \tag{B.45}$$

$$\begin{aligned}\alpha_i^{z0z}(t,4) = -\frac{1}{8} + \frac{\cos^2 J_\perp t}{4}\Big(1+\frac{3}{2}\cos 2J_\parallel t\Big) - \frac{\sin^2 J_\perp t}{8}\cos J_\parallel t\cos J_\times t\\ + \frac{1+3\cos 2J_\perp t}{16}\cos\phi_\times \sin J_\parallel t \sin J_\times t\end{aligned} \tag{B.46}$$

$$\begin{aligned}\beta_i^{z00}(t,4) = -\frac{\cos^2 J_\perp t}{8}\Big(3\sin 2J_\parallel t + \sin J_\parallel t\cos J_\times t + \cos\phi_\times \cos J_\parallel t \sin J_\times t\Big)\\ + \frac{\sqrt{2}}{16}\sin\phi_\times \sin J_\parallel t \sin 2J_\perp t \sin J_\times t = \beta_i^{00z}(t,4)\end{aligned} \tag{B.47}$$

$$\begin{aligned}\beta_i^{0z0}(t,4) = \frac{1+3\cos 2J_\perp t}{16}\cos\phi_\times \cos J_\parallel t \sin J_\times t - \frac{\cos^2 J_\perp t}{8}\sin 2J_\parallel t\\ + \frac{\sin^2 J_\perp t}{8}\sin J_\parallel t\cos J_\times t\end{aligned} \tag{B.48}$$

$$\begin{aligned}\beta_i^{zzz}(t,4) = \frac{\sin^2 J_\perp t}{8}\cos\phi_\times t\cos J_\parallel t\sin J_\times t - \frac{\cos^2 J_\perp t}{8}\sin 2J_\parallel t\\ + \frac{1+3\cos 2J_\perp t}{16}\sin J_\parallel t\cos J_\times t\\ - \frac{\sqrt{2}}{16}\sin\phi_\times \sin J_\parallel t \sin 2J_\perp t \sin J_\times t\end{aligned} \tag{B.49}$$

B.2.2.2 5-qubits

As with the previous examples we change from the computational basis to the canonically ordered excitation basis. We achieve this by using a permutation matrix

$$\mathcal{P}_5 H_{\mathrm{XXZ}}\mathcal{P}_5^\dagger = H^0_{\mathrm{XXZ}} \oplus H^1_{\mathrm{XXZ}} \oplus H^2_{\mathrm{XXZ}} \oplus H^3_{\mathrm{XXZ}} \oplus H^4_{\mathrm{XXZ}} \oplus H^5_{\mathrm{XXZ}} \tag{B.50}$$

and we are interested in finding the stationary states of the middle two blocks, as the others may be found trivially. Now we can go further by changing to a translation eigenbasis

$$\Gamma_5 H^2_{\mathrm{XXZ}} \oplus H^3_{\mathrm{XXZ}}\Gamma_5^\dagger = \bigoplus_{a=0}^{4} H^{2,a}_{\mathrm{XXZ}} \oplus H^{3,a}_{\mathrm{XXZ}} \tag{B.51}$$

where the $q = 2$ blocks take the form

$$H^{2,a}_{\mathrm{XXZ}} = \begin{bmatrix} -h + \frac{1}{2}J_{\parallel} & \left(2\cos\frac{6\pi a}{5}J_{\perp}\right)e^{-\frac{6\pi i a}{5}} \\ \left(2\cos\frac{6\pi a}{5}J_{\perp}\right)e^{\frac{6\pi i a}{5}} & -h - \frac{3}{2}J_{\parallel} + 2\cos\frac{6\pi a}{5}J_{\perp} \end{bmatrix} \tag{B.52}$$

and the $q = 3$ blocks are obtained by sending $h \to -h$. We thus obtain the following parameterization of the non-trivial stationary states

$$\begin{aligned} \tan\psi_a &= \frac{6\pi a}{5} \\ \tan\phi_a &= \frac{2\cos\frac{6\pi a}{5}J_{\perp}}{\left(J_{\parallel} - \cos\frac{6\pi a}{5}J_{\perp}\right)} \\ J_a &= \sqrt{(J_{\parallel} - \cos\frac{6\pi a}{5}J_{\perp})^2 + 4\cos^2\frac{6\pi a}{5}J_{\perp}^2} \end{aligned} \tag{B.53}$$

Due to the length of the expression obtained, we must report the non-unitary parameters by the partial components defined in the main text. Setting $J_{\perp} = J_{\parallel}$ we find

$$\begin{aligned} \lambda^{0000}_{3,i}(t;5) = &\frac{71}{225} + \frac{13}{90}\cos(\frac{3-\sqrt{5}}{2})J_{\perp}t + \frac{1}{10}\cos(\frac{5-\sqrt{5}}{2})J_{\perp}t \\ &+ \frac{1}{45}\cos 3(\frac{1-\sqrt{5}}{2})J_{\perp}t + \frac{32}{225}\cos\sqrt{5}J_{\perp}t \\ &+ \frac{13}{90}\cos(\frac{3+\sqrt{5}}{2})J_{\perp}t + \frac{1}{10}\cos(\frac{5+\sqrt{5}}{2})J_{\perp}t \\ &+ \frac{2}{225}\cos 2\sqrt{5}J_{\perp}t + \frac{1}{45}\cos 3(\frac{1+\sqrt{5}}{2})J_{\perp}t \end{aligned} \tag{B.54}$$

$$\begin{aligned} \lambda^{zz00}_{3,i}(t,5) = &-\frac{6\sqrt{5}+25}{900}\cos(\frac{3+\sqrt{5}}{2})J_{\perp}t + \frac{6\sqrt{5}-25}{900}\cos(\frac{3-\sqrt{5}}{2})J_{\perp}t \\ &+\frac{1}{100}\cos(\frac{5+\sqrt{5}}{2})J_{\perp}t + \frac{1}{100}\cos(\frac{5-\sqrt{5}}{2})J_{\perp}t \\ &-\frac{\sqrt{5}}{450}\cos 3(\frac{1-\sqrt{5}}{2})J_{\perp}t + \frac{\sqrt{5}}{450}\cos 3(\frac{1+\sqrt{5}}{2})J_{\perp}t \\ &-\frac{2}{225}\cos 2\sqrt{5}J_{\perp}t + \frac{2}{45}\cos\sqrt{5}J_{\perp}t = \lambda^{00zz}_{3,i}(t,5) \end{aligned} \tag{B.55}$$

$$\begin{aligned}\lambda_{3,i}^{z0z0}(t,5) =&\frac{1}{100}\cos(\frac{5-\sqrt{5}}{2})J_\perp t-\frac{6\sqrt{5}+25}{900}\cos(\frac{3-\sqrt{5}}{2})J_\perp t\\&+\frac{\sqrt{5}}{450}\cos 3(\frac{1-\sqrt{5}}{2})J_\perp t-\frac{\sqrt{5}}{450}\cos 3(\frac{1+\sqrt{5}}{2})J_\perp t\\&+\frac{6\sqrt{5}-25}{900}\cos(\frac{3+\sqrt{5}}{2})J_\perp t+\frac{1}{100}\cos(\frac{5+\sqrt{5}}{2})J_\perp t\\&-\frac{2}{225}\cos 2\sqrt{5}J_\perp t+\frac{2}{45}\cos\sqrt{5}J_\perp t=\lambda_{3,i}^{0z0z}(t,5)\end{aligned}\tag{B.56}$$

$$\begin{aligned}\lambda_{3,i}^{0zz0}(t,5) =&\frac{1}{45}+\frac{3\sqrt{5}-5}{300}\cos(\frac{3-\sqrt{5}}{2})J_\perp t+\frac{1}{75}\cos 2\sqrt{5}J_\perp t\\&+\frac{1-\sqrt{5}}{100}\cos(\frac{5-\sqrt{5}}{2})J_\perp t-\frac{5-\sqrt{5}}{450}\cos 3(\frac{1-\sqrt{5}}{2})J_\perp t\\&-\frac{3\sqrt{5}+5}{300}\cos(\frac{3+\sqrt{5}}{2})J_\perp t+\frac{1+\sqrt{5}}{100}\cos(\frac{5+\sqrt{5}}{2})J_\perp t\\&-\frac{5+\sqrt{5}}{450}\cos 3(\frac{1+\sqrt{5}}{2})J_\perp t\end{aligned}\tag{B.57}$$

$$\begin{aligned}\lambda_{3,i}^{z00z}(t,5) =&\frac{1}{45}-\frac{3\sqrt{5}+5}{300}\cos(\frac{3-\sqrt{5}}{2})J_\perp t+\frac{1+\sqrt{5}}{100}\cos(\frac{5-\sqrt{5}}{2})J_\perp t\\&-\frac{5+\sqrt{5}}{450}\cos 3(\frac{1-\sqrt{5}}{2})J_\perp t+\frac{3\sqrt{5}-5}{300}\cos(\frac{3+\sqrt{5}}{2})J_\perp t\\&+\frac{1-\sqrt{5}}{100}\cos(\frac{5+\sqrt{5}}{2})J_\perp t+\frac{1}{75}\cos 2\sqrt{5}J_\perp t\\&+\frac{5-\sqrt{5}}{450}\cos 3(\frac{1+\sqrt{5}}{2})J_\perp t\end{aligned}\tag{B.58}$$

$$\begin{aligned}\tau_{3,i}^{z000}(t;5) =&\frac{77}{450}-\frac{1+\sqrt{5}}{40}\cos(\frac{5+\sqrt{5}}{2})J_\perp t-\frac{1-\sqrt{5}}{40}\cos(\frac{5-\sqrt{5}}{2})J_\perp t\\&-\frac{1-\sqrt{5}}{180}\cos 3(\frac{1-\sqrt{5}}{2})J_\perp t-\frac{1+\sqrt{5}}{180}\cos 3(\frac{1+\sqrt{5}}{2})J_\perp t\\&-\frac{13+3\sqrt{5}}{360}\cos(\frac{3+\sqrt{5}}{2})J_\perp t-\frac{13-3\sqrt{5}}{360}\cos(\frac{3-\sqrt{5}}{2})J_\perp t\\&-\frac{1}{450}\cos 2\sqrt{5}J_\perp t-\frac{8}{225}\cos\sqrt{5}J_\perp t=\tau_{3,i}^{000z}(t;5)\end{aligned}\tag{B.59}$$

$$\begin{aligned}\tau_{3,i}^{0z00}(t;5) =&\frac{77}{450}-\frac{1-\sqrt{5}}{40}\cos(\frac{5+\sqrt{5}}{2})J_\perp t-\frac{1+\sqrt{5}}{40}\cos(\frac{5-\sqrt{5}}{2})J_\perp t\\&-\frac{1+\sqrt{5}}{180}\cos 3(\frac{1-\sqrt{5}}{2})J_\perp t-\frac{1-\sqrt{5}}{180}\cos 3(\frac{1+\sqrt{5}}{2})J_\perp t\\&-\frac{13-3\sqrt{5}}{360}\cos(\frac{3+\sqrt{5}}{2})J_\perp t-\frac{13+3\sqrt{5}}{360}\cos(\frac{3-\sqrt{5}}{2})J_\perp t\\&-\frac{1}{450}\cos 2\sqrt{5}J_\perp t-\frac{8}{225}\cos\sqrt{5}J_\perp t=\tau_{3,i}^{00z0}(t;5)\end{aligned}\tag{B.60}$$

$$\begin{aligned}\tau_{3,i}^{zzz0}(t;5) =&-\frac{1}{90}-\frac{3-\sqrt{5}}{200}\cos(\frac{5+\sqrt{5}}{2})J_\perp t-\frac{3+\sqrt{5}}{200}\cos(\frac{5-\sqrt{5}}{2})J_\perp t\\ &+\frac{5+3\sqrt{5}}{900}\cos 3(\frac{1-\sqrt{5}}{2})J_\perp t+\frac{5-3\sqrt{5}}{900}\cos 3(\frac{1+\sqrt{5}}{2})J_\perp t\\ &+\frac{65+3\sqrt{5}}{1800}\cos(\frac{3+\sqrt{5}}{2})J_\perp t+\frac{65-3\sqrt{5}}{1800}\cos(\frac{3-\sqrt{5}}{2})J_\perp t\\ &+\frac{1}{450}\cos 2\sqrt{5}J_\perp t-\frac{2}{45}\cos(\sqrt{5}J_\perp t)=\tau_{3,i}^{0zzz0}(t;5)\end{aligned} \tag{B.61}$$

$$\begin{aligned}\tau_{3,i}^{z0zz}(t;5) =&-\frac{1}{90}-\frac{3+\sqrt{5}}{200}\cos(\frac{5+\sqrt{5}}{2})J_\perp t-\frac{3-\sqrt{5}}{200}\cos(\frac{5-\sqrt{5}}{2})J_\perp t\\ &+\frac{5-3\sqrt{5}}{900}\cos 3(\frac{1-\sqrt{5}}{2})J_\perp t+\frac{5+3\sqrt{5}}{900}\cos 3(\frac{1+\sqrt{5}}{2})J_\perp t\\ &+\frac{65-3\sqrt{5}}{1800}\cos(\frac{3+\sqrt{5}}{2})J_\perp t+\frac{65+3\sqrt{5}}{1800}\cos(\frac{3-\sqrt{5}}{2})J_\perp t\\ &+\frac{1}{450}\cos 2\sqrt{5}J_\perp t+\frac{2}{45}\cos(\sqrt{5}J_\perp t)=\tau_{3,i}^{zz0z}(t;5)\end{aligned} \tag{B.62}$$

B.2.3 Disconnected XX-network

In terms of the following parameterization of the eigendecomposition of $H_{\mathrm{XX}}^{1,2}$

$$\begin{aligned}h_{12}&=\frac{h_1+h_2}{2} \quad \omega_{12}=\mathrm{sgn}(\Delta_{12})\sqrt{\Delta_{12}^2+J_{12}^2}\\ \Delta_{12}&=h_1-h_2 \quad \tan\phi_{12}=\frac{J_{12}}{\Delta_{12}}\end{aligned} \tag{B.63}$$

the Pauli components of the unitary channel may be expressed as

$$
\begin{aligned}
&\mathcal{U}^{x0}_{zy} = \mathcal{U}^{zx}_{y0} = \mathcal{U}^{0x}_{yz} = \mathcal{U}^{xz}_{0y} = -\mathcal{U}^{y0}_{zx} = -\mathcal{U}^{zy}_{x0} = -\mathcal{U}^{0y}_{xz} = -\mathcal{U}^{yz}_{0x} = \sin\phi_{12}\sin\omega_{12}t\cos 2h_{12}t \\
&\mathcal{U}^{xx}_{0z} = \mathcal{U}^{yy}_{z0} = \mathcal{U}^{z0}_{xx} = \mathcal{U}^{z0}_{yy} = -\mathcal{U}^{xx}_{0z} = -\mathcal{U}^{yy}_{0z} = -\mathcal{U}^{0z}_{xx} = -\mathcal{U}^{0z}_{yy} = \cos\phi_{12}\sin\phi_{12}\sin^2\omega_{12}t \\
&\mathcal{U}^{xy}_{z0} = \mathcal{U}^{yx}_{z0} = \mathcal{U}^{z0}_{yx} = \mathcal{U}^{0z}_{xy} = -\mathcal{U}^{xy}_{0z} = -\mathcal{U}^{yx}_{z0} = -\mathcal{U}^{z0}_{xy} = -\mathcal{U}^{0z}_{yx} = \frac{1}{2}\sin\phi_{12}\sin 2\omega_{12}t \\
&\mathcal{U}^{0x}_{xz} = \mathcal{U}^{0y}_{yz} = \mathcal{U}^{xz}_{0x} = \mathcal{U}^{yz}_{0y} = \mathcal{U}^{x0}_{zx} = \mathcal{U}^{y0}_{zy} = \mathcal{U}^{zx}_{x0} = \mathcal{U}^{zy}_{y0} = \sin\phi_{12}\sin\omega_{12}t\sin 2h_{12}t \\
&\mathcal{U}^{y0}_{x0} = -\mathcal{U}^{x0}_{y0} = \mathcal{U}^{yz}_{xz} = -\mathcal{U}^{xz}_{yz} = \cos\omega_{12}t\sin 2h_{12}t + \cos\phi_{12}\sin\omega_{12}t\cos 2h_{12}t \\
&\mathcal{U}^{0y}_{0x} = -\mathcal{U}^{0x}_{0y} = \mathcal{U}^{zy}_{zx} = -\mathcal{U}^{zx}_{zy} = \cos\omega_{12}t\sin 2h_{12}t - \cos\phi_{12}\sin\omega_{12}t\cos 2h_{12}t \\
&\mathcal{U}^{x0}_{x0} = \mathcal{U}^{y0}_{y0} = \mathcal{U}^{xz}_{xz} = \mathcal{U}^{yz}_{yz} = \cos\omega_{12}t\cos 2h_{12}t - \cos\phi_{12}\sin\omega_{12}t\sin 2h_{12}t \\
&\mathcal{U}^{0x}_{0x} = \mathcal{U}^{0y}_{0y} = \mathcal{U}^{zx}_{zx} = \mathcal{U}^{zy}_{zy} = \cos\omega_{12}t\cos 2h_{12}t + \cos\phi_{12}\sin\omega_{12}t\sin 2h_{12}t \\
&\mathcal{U}^{yx}_{xx} = \mathcal{U}^{yy}_{xy} = -\mathcal{U}^{xx}_{yx} = -\mathcal{U}^{xy}_{yy} = \frac{1}{2}\Big(\sin 4h_{12}t + \cos\phi_{12}\sin 2\omega_{12}t\Big) \\
&\mathcal{U}^{xy}_{xx} = \mathcal{U}^{yy}_{yx} = -\mathcal{U}^{xx}_{xy} = -\mathcal{U}^{yx}_{yy} = \frac{1}{2}\Big(\sin 4h_{12}t - \cos\phi_{12}\sin 2\omega_{12}t\Big) \\
&\mathcal{U}^{yy}_{xx} = \mathcal{U}^{xx}_{yy} = \frac{1}{2}\Big(-\cos 4h_{12}t + \cos^2\phi_{12}\cos 2\omega_{12}t + \sin^2\phi_{12}\Big) \\
&\mathcal{U}^{xx}_{xx} = \mathcal{U}^{yy}_{yy} = \frac{1}{2}\Big(\cos 4h_{12}t + \cos^2\phi_{12}\cos 2\omega_{12}t + \sin^2\phi_{12}\Big) \\
&\mathcal{U}^{xy}_{xy} = \mathcal{U}^{yx}_{yx} = \frac{1}{2}\Big(\cos 4h_{12}t + \cos 2\omega_{12}t\Big) \\
&\mathcal{U}^{xy}_{yx} = \mathcal{U}^{yx}_{xy} = \frac{1}{2}\Big(\cos 4h_{12}t - \cos 2\omega_{12}t\Big) \\
&\mathcal{U}^{z0}_{z0} = \mathcal{U}^{0z}_{0z} = 1 - \sin^2\phi_{12}\sin^2\omega_{12}t \\
&\mathcal{U}^{z0}_{0z} = \mathcal{U}^{0z}_{z0} = \sin^2\phi_{12}\sin^2\omega_{12}t
\end{aligned}
\tag{B.64}
$$

Constructing the 1-qubit dynamical map, a non-unital dynamical map is obtained as given in Section 2. But enforcing a noise-distribution over ϕ_{12} that is an even function, the noise-averaged dynamical map takes the form Eq.(B.12).

Appendix C
Emergent Quantum Subsystems

C.1 Curvature functionals from the structure constants

To begin, a non-holonomic basis is a choice of basis over the tangent manifold that is non-commutative. Assume that $\{X_a\}$ forms a basis for the tangent manifold with

$$[X_a, X_b] = C^c{}_{ab} X_c \tag{C.1}$$

defining the structure constants associated to the chosen basis. The Christoffel connection (the unique connection that is torsion-less and compatible with the metric) in a non-coordinate basis is

$$\Gamma_{abc} = \frac{1}{2}\left[\partial_c g_{ab} + \partial_b g_{ac} - \partial_a g_{bc} + C_{abc} - C_{bca} - C_{cba}\right] . \tag{C.2}$$

Assuming $\{X_a\}$ is an orthonormal basis of the metric and that the metric is left invariant, the terms involving the metric vanish leaving

$$\Gamma_{abc} = \frac{1}{2}(C_{abc} - C_{bca} - C_{cba}) . \tag{C.3}$$

Notice that $\Gamma_{abc} = -\Gamma_{cba}$. The components of the Christoffel connection in an orthonormal, non-holonomic basis are referred to as the Ricci rotation coefficients [128]. The Riemann tensor and its various traces are computed as functions of the Christoffel connection and

structure constants [129]

$$
\begin{aligned}
R_{abcd} =& \Gamma^{e}{}_{db}\Gamma_{ace} - \Gamma^{e}{}_{cb}\Gamma_{ade} - C^{e}{}_{cd}\Gamma_{aeb} \\
R_{ab} =& -\frac{1}{2}g_{eb}\left(C_{dac}C^{ced} + C_{cad}C^{ced} - \frac{1}{2}C_{acd}C^{ecd}\right) \\
R =& -\frac{1}{2}C_{abc}C^{cba} - \frac{1}{4}C_{abc}C^{abc}\,.
\end{aligned}
\tag{C.4}
$$

Using the graphical method described in Appendix C.2, we compute the second order curvatures functionals in terms of structure constant networks. We have found

$$
\begin{aligned}
\mathcal{R}_2[g] = \frac{1}{16}g^{ef}g_{lk}\Bigg(& C_{dbf}\left[4C_{ace}C^{dbk}C^{acl} - 4C_{ace}C^{bdk}C^{cla} - 8C_{ace}C^{dbk}C^{cla}\right] \\
&+C_{fdb}\left[C_{eca}C^{kdb}C^{lca} - 4C_{ace}C^{kdb}C^{acl} + 4C_{ace}C^{kdb}C^{cla}\right]\Bigg)
\end{aligned}
$$

$$
\begin{aligned}
\mathcal{R}_4[g] = \frac{1}{8}g^{ef}g_{lk}\Bigg(& C_{dbf}\Big[4C_{ace}C^{dbk}C^{acl} - 4C_{ace}C^{bdk}C^{cla} - 8C_{ace}C^{dbk}C^{cla}\Big] \\
&+C_{fdb}\Big[3C_{eca}C^{kdb}C^{lca} + 8C_{ace}C^{kdb}C^{acl} + 8C_{ace}C^{kdb}C^{lca}\Big] \\
&-C_{fcd}\Big[C_{eba}C^{kdb}C^{lca} + 2C_{aeb}C^{dbk}C^{lca} + 4C_{aeb}C^{bdk}C^{acl} \\
&\quad 8C_{aeb}C^{kdb}C^{lca} - 8C_{aeb}C^{kdb}C^{cla} + 28C_{aeb}C^{kdb}C^{acl}\Big]\Bigg)\,.
\end{aligned}
$$

C.2 Graphical representation of structure networks

The fundamental information about the group structure and the metric on the manifold is carried in the structure constants, organized into the connection, and the metric. Any functionals one might want to define, including the Ricci scalar R, $\mathcal{R}_2[g]$, and $\mathcal{R}_4[g]$ can be built from the totally contracted combinations of C_{ijk}, C^{ijk}, $g^{\ell m}$, and $g_{\ell m}$. A diagrammatic representation of the terms is useful, where each C_{ijk} is represented by a node and contractions are indicated with edges. The line style of the edge carries relevant information about the contraction, i.e., whether it involves the metric and any symmetry

information.

We define the following notation for the placement and style of nodes and edges: C_{ijk} is a node with edges emerging upward, while C^{ijk} is a node with edges emerging downward. Contractions via the metric will then always be represented by horizontal lines, while others appear as vertical or diagonal lines. Since the C_{ijk} are antisymmetric in the last two indices, we differentiate contractions between indices in different positions. Contractions of indices both in the first position are drawn with a solid line, both indices in the second or both in the third position with a dashed line, and contractions between an index in the first position and one in the second or third is a solid line with arrows pointing from the node containing the first-position index to the node containing the second- or third-position index.

For example, the two terms contributing to the $R = -\frac{1}{2}C_{abc}C^{cba} - \frac{1}{4}C_{abc}C^{abc}$ can be drawn as

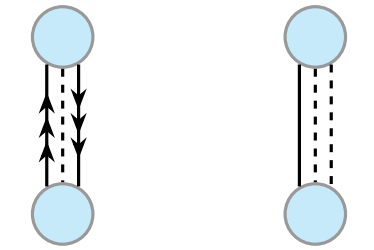

These are similar to the theta diagrams defined in [103]. The remaining curvature structures we consider, $\mathcal{R}_2$ and $\mathcal{R}_4$, have terms containing four structure constants, so all additional graphs have four nodes. There are two classes of graphs, depending on whether each node is connected to two others ("tin cans") or to three ("tetrahedra"). $\mathcal{R}_2$ contains only tin cans while $\mathcal{R}_4$ has both types of graphs.

Tin can terms from the product of four Christoffel symbols have a symmetry structure that helps to simplify the large number of terms. Consider, for example, the term

$$g^{ef}g_{\ell k}\Gamma_{fdb}\Gamma_{ace}\Gamma^{kdb}\Gamma^{ac\ell} = \frac{1}{4}g^{ef}g_{\ell k}(C_{fdb} - C_{dbf} - C_{bdf})(C^{kdb} - C^{dbk} - C^{bdk})\Gamma_{ace}\Gamma^{ac\ell} \ . \quad \text{(C.5)}$$

Here there are two pairs of terms that cancel, among the nine terms coming from expanding $\Gamma_{fdb}\Gamma^{kdb}$, due to the anti-symmetry of the full contraction under permutations of indices. On the other hand, there are two pairs of terms that add, containing $C_{dbf}C^{dbk}$ and $C_{bdf}C^{bdk}$, for example. There are therefore three sets of nine diagrams that remain

to be evaluated. For example, one such term is

$$g^{ef}g_{\ell k}C_{dbf}C^{dbk}\Big[C_{ace}C^{ac\ell}-C_{acd}C^{c\ell a}-C_{ace}C^{\ell ca} \\ -C_{cea}C^{ac\ell}+C_{cea}C^{c\ell a}+C_{cea}C^{\ell ca} \\ -C_{eca}C^{ac\ell}+C_{eca}C^{c\ell a}+C_{cea}C^{\ell ca}\Big]\subset g^{ef}g_{\ell k}\Gamma_{fdb}\Gamma_{ace}\Gamma^{kdb}\Gamma^{ac\ell}\,. \tag{C.6}$$

The nine terms in this sum can be represented diagramatically as:

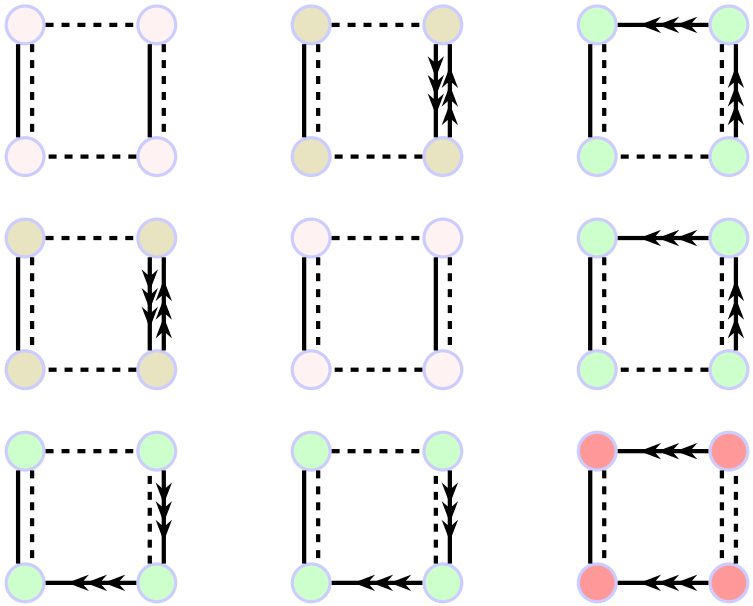

As the graph structure (and colors) indicate, the nine terms contain only four distinct constructions. Note that the graph structure does not directly indicate the relative sign between graphs related by a rotation of the structure nodes, for example between the upper right diagram and the lower left diagram. Furthermore, the signs of the terms are inherited from the signs in the expansions $\Gamma_{abc}=\frac{1}{2}(C_{abc}-C_{bca}-C_{cba})$. Collecting all relative signs, the two identical (green) diagrams in the right column cancel, as do the two identical (green) diagrams in the bottom row. The other pairs add so that there are three distinct diagrams. Within the four-gamma term that contains the above set, $g^{ef}g_{\ell k}\Gamma_{fdb}\Gamma_{ace}\Gamma^{kdb}\Gamma^{ac\ell}$, there are two other sets of nine terms that must be evaluated. The pattern of colors (identical graphs) and cancellations repeats in each of the nine sets of nine graphs, and there are ultimately three additional types of diagrams.

A different contraction structure occurs in terms like $g^{ef}g_{\ell k}C_{fcd}\Gamma_{aeb}\Gamma^{kdb}\Gamma^{ac\ell}$. This term can be represented by tetrahedron diagrams. Among the (seven) terms that do not cancel, there are just three diagrams:

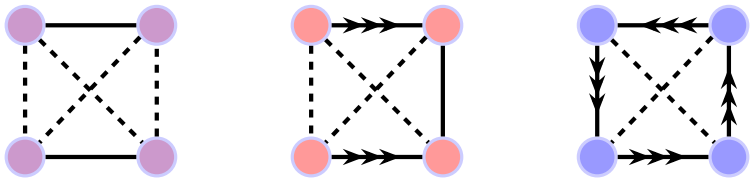

One can certainly consider other loss functionals. For example, the function primarily studied in [103], given by Eq.(4.58), contains terms with all even numbers of C_{ijk}. That work considered an expansion of terms up to third order, giving rise to graphs with two, four, and six nodes. However, only a subset of the four-vertex graphs appeared. The set of four-vertex graphs needed for the curvature terms is larger.

Bibliography

[1] Breuer and Petruccione (2002) The Theory of Open Quantum Systems, Oxford University Press, Oxford.

[2] Nielsen, M. A. and I. L. Chuang (2010) Quantum Computation and Quantum Information: 10th Anniversary Edition, Cambridge University Press.

[3] Rivas, A. and S. F. Huelga (2012) Open Quantum Systems: An Introduction, Springer Berlin Heidelberg.
URL http://dx.doi.org/10.1007/978-3-642-23354-8

[4] Kraus, K., W. Wootters, J. Dollard, and A. Böhn (1983) States, Effects, and Operations: Fundamental Notions of Quantum Theory, Lecture notes in physics, Springer-Verlag.
URL https://books.google.com/books?id=jbqxswEACAAJ

[5] Choi, M.-D. (1975) "Completely positive linear maps on complex matrices," Linear Algebra and its Applications, **10**(3), pp. 285–290.
URL https://www.sciencedirect.com/science/article/pii/0024379575900750

[6] Ruskai, M. B., S. Szarek, and E. Werner (2000) "An Analysis of Completely-Positive Trace-Preserving Maps on 2x2 Matrices," arXiv e-prints, quant-ph/0101003, quant-ph/0101003.

[7] Stinespring, W. F. (1955) "Positive Functions on C*-Algebras," Proceedings of the American Mathematical Society, **6**(2), pp. 211–216.
URL http://www.jstor.org/stable/2032342

[8] Wolf, M. M. and J. I. Cirac (2008) "Dividing Quantum Channels," Communications in Mathematical Physics, **279**(1), pp. 147–168.
URL https://doi.org/10.1007%2Fs00220-008-0411-y

[9] Milz, F. A., Pollock and Modi (2019) "Completely Positive Divisibility Does Not Mean Markovianity," Physical Review Letters, **123**(4).
URL http://dx.doi.org/10.1103/PhysRevLett.123.040401

[10] Chakraborty, S. and D. Chruściński (2019) "Information flow versus divisibility for qubit evolution," Physical Review A, **99**(4).
URL http://dx.doi.org/10.1103/PhysRevA.99.042105

[11] Davalos, D., M. Ziman, and C. Pineda (2019) "Divisibility of qubit channels and dynamical maps," Quantum, **3**, p. 144.
URL http://dx.doi.org/10.22331/q-2019-05-20-144

[12] Wissmann, S., H.-P. Breuer, and B. Vacchini (2015) "Generalized trace-distance measure connecting quantum and classical non-Markovianity," Physical Review A, **92**(4).
URL http://dx.doi.org/10.1103/PhysRevA.92.042108

[13] Lindblad, G. (1976) "On the generators of quantum dynamical semigroups," Communications in Mathematical Physics, **48**(2), pp. 119–130.

[14] Gorini, V., A. Kossakowski, and E. C. G. Sudarshan (1976) "Completely positive dynamical semigroups of N-level systems," Journal of Mathematical Physics, **17**(5), pp. 821–825.

[15] Nakajima, S. (1958) "On Quantum Theory of Transport Phenomena —Steady Diffusion—," Progress of Theoretical Physics, **20**(6), pp. 948–959.

[16] Zwanzig, R. (1960) "Ensemble Method in the Theory of Irreversibility," jcp, **33**(5), pp. 1338–1341.

[17] Shabani, A. and D. A. Lidar (2005) "Completely positive post-Markovian master equation via a measurement approach," Physical Review A, **71**(2).
URL http://dx.doi.org/10.1103/PhysRevA.71.020101

[18] Kaplanek, G. and C. P. Burgess (2020) "Hot Accelerated Qubits: Decoherence, Thermalization, Secular Growth and Reliable Late-time Predictions," JHEP, **03**, p. 008, 1912.12951.

[19] ——— (2020) "Hot Cosmic Qubits: Late-Time de Sitter Evolution and Critical Slowing Down," JHEP, **02**, p. 053, 1912.12955.

[20] ——— (2021) "Qubits on the Horizon: Decoherence and Thermalization near Black Holes," JHEP, **01**, p. 098, 2007.05984.

[21] Kaplanek, G. and E. Tjoa (2023) "Effective master equations for two accelerated qubits," Phys. Rev. A, **107**(1), p. 012208, 2207.13750.

[22] Colas, T., J. Grain, and V. Vennin (2022) "Benchmarking the cosmological master equations," Eur. Phys. J. C, **82**(12), p. 1085, 2209.01929.

[23] Colas, T., C. de Rham, and G. Kaplanek (2024) "Decoherence out of fire: purity loss in expanding and contracting universes," JCAP, **05**, p. 025, 2401.02832.

[24] Shandera, S., N. Agarwal, and A. Kamal (2018) "Open quantum cosmological system," Physical Review D, **98**(8).
URL http://dx.doi.org/10.1103/PhysRevD.98.083535

[25] Prudhoe, S. and S. Shandera (2023) "Classifying the non-time-local and entangling dynamics of an open qubit system," Journal of High Energy Physics, **2023**(2).
URL http://dx.doi.org/10.1007/JHEP02(2023)007

[26] Rivas, A., S. F. Huelga, and M. B. Plenio (2014) "Quantum non-Markovianity: characterization, quantification and detection," Reports on Progress in Physics, **77**(9), p. 094001.
URL http://dx.doi.org/10.1088/0034-4885/77/9/094001

[27] Calzetta, E. and B. L. Hu (1989) "Dissipation of quantum fields from particle creation," Phys. Rev. D, **40**, pp. 656–659.
URL https://link.aps.org/doi/10.1103/PhysRevD.40.656

[28] Koks, D., A. Matacz, and B. L. Hu (1997) "Entropy and uncertainty of squeezed quantum open systems," Phys. Rev. D, **55**, pp. 5917–5935.
URL https://link.aps.org/doi/10.1103/PhysRevD.55.5917

[29] Achúcarro, A. et al. (2022) "Inflation: Theory and Observations," 2203.08128.

[30] Shandera, S., N. Agarwal, and A. Kamal (2018) "Open quantum cosmological system," Phys. Rev. D, **98**(8), p. 083535, 1708.00493.

[31] Ooguri, H. and C. Vafa (2007) "On the Geometry of the String Landscape and the Swampland," Nucl. Phys. B, **766**, pp. 21–33, hep-th/0605264.

[32] Garg, S. K. and C. Krishnan (2019) "Bounds on Slow Roll and the de Sitter Swampland," JHEP, **11**, p. 075, 1807.05193.

[33] Ooguri, H., E. Palti, G. Shiu, and C. Vafa (2019) "Distance and de Sitter Conjectures on the Swampland," Phys. Lett. B, **788**, pp. 180–184, 1810.05506.

[34] Burgess, C. P., L. Leblond, R. Holman, and S. Shandera (2010) "Super-Hubble de Sitter Fluctuations and the Dynamical RG," JCAP, **03**, p. 033, 0912.1608.

[35] Agon, C., V. Balasubramanian, S. Kasko, and A. Lawrence (2018) "Coarse grained quantum dynamics," Physical Review D, **98**(2).
URL http://dx.doi.org/10.1103/PhysRevD.98.025019

[36] Weinberg, S. (2008) "Effective Field Theory for Inflation," Phys. Rev. D, **77**, p. 123541, 0804.4291.

[37] Banks, T., L. Susskind, and M. E. Peskin (1984) "Difficulties for the Evolution of Pure States Into Mixed States," Nucl. Phys. B, **244**, pp. 125–134.

[38] Unruh, W. G. and R. M. Wald (1995) "On evolution laws taking pure states to mixed states in quantum field theory," Phys. Rev. D, **52**, pp. 2176–2182, hep-th/9503024.

[39] Burgess, C. P., R. Holman, G. Tasinato, and M. Williams (2015) "EFT Beyond the Horizon: Stochastic Inflation and How Primordial Quantum Fluctuations Go Classical," JHEP, **03**, p. 090, 1408.5002.

[40] Burgess, C. P., R. Holman, and G. Tasinato (2016) "Open EFTs, IR effects \& late-time resummations: systematic corrections in stochastic inflation," JHEP, **01**, p. 153, 1512.00169.

[41] Burgess, C. P., R. Holman, and G. Kaplanek (2022) "Quantum Hotspots: Mean Fields, Open EFTs, Nonlocality and Decoherence Near Black Holes," Fortsch. Phys., **70**(4), p. 2200019, 2106.10804.

[42] Nielsen, M. A. and I. L. Chuang (2000) Quantum Computation and Quantum Information, Cambridge University Press.

[43] Braun, D., O. Giraud, I. Nechita, C. Pellegrini, and M. Žnidarič (2014) "A universal set of qubit quantum channels," Journal of Physics A: Mathematical and Theoretical, **47**(13), p. 135302.
URL https://doi.org/10.1088%2F1751-8113%2F47%2F13%2F135302

[44] Rodriguez, C. A., A. Shaji, and E. C. G. Sudarshan (2005), "Dynamics of Two Qubits: Decoherence and an Entanglement Optimization Protocol," .
URL https://arxiv.org/abs/quant-ph/0504051

[45] Niu, C.-S. and R. B. Griffiths (1999) "Two-qubit copying machine for economical quantum eavesdropping," Physical Review A, **60**(4), p. 2764–2776.
URL http://dx.doi.org/10.1103/PhysRevA.60.2764

[46] King, C. and M. B. Ruskai (2001) "Capacity of quantum channels using product measurements," Journal of Mathematical Physics, **42**(1), pp. 87–98.
URL https://doi.org/10.1063%2F1.1327598

[47] Berry, D. W. (2005) "Qubit channels that achieve capacity with two states," Physical Review A, **71**(3).
URL https://doi.org/10.1103%2Fphysreva.71.032334

[48] Kechrimparis, S. and J. Bae (2020), "Optimal measurement preserving qubit channels," .
URL https://arxiv.org/abs/2006.16366

[49] Ghosal, A., D. Das, and S. Banerjee (2021) "Characterizing qubit channels in the context of quantum teleportation," Physical Review A, **103**(5).
URL https://doi.org/10.1103%2Fphysreva.103.052422

[50] Gorini, V., A. Kossakowski, and E. C. G. Sudarshan (1976) "Completely positive dynamical semigroups of N-level systems," Journal of Mathematical Physics, **17**(5), pp. 821–825, https://aip.scitation.org/doi/pdf/10.1063/1.522979.
URL https://aip.scitation.org/doi/abs/10.1063/1.522979

[51] Shibata, F., Y. Takahashi, and N. Hashitsume (1977) "A generalized stochastic liouville equation: Non-Markovian versus memoryless master equations," J. Stat Phys., **17**, p. 171–187.

[52] Chaturvedi, S. and F. Shibata (1979) "Time-convolutionless projection operator formalism for elimination of fast variables. Applications to Brownian motion," Z Physik B, **35**, p. 297–308.

[53] Chruś ciński, D. and S. Maniscalco (2014) "Degree of Non-Markovianity of Quantum Evolution," Physical Review Letters, **112**(12).
URL https://doi.org/10.1103%2Fphysrevlett.112.120404

[54] Chruściński, D. and A. Kossakowski (2010) "Non-Markovian Quantum Dynamics: Local versus Nonlocal," Physical Review Letters, **104**(7), 0912.1259.
URL http://dx.doi.org/10.1103/PhysRevLett.104.070406

[55] Hulse, A. and B. Schumacher (2019) "Quantum meronomic frames," arXiv e-prints, arXiv:1907.04899, 1907.04899.

[56] Dann, R., N. Megier, and R. Kosloff (2021), "Non-Markovian dynamics under time-translation symmetry," .
URL https://arxiv.org/abs/2106.05295

[57] Makhlin, Y. (2000) "Nonlocal properties of two-qubit gates and mixed states and optimization of quantum computations," arXiv e-prints, quant-ph/0002045, quant-ph/0002045.

[58] Zhang, J., J. Vala, S. Sastry, and K. B. Whaley (2003) "Geometric theory of nonlocal two-qubit operations," Phys. Rev. A, **67**, p. 042313, quant-ph/0209120.

[59] Laine, E.-M., J. Piilo, and H.-P. Breuer (2010) "Measure for the non-Markovianity of quantum processes," Physical Review A, **81**(6).
URL http://dx.doi.org/10.1103/PhysRevA.81.062115

[60] Chen, J.-L., L. Fu, A. A. Ungar, and X.-G. Zhao (2002) "Geometric observation for Bures fidelity between two states of a qubit," Physical Review A, **65**(2).
URL http://dx.doi.org/10.1103/PhysRevA.65.024303

[61] Puebla, R. (2020) "Finite-component dynamical quantum phase transitions," Phys. Rev. B, **102**, p. 220302.
URL https://link.aps.org/doi/10.1103/PhysRevB.102.220302

[62] Smirne, A. and B. Vacchini (2010) "Nakajima-Zwanzig versus time-convolutionless master equation for the non-Markovian dynamics of a two-level system," Physical Review A, **82**(2).
URL http://dx.doi.org/10.1103/PhysRevA.82.022110

[63] Burgess, C. P., R. Holman, G. Kaplanek, J. Martin, and V. Vennin (2022) "Minimal decoherence from inflation," 2211.11046.

[64] Brahma, S., A. Berera, and J. Calderón-Figueroa (2022) "Quantum corrections to the primordial tensor spectrum: open EFTs & Markovian decoupling of UV modes," JHEP, **08**, p. 225, 2206.05797.

[65] Prudhoe, S., U. Akhouri, T. Chin, and S. Shandera (2024), "Effective dynamics of qubit networks via phase-covariant quantum ensembles," 2404.15223.

[66] Deshpande, A., P. Niroula, O. Shtanko, A. V. Gorshkov, B. Fefferman, and M. J. Gullans (2022) "Tight Bounds on the Convergence of Noisy Random Circuits to the Uniform Distribution," PRX Quantum, **3**, p. 040329.
URL https://link.aps.org/doi/10.1103/PRXQuantum.3.040329

[67] Fefferman, B., S. Ghosh, M. Gullans, K. Kuroiwa, and K. Sharma (2023) "Effect of non-unital noise on random circuit sampling," arXiv e-prints, arXiv:2306.16659, 2306.16659.

[68] Holevo, A. S. (1993) "A note on covariant dynamical semigroups," Reports on mathematical physics, **32**(2), pp. 211–216.

[69] Lankinen, J., H. Lyyra, B. Sokolov, J. Teittinen, B. Ziaei, and S. Maniscalco (2016) "Complete positivity, finite-temperature effects, and additivity of noise for time-local qubit dynamics," Physical Review A, **93**(5), 052103, 1511.07202.

[70] Kropf, C. M., C. Gneiting, and A. Buchleitner (2016) "Effective Dynamics of Disordered Quantum Systems," Physical Review X, **6**(3), 031023, 1511.08764.

[71] Denisov, S., T. Laptyeva, W. Tarnowski, D. Chruściński, and K. Życzkowski (2019) "Universal Spectra of Random Lindblad Operators," Physical Review Letters, **123**(14), 140403, 1811.12282.

[72] Can, T. (2019) "Random Lindblad dynamics," Journal of Physics A Mathematical General, **52**(48), 485302, 1902.01442.

[73] Can, T., V. Oganesyan, D. Orgad, and S. Gopalakrishnan (2019) "Spectral Gaps and Midgap States in Random Quantum Master Equations," Physical Review Letters, **123**(23), 234103, 1902.01414.

[74] Lieu, S., M. McGinley, and N. R. Cooper (2020) "Tenfold Way for Quadratic Lindbladians," Physical Review Letters, **124**(4), 040401, 1908.08834.

[75] Li, J., T. Prosen, and A. Chan (2021) "Spectral Statistics of Non-Hermitian Matrices and Dissipative Quantum Chaos," Physical Review Letters, **127**(17), 170602, 2103.05001.

[76] Tarnowski, W., D. Chruściński, S. Denisov, and K. Życzkowski (2023) "Random Lindblad Operators Obeying Detailed Balance," Open Systems and Information Dynamics, **30**(02).
URL http://dx.doi.org/10.1142/S1230161223500075

[77] Bruzda, W., V. Cappellini, H.-J. Sommers, and K. Życzkowski (2009) "Random quantum operations," Physics Letters A, **373**(3), pp. 320–324, 0804.2361.

[78] Bruzda, W., M. Smaczyński, V. Cappellini, H.-J. Sommers, and K. Życzkowski (2010) "Universality of spectra for interacting quantum chaotic systems," Physical Review E, **81**(6), 066209, 1003.2931.

[79] Sá, L., P. Ribeiro, T. Can, and T. Prosen (2020) "Spectral transitions and universal steady states in random Kraus maps and circuits," Physical Review B, **102**(13), 134310, 2007.04326.

[80] Filippov, S. N., A. N. Glinov, and L. Leppäjärvi (2019) "Phase covariant qubit dynamics and divisibility," arXiv e-prints, arXiv:1911.09468, 1911.09468.

[81] Siudzińska, K. (2023) "Geometry of phase-covariant qubit channels," Journal of Physics Communications, **7**(7), 075002, 2210.17448.

[82] Smirne, A., J. Kołodyński, S. F. Huelga, and R. Demkowicz-Dobrzański (2016) "Ultimate Precision Limits for Noisy Frequency Estimation," Phys. Rev. Lett., **116**, p. 120801.
URL https://link.aps.org/doi/10.1103/PhysRevLett.116.120801

[83] Haase, J. F., A. Smirne, J. Kołodyński, R. Demkowicz-Dobrzański, and S. F. Huelga (2018) "Fundamental limits to frequency estimation: a comprehensive microscopic perspective," New Journal of Physics, **20**(5), 053009, 1710.04673.

[84] Haase, J. F., A. Smirne, and S. F. Huelga (2019) "Non-monotonic Population and Coherence Evolution in Markovian Open-System Dynamics," in Advances in Open Systems and Fundamental Tests of Quantum Mechanics (B. Vacchini, H.-P. Breuer, and A. Bassi, eds.), Springer International Publishing, Cham, pp. 41–57.

[85] Siudzińska, K. and M. Studziński (2023) "Adjusting phase-covariant qubit channel performance with non-unitality," Journal of Physics A Mathematical General, **56**(20), 205301, 2212.04876.

[86] Siudzińska, K. (2023) "Improving classical capacity of qubit dynamical maps through stationary state manipulation," Journal of Physics A Mathematical General, **56**(23), 235301, 2302.11519.

[87] Chruściński, D. (2022) "Dynamical maps beyond Markovian regime," Physics Reports, **992**, pp. 1–85, 2209.14902.

[88] Siudzińska, K. (2022) "Phase-covariant mixtures of non-unital qubit maps," Journal of Physics A Mathematical General, **55**(40), 405303, 2206.10742.

[89] Macdonald, I. (1998) Symmetric Functions and Hall Polynomials, Oxford classic texts in the physical sciences, Clarendon Press.
URL https://books.google.com/books?id=srv90XiUbZoC

[90] Cleve, R. and C. Wang (2016) "Efficient Quantum Algorithms for Simulating Lindblad Evolution," 1612.09512.

[91] Pocrnic, M., D. Segal, and N. Wiebe (2023) "Quantum Simulation of Lindbladian Dynamics via Repeated Interactions," arXiv e-prints, arXiv:2312.05371, 2312.05371.

[92] Kashyap, V., G. Styliaris, S. Mouradian, J. I. Cirac, and R. Trivedi (2024) "Accuracy guarantees and quantum advantage in analogue open quantum simulation with and without noise," 2404.11081.

[93] Prudhoe, S., R. Kumar, and S. Shandera (2024) "Spontaneously interacting qubits from Gauss-Bonnet," Journal of High Energy Physics, **2024**(2), pp. 1–29.

[94] Freedman, M. and M. S. Zini (2021) "The universe from a single particle," Journal of High Energy Physics, **2021**(1).
URL https://doi.org/10.1007%2Fjhep01%282021%29140

[95] ——— (2021) "The universe from a single particle. Part II," Journal of High Energy Physics, **2021**(10).
URL https://doi.org/10.1007%2Fjhep10%282021%29102

[96] ——— (2022) "Symmetry breaking to Majorana Brown-Susskind metric," Journal of High Energy Physics, **2022**(4).
URL https://doi.org/10.1007%2Fjhep04%282022%29041

[97] Ishibashi, N., H. Kawai, Y. Kitazawa, and A. Tsuchiya (1997) "A large- N reduced model as superstring," Nuclear Physics B, **498**(1), pp. 467–491, hep-th/9612115.

[98] Konopka, T., F. Markopoulou, and S. Severini (2008) "Quantum graphity: A model of emergent locality," Physical Review D, **77**(10), 104029, 0801.0861.

[99] Hu, B. L. (2009) "Emergent/Quantum Gravity: Macro/Micro Structures of Spacetime," J. Phys. Conf. Ser., **174**, p. 012015, 0903.0878.

[100] Hamma, A., F. Markopoulou, S. Lloyd, F. Caravelli, S. Severini, and K. Markström (2010) "Quantum Bose-Hubbard model with an evolving graph as a toy model for emergent spacetime," Physical Review D, **81**(10), 104032, 0911.5075.

[101] Verlinde, E. P. (2011) "On the Origin of Gravity and the Laws of Newton," JHEP, **04**, p. 029, 1001.0785.

[102] Swingle, B. and M. Van Raamsdonk (2014) "Universality of Gravity from Entanglement," arXiv e-prints, arXiv:1405.2933, 1405.2933.

[103] Freedman, M. and M. S. Zini (2021) "The universe from a single particle," Journal of High Energy Physics, **2021**(1), 140, 2011.05917.

[104] Freedman, M. and M. Shokrian Zini (2021) "The Universe from a Single Particle II," arXiv e-prints, arXiv:2108.12709, 2108.12709.

[105] Freedman, M. and M. S. Zini (2021) "The universe from a single particle. Part III," Journal of High Energy Physics, **2021**(10), 102, 2112.08613.

[106] Kobayashi, S. and K. Nomizu (1996) Foundations of Differential Geometry, Volume 1, A Wiley Publication in Applied Statistics, Wiley.
URL https://books.google.com/books?id=ajN0aD65Ez8C

[107] Caselle, M. and U. Magnea (2004) "Random matrix theory and symmetric spaces," **394**(2-3), pp. 41–156, cond-mat/0304363.

[108] Gallier, J. and J. Quaintance (2020) Differential Geometry and Lie Groups: A Computatio
Springer Cham.

[109] Berger, M. (1970) "Quelques formules de variation pour une structure riemannienne," Ann. sci. Ecole Norm. Sup.,, **4e serie**(3), pp. 285–294.

[110] MUTO, Y. (1974) "Curvature and critical Riemannian metric," Journal of the Mathematical Society of Japan, **26**(4), pp. 686–697.

[111] ——— (1977) "Riemannian submersions and critical Riemannian metrics," Journal of the Mathematical Society of Japan, **29**(3), pp. 493–511.

[112] Patterson, E. M. (1981) "A Class of Critical Riemannian Metrics," Journal of the London Mathematical Society, **s2-23**(2), pp. 349–358, https://londmathsoc-onlinelibrary-wiley-com.ezaccess.libraries.

psu.edu/doi/pdf/10.1112/jlms/s2-23.2.349.
URL https://londmathsoc-onlinelibrary-wiley-com.ezaccess.libraries.psu.edu/doi/abs/10.1112/jlms/s2-23.2.349

[113] JENSEN, G. R. and S. S. Chern (1971) "The Scalar Curvature of Left-Invariant Riemannian Metrics," Indiana University Mathematics Journal, **20**(12), pp. 1125–1144.
URL http://www.jstor.org/stable/24890189

[114] Wigner, E. P. (1955) "Characteristic Vectors of Bordered Matrices With Infinite Dimensions," Annals of Mathematics, **62**(3), pp. 548–564.

[115] Dyson, F. J. (1962) "Statistical theory of the energy levels of complex systems. I," Journal of Mathematical Physics, **3**(1), pp. 140–156.

[116] MUTO, Y. (1977) "Riemannian submersions and critical Riemannian metrics," Journal of the Mathematical Society of Japan, **29**(3), pp. 493–511.

[117] Khaneja, N. and S. Glaser (2000) "Cartan Decomposition of SU(2n̂), Constructive Controllability of Spin systems and Universal Quantum Computing," arXiv e-prints, quant-ph/0010100, quant-ph/0010100.

[118] Bossion, D. and P. Huo (2021) "General Formulas of the Structure Constants in the $\mathfrak{su}(N)$ Lie Algebra," 2108.07219.

[119] Helgason, S. (2001) Differential Geometry, Lie Groups, and Symmetric Spaces, Crm Proceedings & Lecture Notes, American Mathematical Society.
URL https://books.google.com/books?id=a9KFAwAAQBAJ

[120] D'Atri, J. and W. Ziller (1979) "Naturally reductive metrics and Einstein metrics on compact Lie groups," Memoirs of the American Mathematical Society, **215**.

[121] Arvanitoyeorgos, A., Y. Sakane, and M. Statha (2020) "Invariant Einstein metrics on SU(N) and complex Stiefel manifolds," arXiv e-prints, arXiv:2002.10359, 2002.10359.

[122] Earp, H. N. S. and J. K. Pachos (2005) "A constructive algorithm for the Cartan decomposition of SU(2^N)," Journal of Mathematical Physics, **46**(8), 082108, quant-ph/0505128.

[123] Nielsen, M. A. (2005) "A geometric approach to quantum circuit lower bounds," arXiv e-prints, quant-ph/0502070, quant-ph/0502070.

[124] Nielsen, M. A., M. R. Dowling, M. Gu, and A. C. Doherty (2006) "Quantum Computation as Geometry," Science, **311**(5764), pp. 1133–1135, quant-ph/0603161.

[125] Brown, A. R. and L. Susskind (2018) "Second law of quantum complexity," Physical Review D, **97**(8).
URL https://doi.org/10.1103%2Fphysrevd.97.086015

[126] Brown, A. R., M. H. Freedman, H. W. Lin, and L. Susskind (2021), "Effective Geometry, Complexity, and Universality," 2111.12700.

[127] Su, Z.-Y. (2006) "A Scheme of Cartan Decomposition for su(N)," arXiv e-prints, quant-ph/0603190, quant-ph/0603190.

[128] Wald, R. M. (1984) General relativity, Chicago Univ. Press, Chicago, IL.
URL https://cds.cern.ch/record/106274

[129] Santos, W. C. d. (2017), "Non-coordinates basis in General Relativity and Cartan's structure equations," .
URL https://arxiv.org/abs/1711.09503

Vita

Sean T. Prudhoe

2018 B.S in Physics, The Pennsylvania State University

2018 B.S in Mathematics, The Pennsylvania State University

2018 Teaching Assistant, Department of Physics, The Pennsylvania State University

2019-21 Research Assistant, Department of Physics, The Pennsylvania State University

2022 Teaching Assistant, Department of Physics, The Pennsylvania State University

2023 Research Assistant, Department of Physics, The Pennsylvania State University

2024 Ph.D in Physics, The Pennsylvania State University

FIELD OF STUDY

Open Quantum Systems and Quantum Information

PUBLICATIONS

Sean Prudhoe and Sarah Shandera. "Classifying the non-time-local and entangling dynamics of an open qubit system". Journal of High Energy Physics, 2023

Sean Prudhoe, Sarah Shandera, and Rishabh Kumar. "Spontaneously interacting qubits from Gauss-Bonnet". Journal of High Energy Physics, 2024

Sean Prudhoe, Unnati Akhouri, Tommy Chin, Sarah Shandera. "Effective dynamics of qubit-networks via phase-covariant ensembles". Open Systems and Information Dynamics, 2024 (under review)